PARAMETRIC LIFE CYCLE ASSESSMENT OF COMBINED COOLING, HEATING, AND POWER INTEGRATED WITH RENEWABLE ENERGY AND ENERGY STORAGE

A Dissertation
Presented to
The Academic Faculty

by

Junchen Yan

In Partial Fulfillment
of the Requirements for the Degree
Doctor of Philosophy in the
School of Civil and Environmental Engineering

Georgia Institute of Technology
May 2020

PARAMETRIC LIFE CYCLE ASSESSMENT OF COMBINED COOLING, HEATING, AND POWER INTEGRATED WITH RENEWABLE ENERGY AND ENERGY STORAGE

Approved by:

Dr. John C. Crittenden, Advisor
School of Civil and Environmental Engineering
Georgia Institute of Technology

Dr. Santiago Carlos Grijalva
School of Electrical and Computer Engineering
Georgia Institute of Technology

Dr. Yongsheng Chen
School of Civil and Environmental Engineering
Georgia Institute of Technology

Dr. John E. Taylor
School of Civil and Environmental Engineering
Georgia Institute of Technology

Dr. Marilyn A. Brown
School of Public Policy
Georgia Institute of Technology

Dr. Valerie Thomas
H. Milton Stewart School of Industrial and Systems Engineering
Georgia Institute of Technology

Date Approved: December 13th, 2019

I want to dedicate my work to my parents for their selfless support.

ACKNOWLEDGMENTS

First, I thank my advisor, Dr. John C. Crittenden, for his thoughtful and patient support and guidance throughout my study at the Georgia Institute of Technology. I feel fortunate to be his student. Dr. Crittenden is a great mentor and scholar. I am impressed by his persistence and graveness in research and work. His global vision in sustainable development inspired me a lot. The work and life principle he taught me will have a profound influence on my future life. I would thank my committee members Dr. Yongsheng Chen, Dr. Santiago Carlos Grijalva, Dr. Marilyn A. Brown, Dr. Valerie Thomas, and Dr. John E. Taylor for their guidance, patience, and interest in my Ph.D. work. I would thank all staff at Brook Byers Institute of Sustainable Systems, Michael E. Chang, Susan Ryan, Brent Verrill, and Gay Burchfield for their kindly help during my working. I would thank the Academic Professional, Robert Simon, for his patience guidance during my graduate study. I would thank Mr. Duo Li, who is the ex-vice director at the Brook Byers Institute for Sustainable Systems, who treats me like his brother. I would thank my chiropractor Muquan Zhang who cures my spondylosis and my depression. I would appreciate all my friends and colleagues at the Brook Byers Institute for Sustainable Systems: Osvaldo A. Broesicke, Weiqiu Zhang, Kaihang Zhang, Dong Wang, Xiaoyang Meng, Su Liu, Xin Tong, Zefang Chen, Zhongming Lu, Jinming Luo, Siyu Zhang, Deyou Yu, Liping Wang, Guangpeng Yang, Guanglan Di, Thomas Igou, Xiao Sun, Yuling Zhang, Songyan Qin, Dan Qu, Jing Chen, Jingge Shang, Jialiang Zhang, Feilong Dong, Xiaojun Wang, Saige Wang, Zhilin Ran, Feng Gao, Fatao Wang, Dongjin Wan, Wei He, et al.

TABLE OF CONTENTS

LIST OF TABLES

LIST OF FIGURES

LIST OF SYMBOLS AND ABBREVIATIONS

ACAES	Adiabatic Compressed Air Energy Storage
AHP	Analytic Hierarchy Process
AMT	Alternative Minimum Tax
APEEP	Air Pollution Emissions Experiments and Policy
CAES	Compressed Air Energy Storage
CCHP	Combine Cooling, Heating, and Power
CCHP-RE-ESS	Combine Cooling, Heating and Power integrated with Renewable Energy and energy storage system
CHP	Combined Heating and Power
COP	Coefficient of Performance
DOE	Department of Energy
eGRID	Emissions and Generation Resource Integrated Database
FEL	Following the Electrical Load
FTL	Following the Thermal Load
IRS	Internal Revenue Service
ITC	Investment Tax Credit
LCA	Life Cycle Assessment
LCC	Life Cycle Cost
MACR	Modified Accelerated Cost Recovery System
MCFC	Molten Carbonate Fuel Cell
MDO	Multi-Disciplinary Design Optimization
NERC	The North American Electric Reliability Corporation
O & M	Operation and Maintenance
PAFC	Phosphoric Acid Fuel Cell
PEMFC	Proton Exchange Membrane Fuel Cell
SOFC	Solid Oxide Fuel Cell
TMY	Typical Meteorological Year
TRACI	Tool for Reduction and Assessment of Chemicals and Other Environmental impacts
USEEIO	U.S. Environmentally Extended Input-Output Model

SUMMARY

Buildings use about 40% of global energy supply, mainly from natural gas and electric grids powered by fossil fuel-based centralized power plants. This study examines a more sustainable energy generation system --- the distributed combined cooling, heat, and power integrated with renewable energy and energy storage system. A parametric hybrid life cycle assessment framework approach is used to evaluate the environmental, economic, and social impacts of the proposed distributed energy generation system. The rationale for a parametric LCA approach is that it extends conventional LCA, which is cases-specific and shows how impacts change with different input factors such as ambient temperature, pressure, climate, and operation strategies. Then, the impact results integrate with a multi-disciplinary design optimization method, Pareto front, to find the optimal environmental and economic impact trade-offs for different building energy demand scenarios. Finally, the federal policy incentive and social cost models are used to assess the economic cost-saving potential for the distributed energy generation system.

In Chapter 2, a distributed energy generation system that is composed of microturbines, heat recovery units, solar panels, lithium-ion batteries, adsorption chillers, and auxiliary components is simulated by the model. The Pareto front finds the optimal sizes of solar PVs and batteries for different building types and locations. The simulation result shows that the system can primarily reduce the environmental impact as compared to the conventional energy system. However, the life cycle cost is higher than traditional energy generation while it is more economical for the small and large office than the medium office.

In Chapter 3, more commercially available technologies submodules are integrated into the parametric hybrid LCA framework, including small wind turbines, solid oxide fuel cells, and adiabatic compressed air energy storage. The model finds the best technology combinations and corresponding sizes for three types of office buildings in five cities. Microturbine-Solar PVs-Lithium ion Battery and Solid Oxide Fuel Cells-Solar PVs-Lithium-ion Battery are two optimal distributed energy solutions according to the simulation results. However, the life cycle cost for the SOFC-based CCHP-RE-ESS system is even higher than the microturbine-based energy system due to the high capital and operational costs of the fuel cell system.

Finally, in Chapter 4, the model evaluates the social cost and the current U.S. clean energy policy incentives impacts on the distributed CCHP-RE-ESS system. The model uses the Air Pollution Emission Experiments and Policy model to evaluate the marginal damages emissions on a dollar per ton basis. Results show that the social cost of conventional energy is significantly higher than the distributed energy generation. It is estimated that the installation of the distributed CCHP-RE-ESS can help avoid more than 50 billion dollars of social cost per year for commercial buildings in U.S. Besides, the model studies the cost-saving potential of current U.S. clean energy policy incentives, including federal tax credit, low-interest loan, Modified Accelerated Cost Recovery System, and 100-percent first-year bonus depreciation. From calculation results based on current U.S. accounting standards, these policies can primarily reduce the cost of distributed energy. In some scenarios, the after-policy life cycle cost of distributed energy generation is competitive compared to conventional power, but for most situations, the life cycle cost is still higher especially for SOFC based CCHP-RE-ESS. However, if the social

cost of energy-related emissions is considered, 50% of building energy supply scenarios for the distributed CCHP-RE-ESS are cost-competitive as compared to conventional energy generation.

CHAPTER 1. INTRODUCTION

1.1 The Global Energy Challenge

Driven by rapid economic and population growth in the past few decades, cities consume over two-thirds of the world's energy and account for more than 70% of global CO2 emissions [1]. The United Nations and International Energy Agency estimate that the continuing urbanization and growth of the world's population is projected to add 2.5 billion people to the urban population and a 70% increase in energy demand by 2050 [2]. The increase in energy consumption will cause more energy-related water usage, as well as carbon dioxide and pollutant emissions. Cities are looking for a more efficient and less polluting way to meet the increasing energy demand.

The Trigeneration or combined cooling, heat, and power (CCHP) refers to the simultaneous generation of electricity and useful heating and cooling supply. Combined cooling, heat, and power (CCHP) has higher efficiency than conventional energy generation because waste heat can be recovered and used to meet the heating and cooling loads. Previous researches focused on both centralized large gas turbines and those applicable for distributed generations [3,4]. However, the distributed energy generation is closer to the end-users and hence can avoid energy transmission losses. The distributed CCHP can be integrated with renewable energy technologies and energy storage systems (CCHP-RE-ESS) to enhance local power reliability and sustainability performance (e.g., less energy-related emissions and water usage) [5].

For the CCHP system itself, the reported combined efficiency ranges from 60% to 80% [3]. The CCHP has two wildly used operation strategies: following the electrical load

(FEL) [6] and following the thermal load (FTL) [7]. It is reported that if there is no net metering policy, following the thermal load (FTL) operation strategy results in the most significant environmental benefit and cost savings [8]. This is because a combustion-based energy generation unit usually produces more heat than electrical power. Hence, the integration of the CCHP with renewable energy and energy storage system (CCHP-RE-ESS) can further reduce the emission and become more reliable in peak hours. The distributed CCHP-RE-ESS is composed of a prime mover, a heat recovery unit, an absorption chiller, a set of renewable energy sources, and energy storage device, and electrical interconnections. One example of CCHP-RE-ESS is shown in Figure 1.1. The prime mover (a microturbine, as shown in Figure 1.1) generates the majority of electrical power, and the waste heat produced during the combustion process is recovered by the heat recovery unit. The recovered heat can be used for space heating, hot water, and absorption chiller for space cooling. The renewable energy source can generate extra electricity, which can be stored in the electrical energy storage device for later use.

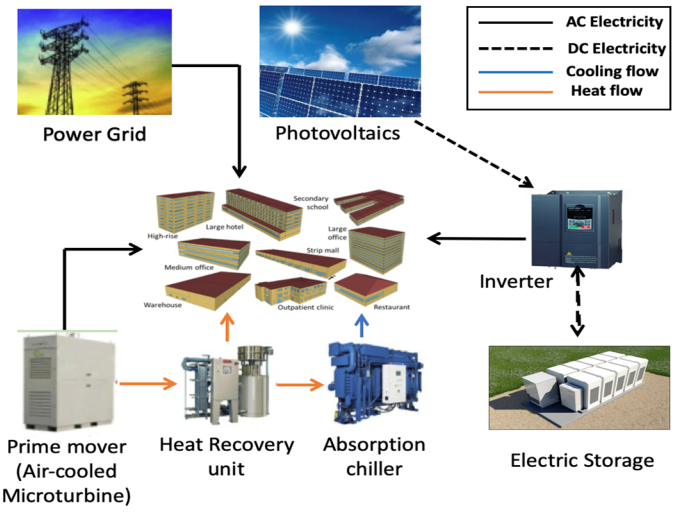

Figure 1.1. An example of distributed CCHP-RE-ESS.
A microturbine-based combined cooling, heating, and power integrated with solar power and the lithium-ion battery.

Also, an essential advantage of distributed generation is that it has a degree of modularity and scalability that is not possessed by a conventional centralized power plant [9,10]. For example, once a centralized power plant is built based on local energy demand capacity. As the regional population growth, we need to build another large and expensive plant for the increasing energy demand. We cannot just build a small power plant and add to local capacity. The new plant may have more capacity than we need.

In the following chapters, we use a parametric life cycle assessment framework to evaluate the environmental, economic, and social impacts of the distributed CCHP-RE-ESS energy system with various prime mover, renewable energy, and energy storage technologies. We also adopt multi-disciplinary design optimization to find the best technology combinations and corresponding sizes for different building types and climate zones. Besides, we study and calculate the current U.S. clean and renewable energy policies (such as the investment tax credit, the low-interest loan, the Modified Accelerated Cost Recovery System, and the 100-percent first-year bonus depreciation.) impact on investment savings for the distributed energy generation for commercial entities.

The parametric LCA framework is comprised of: (1) a scenario-based energy demand simulation for various commercial building types under different geospatial conditions; (2) parametric submodules for different system technologies (3) process-based and economic input-output based life cycle impact inventories for environmental and economic impact assessment; (4) life cycle cost model that include different policy incentives and depreciation of assets; and (5) social cost model and inventory for energy-related air pollutant emissions.

1.2 Background of Research and Literature Review

1.2.1 The CCHP-RE-ESS

By and large, previous research studies evaluated four aspects of the distributed CCHP integrated with renewable energy and energy storage system (CCHP-RE-ESS): operational performance [11–19], system design [20–24], economic cost [25–30], and emissions and impacts in operational stage [18,25,31–33]. However, there are few cradle-to-grave life cycle assessment studies on CCHP-RE-ESS. The life-cycle assessment (LCA) of CCHP-RE-ESS for commercial building energy supply is scant, especially in the U.S. context.

Bahman Shabani et al. [29] conducted a techno-economic analysis of solar-hydrogen combined heat and power systems, but they did not consider the optimal trade-offs between impact and cost. Also, most researchers designed the CCHP-RE-ESS only for residential houses rather than commercial buildings. However, CHP or CCHP systems have been widely employed in industrial, large commercial and institutional applications [34]. Although different technologies for CCHP-RE-ESS has been evaluated, the technologies combination of microturbine, solar PVs, and lithium-ion batteries have not yet been studied. In Chapter 2, we studied the CCHP-RE-ESS that consist of the microturbine, solar PVs, and lithium-ion batteries and find the optimal sizes for solar and energy storage system.

1.2.2 Parametric Life Cycle Assessment for CCHP-RE-ESS

The performance and emissions of different CCHP-RE-ESS technologies depend on their operation conditions such as ambient temperature, operating temperature, fuel utilization rate, and partial load ratio. For example, the emission of microturbine per kWh

of energy generated is a function of ambient temperature and part load ratio, as reported by the manufacturers. Previous studies [25] only consider average emission data and reports case-specific impact results. They failed to show why and how much results vary with different operating conditions.

On the other hand, a transportation LCA study conducted by Dong-Yeon Lee et al. [31] used a parametric approach to evaluate the economic and environmental life cycle impacts of medium-duty trucks. They compared medium-duty electric trucks with various types of truck power by fossil fuel that operate at different speeds. Besides, compared to conventional LCA, the parametric LCA is more accurate since it reveals how impact changes with different operating conditions. Hence, in this research, we used MATLAB [35] to develop a parametric LCA framework for the CCHP-RE-ESS that was able to show how and why impacts change with the input parameter.

1.2.3 Trigeneration Technologies

Although different technologies for CCHP-RE-ESS have been evaluated, most previous researches studied one single combination of technologies, with constant system component sizes [27,32,33,36]. The detailed technology or technologies combinations for CHP, CCHP, and CCHP-RE-ESS system are summarised in Table 1.1 below. In our research (Chapter 3), we simulate nine commercially available trigeneration technologies and find the optimal trade-offs via Multi-disciplinary design optimization. The studied technologies of our research are listed in Table 1.2.

Table 1.1. Literature summary of CHP, CCHP, and CCHP-RE-ESS technologies.

	Prime Mover	Renewables	Energy Storage
Pruitt et al. (2013)	SOFC	None	None
Angrisani et al. (2015)	ICE	None	None
Cappa et al. (2015)	ICE and PEMFC	None	None
Balcombe et al. (2015a; 2015b)	SE	None	None
James et al. (2015) [37]	MT	None	None
Tempestic (2012) [38]	Microturbine	Geothermal	None
Ma (2012) [39]	ICE	Solar and Wind	None
Yang et al. (2012) [40]	Gas turbine	Solar Thermal	Thermal Energy Storage
Hosseini (2013) [32]	SOFC	Solar PVs	Hydrogen Storage Tank
Alipour et al. (2015) [33]	Fuel Cell	Wind Turbine	Battery
Rodriguez (2015) [41]	NG engine	Solar PV	Heating Tank
Levihn (2017) [36]	CHP	Heat Pump	None
Maleki (2017) [27]	Fuel cell	Wind and Solar PVs	None
Prime movers: ICE – internal combustion engine, SE – Stirling engine, SOFC – solid oxide fuel cell, PEMFC – proton exchange membrane fuel cell, MT – microturbine.			

Table 1.2. Selected technologies for CCHP-RE-ESS.

Technology	Category	Service Provided
Power Grid	Centralized Energy	Electricity
Furnace (conventional energy)	Centralized Heating	Heating
Boiler (conventional energy)	Centralized Heating	Heating
Microturbine	Prime Mover	Electricity, Heating
Solid Oxide Fuel Cells	Prime Mover	Electricity, Heating
Heat Recovery Unit	CHP System Components	Heat Exchange
Absorption Chiller	CHP System Components	Cooling
Air Conditioning	Plug Loads	Cooling
Solar Photovoltaics	Renewables	Electricity
Small Wind Turbine	Renewables	Electricity
Li-ion Batteries	Energy Storage	Electricity Storage
Compressed Air Energy Storage	Energy Storage	Electricity Storage

1.2.4 Multi-Disciplinary Design Optimization

The goal of multi-disciplinary design optimization (MDO) is to generate the Pareto front or surface, such that each point on the surface is a design that optimally satisfies all objectives [42]. It is developed to deal with the complexity of the multi-criteria design, combines with parametric design in order to evaluate the trade-offs between objectives of each design [43,44]. MDO is originally used in the field of aerospace engineering for aircraft shape design [45]. A recent study has shown the application of MDO in distributed energy generation and urban district design [46]. However, the main focus of this paper is on building energy mix and no renewable sources integrated. Currently, few studies have applied MDO in the CCHP-RE-ESS energy generation for the best technology and size combinations. In this research (Chapter 2 and Chapter 3), the MDO approach is used to find the optimal combination of technologies and their corresponding sized for the distributed CCHP-RE-ESS under different scenarios.

1.2.5 Current Policy Incentives

The development of clean and renewable energy technologies, such as solar energy, geothermal energy, combined heat and power, fuel cells wind energy, etc., have been aided by federal policy incentives aimed at sustainable energy generation. Federal initiatives aimed at developing and deploying sustainable energy technologies include the Energy Policy Act of 2005, the Energy Independence and Security Act of 2007, the American Recovery and Reinvestment Act of 2009, and the Clean Air Act under Section 111(d) (the Clean Power Plan).

Current US federal policies for developing clean and renewable technologies for energy consumers include renewable portfolio standards (RPS) [47], the renewable energy credit (REC) [48], the feed-in-tariff [49], net metering tariffs, federal production tax credits (PTC) [50] and bonus tax depreciation system. Previous life cycle cost researches mainly focus on investment cost, operation & maintenance cost, and disposals cost but failed to consider the cost-saving potentials of the policy incentives and depreciation using business accounting standards [51–53]. Nevertheless, these factors have a significant impact on commercial entities' financial performance. Several researchers considered the policy impacts of individual technologies, such as renewable [54–56], CHP or CCHP [57–60], but none investigated the impacts associated with the integrated system comprising all three categories(CCHP, renewable, and energy storage) of technologies and considering its dynamic operation with respect to daily and seasonal energy demand.

1.3 Research Objectives

This research contributes a more detailed and systematic understanding of the distributed Combined Cooling, Heating, and Power---Renewable Energy---Energy Storage System (CCHP-RE-ESS) and its life cycle environmental, economic, and social impact. The research objectives are:

1. To develop a modular and parametric life cycle assessment (LCA) framework for the distributed CCHP-RE-ESS energy generation that can evaluate the environmental, economic and social impact.
2. To assess various trigeneration combination of technologies that can be applied to the distributed CCHP-RE-ESS: prime mover (e.g., microturbine, fuel cell), renewable energy source (e.g., solar PV, wind turbine) and energy storage (e.g., lithium-ion battery, compressed air energy storage).
3. To find optimal environmental and economic trade-offs of different combinations of technologies and their corresponding sizes for the distributed CCHP-RE-ESS under various scenarios (e.g., climate zones and building types).
4. To evaluate the social cost of the distributed CCHP-RE-ESS compared to conventional centralized power generation.
5. To evaluate the cost-saving potential of the current policy incentives and depreciation accounting method for the distributed CCHP-RE-ESS system.

CHAPTER 2. THE PARAMETRIC LCA FRAMEWORK FOR DISTRIBUTED CCHP-RE-ESS GENERATION

2.1 Chapter Summary

The objective of this section is to illustrate the parametric life cycle assessment framework and evaluate the environmental, economic impact, and trade-offs of a distributed CCHP-RE-ESS energy generation system that consists of microturbines, solar PVs, lithium-ion batteries, and other auxiliary system components. The parametric life cycle assessment framework was developed via MATLAB. We used a multi-disciplinary design optimization method, Pareto front, to find the optimal environmental and economic impact trade-off and corresponding solar and battery sizes for different commercial building types at various climate zones. The simulation results show that the CCHP-RE-ESS and proposed technologies have less life cycle environmental impact compared to conventional power generation. By adopting the CCHP-RE-ESS system, buildings require much less electricity demand from the grid. For example, it has been shown that the proposed system could help a medium office in Atlanta save 21-46% of global warming impact and 70%-98% of water usage at different sizes of solar PVs and lithium-ion batteries. The distributed CCHP-RE-ESS can also stay more than 90% off-grid by following the thermal load of a medium office. From the results, the medium office building can have the largest environmental benefit in terms of life cycle single score by adopting the CCHP-RE-ESS. In terms of cost, the life cycle cost of the proposed system is often higher than conventional energy generation while it is more economical for the small and large office than the medium office [61].

2.2 Methodology

2.2.1 The System Framework

Figure 2.1 shows the system framework of the CCHP-RE-ESS system versus conventional energy generation. In the United States, the conventional energy generation for buildings are comprised of electricity from the central electricity grid and heat from a furnace or boiler [62,63], cooling demand is met by air conditioner powered by electricity. However, the heat generated from a centralized power plant is wasted and cannot be recovered and transported to buildings in the city area.

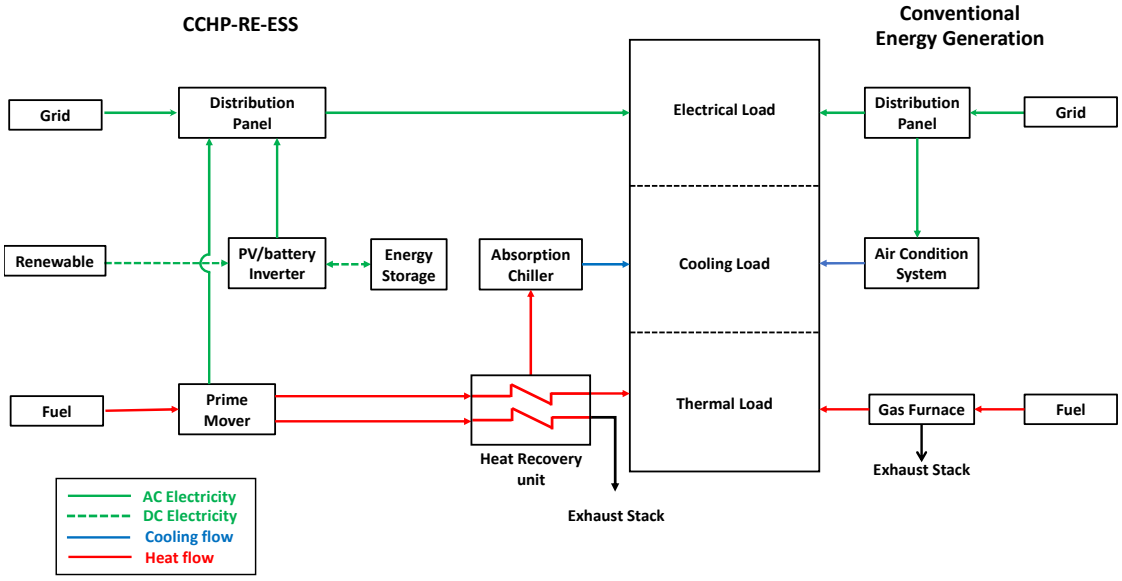

Figure 2.1 The system framework.

The distributed CCHP-RE-ESS is composed of a prime mover, a heat recovery unit, an absorption chiller, a set of renewable energy sources, energy storage devices, and electrical interconnections. The prime mover is for the main electrical power generation, and the heat recovery unit recovers the waste heat. The recovered heat is used for space

heating, hot water, and absorption chiller for space cooling. The renewable energy source can generate extra electricity, which can be complementary if there is more electricity demand. Extra electricity can be stored in the electrical energy storage device for later use. In this chapter, we choose the microturbine as the prime mover (of CCHP), solar PVs as the renewable energy source (RE), and lithium-ion batteries as energy storage (ESS) and find the optimal sizes for solar and energy storage system.

2.2.2 The Environmental Life Cycle Assessment

The Goal and Scope

The goal of this environmental life cycle assessment (LCA) framework is to compare the distributed CCHP-RE-ESS with various conventional energy generation in terms of freshwater consumption, air emissions impacts (i.e., acidification, eutrophication, global warming, ecotoxicity), and fossil fuel depletion under various spatial conditions and building types.

Functional Unit

The functional unit is the annual energy generation and resulted impact for each foot square of the building. There are three forms of building energy demand: electrical, heating, and cooling loads. The conventional energy supply meets the cooling demand using electricity, while the proposed system uses an absorption chiller to convert waste heat into cooling. Hence, we cannot just add three loads together and use a per kWh based functional unit. We assumed that the service life of the proposed distributed energy

generation was 20 years. For system components (e.g., battery) that have not enough lifetime will be replaced during the service.

System Boundary

As shown in Figure 2.2, our cradle-to-grave LCA for the proposed system mainly includes three stages: (1) hardware manufacturing, (2) operation & maintenance (O & M), and (3) end-of-life treatment. We excluded components related to building electrical interconnections, construction, and operations because these would be similar for the centralized and decentralized systems. We used process-based LCA for most of the stage processes. The economic input-output-based (EIO) methods [64] was only for determining the impact during routine maintenance. The U.S. Life Cycle Inventory Database [65] process-based inventory data was used for on-site power generation and end of life treatment. For product manufacturing, pipeline natural gas, and end-of-life waste disposal, We used the inventory from the Ecoinvent 3 database in Simapro 8 [66].

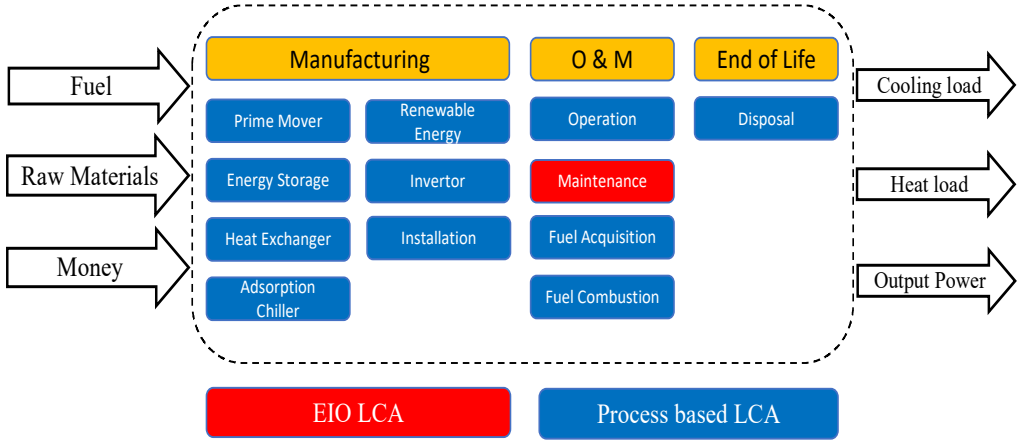

Figure 2.2. System boundary.

For EIO, a new and transparent the United States Environmentally Extended Input-Output Model (USEEIO) [67] was adopted. This model melds data on economic transactions between 389 industry sectors with environmental data for these sectors covering water, energy and mineral usage, emissions of greenhouse gases, criteria air pollutants, nutrients, and toxics, to build a life cycle model of 385 US goods and services.

For conventional energy generation, the United States uses different types of energy sources. By and large, fossil fuels have dominated the energy mix. The energy-related emissions can also vary due to the different energy mixes of each state. The grid emissions data were obtained from the Emissions and Generation Resource Integrated Database (eGRID) [68]. We calculated state-level emission information as the inventory of conventional electricity supply. Since the losses from transmission and distribution infrastructures are not considered by eGRID, we assumed a 7% transmission loss. The emission inventory of different states (involved in this study) for conventional energy is presented in Appendix A. We also evaluated the process-based impact for power plant construction and decommissioning via Simapro 8.

Life Cycle Impact Inventory

The life cycle emissions inventory includes greenhouse gases (GHGs – CO_2, N_2O, and CH_4), carbon monoxide (CO), ammonia (NH_3), nitrogen oxides (NO_X), particulate matter ($PM_{2.5}$ and PM_{10}), sulfur dioxide (SO_2), and volatile organic compounds (VOCs). We assessed their midpoint life cycle environmental impacts – climate change, acidification, eutrophication, ecotoxicity, ozone depletion, and fossil fuel depletion based on TRACI 2.1 [69]. The detailed input inventory for CCHP-RE-ESS system components

manufacturing (microturbine, solar PVs, lithium-ion batteries, adsorption chillers, etc.) is provided in Appendix A. The life cycle water consumption was presented in gallons of fresh water used. We normalized the environmental impact to a percentage by dividing the impact by the average impact of a US resident. For the US, total and per-capita year normalization factors have been published for use in the TRACI 2.1 LCIA model [70], as shown in Table 2.1. The normalized mid-point impact results are multiplied by the weighting factors to generate a single overall score. We used the long-term environmental impact importance weights developed by the Analytic Hierarchy Process (AHP) technique at the panel event [71]. The weighting factors are tabulated in Table 2.2.

Table 2.1. Normalization factors for the US, 2008.

Impact category	Annual (impact per year)	Per-capita (impact per person-year)
Ecotoxicity-non-metals (CTUe)	2.3E+10	7.6E+01
Ecotoxicity-metals (CTUe)	3.3E+12	1.1E+04
Global warming (kg CO_2 eq)	7.4E+12	2.4E+04
Ozone depletion (kg CFC-11 eq)	4.9E+07	1.6E-01
Acidification (kg SO_2 eq)	2.8E+10	9.1E+01
Eutrophication (kg N eq)	6.6E+09	2.2E+01
Fossil fuel depletion (MJ surplus)	5.3E+12	1.7E+04

Table 2.2. Environmental impact importance.

Long-term time horizon (%)				
Impact category	all	producer	user	LCA expert
Global warming	52	30	57	68
Fossil fuel depletion	4	10	1	5
Criteria air pollutants	1	2	0	1
Water intake	8	8	9	6
cancerous	9	9	6	7
Ecological toxicity	9	9	13	5
eutrophication	3	4	2	2
Land use	5	6	6	3
noncancerous	6	17	2	2
Smog formation	0	1	0	1
Indoor air quality	0	0	0	0
acidification	2	2	2	1
Ozone depletion	2	3	1	1
inconsistency	0.06	0.11	0.08	0.13

2.2.3 The life Cycle Cost

We broke all the costs of the proposed system into two main categories: fixed costs and variable costs. Fixed costs are costs that are independent of output, while variable costs are costs that vary with the amount of energy required. For the CCHP-RE-ESS, fixed costs include purchase for prime mover, renewable energy, energy storage device, heat recovery unit, absorption chiller, other auxiliary system components, and installation service [72]. Fixed cost of conventional energy supply consisting of the construction of power generation and transmission infrastructures and is assumed to be included in the electricity and heating service fees.

Variable costs of the proposed system include purchase for fuel, operation and maintenance service. Variable costs of the conventional energy system include purchases for electricity and heating. The cost inventory is shown in Table 2.3. All monetary values are in constant 2019 dollars in net present value over 20 years of system lifetime, at a 7% discount rate. Equation 2.1 and Equation 2.2 shows the average annual LCC for conventional and proposed system respectively.

$$\boldsymbol{LCC_{conventional}}\left(\frac{\$}{\boldsymbol{ft^2}}\right) = \sum \frac{\boldsymbol{C_{electricity,i} + C_{fuel}}}{\boldsymbol{(1+r)^i * 20}} \qquad \textbf{Equation 2.1}$$

$$\boldsymbol{LCC_{CCHP-RE-ESS}}\left(\frac{\$}{\boldsymbol{ft^2}}\right) = \sum \frac{\boldsymbol{C_{system} + \sum \frac{C_{fuel}}{(1+r)^i}}}{\boldsymbol{20}} \qquad \textbf{Equation 2.2}$$

Where i stands for i-th year, C is the cost in dollars, r is the discount rate.

Table 2.3. Cost inventories for microturbine, solar PVs, and Li-ion battery.

	Cost Category	Cost
CCHP-RE-ESS		
·Turbine	**fixed**	**$700-1100/kW**
·Solar Panels	**fixed**	**$2.67-$3.43/W**
·Tesla Powerpack	**fixed**	**$400-500/kWh**
·Heat Recovery Unit	**fixed**	**$75-350/kW**
·Absorption Chiller	**fixed**	**$820-$2010/ton**
·Inverter	**fixed**	
·O&M Absorption Chiller	**variable**	**0.1-0.6/ton-hr**
·Natural gas	**variable**	**Depend on states $6.6-$44 per ft^3**
·O&M (CCHP)	**variable**	**$0.003-$0.004/kWh**
·O&M (PVs)	**variable**	**$10-$20 per panel**
Conventional Energy Generation		
·Electricity	**variable**	**Depend in states 8-36 cents per kWh**
·Heating (natural gas)	**variable**	**Depend on state $6.6-$44 per ft^3**

2.2.4 The Operation Strategy and Sizing

The microturbine was designed to be a "follow the thermal load (FTL)" model since previous research studies show that systems of this type have lower emissions than following the electrical load of the building [7,73]. To be more specific, microturbine generates more heat than electricity, and "follow the electric load (FEL)" will produce more heat than what can be used by the building. For the system that used only CCHP and FEL, extra electricity comes from the grid. The integration of renewable energy and energy storage can help increase off-grid electricity generation.

Hence, the selection of microturbine size is based on the maximum hourly thermal energy required by the building. The absorption chiller for each building was sized to satisfy the cooling requirement of the building. Sizes of energy storage and solar energy

can vary, we plotted the Pareto front to find the optimal size combinations. The maximum energy storage capacity is limited by maximum daily electricity demand, and the maximum usable roofing area for solar PV is assumed to be 80 percent of the total roof area. We choose a tandem configuration for all components, especially microturbine because it cannot be turned off completely.

2.2.5 Dispatch Strategy

The electricity control dispatch strategy for the CCHP-RE-ESS is shown in Figure 2.3. This is the priority for electricity dispatch: first is the prime mover, second is renewable energy, third is energy storage, and the grid in order. If the electricity demand is fulfilled, the remaining energy is stored in the energy storage device if it is not fully charged. The energy stored in the battery will be used during times when there is insufficient electricity generated from the prime mover and renewable energy to match the electrical demand. Due to electrical current and voltage constraints, the battery can only be charged by solar panels. If the battery is fully charged, extra electricity produced is assumed to be wasted. We did not consider net metering in this research since some states in the U.S. did not build related infrastructure and had sustainable energy generation rules other than net metering.

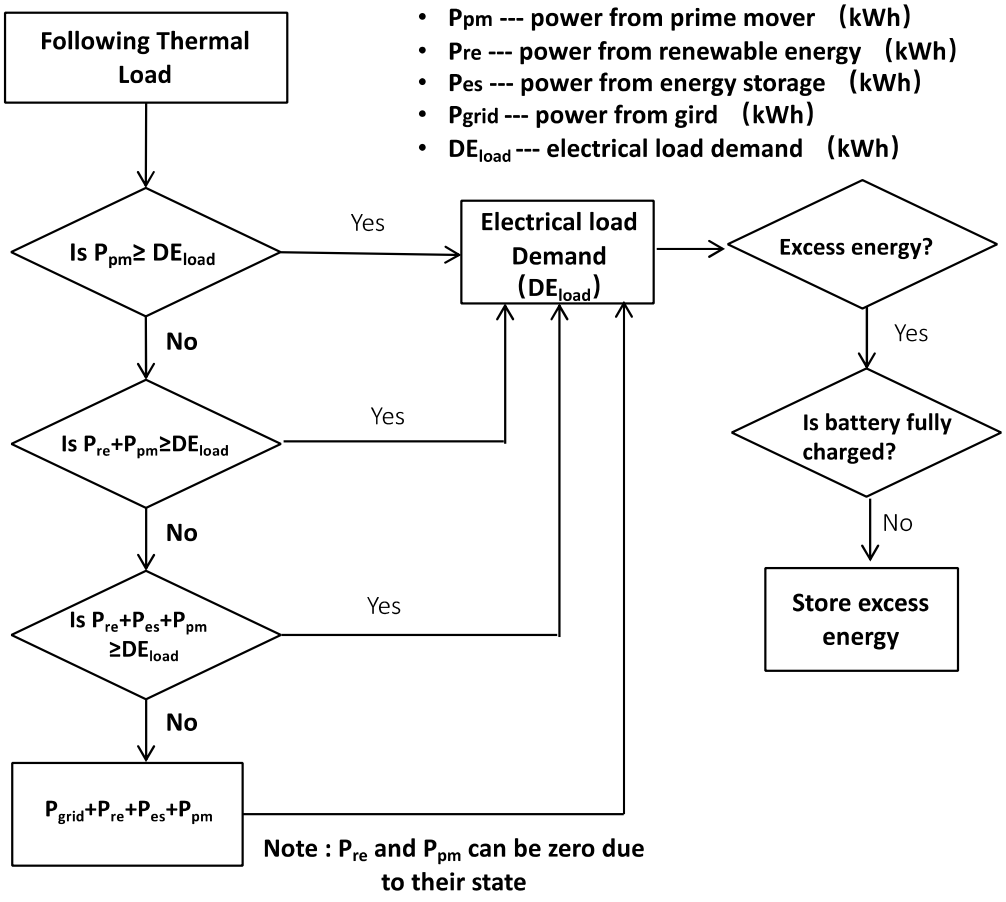

Figure 2.3. The dispatch strategy.

2.2.6 Building Energy Demand Simulation

We used EnergyPlus [74,75] to model the building energy consumption for heating, cooling, plug loads. According to the National Renewable Energy Laboratory and U.S. DOE, 16 building types represent approximately 70% of the commercial buildings in the U.S. [76,77]. In this research, we simulated three building types (large, medium and small) and their characteristics shown in Table 2.4 were modeled into the commercial reference benchmark models developed by DOE. We also incorporated the commercial reference

benchmark models and TMY3 weather file [78] to the EnergyPlus simulation software to provide energy demand for buildings at different climate zones. Table 2.5 shows 16 climate zones and the corresponding cities in U.S.

Table 2.4. Characteristics of some commercial reference buildings.

Building	Floor Area	Floors	Heating Equipment	Cooling
Large office	46320	12	Gas boiler	2 water-cooled
Medium	4982	3	Gas furnace and	PACU
Small office	511	1	Gas furnace	Unitary DX

Table 2.5. TMY3 climate zones.

Climate	Representative City	Climate	Representative City
1A	Miami, Florida	4B	Albuquerque, New
2A	Houston, Texas	4C	Seattle, Washington
2B	Phoenix, Arizona	5A	Chicago, Illinois
3A	Atlanta, Georgia	5B	Boulder, Colorado
3B-Coast	Los Angeles, California	6A	Minneapolis, Minnesota
3B	Las Vegas, Nevada	6B	Helena, Montana
3C	San Francisco,	7	Duluth, Minnesota
4A	Baltimore, Maryland	8	Fairbanks, Alaska

The energy demand simulation provides hourly-based energy demand data in terms of electricity for appliances and natural gas for heating. Equation 2.3 and Equation 2.4 calculate the conventional electrical and thermal energy demand for buildings. Facilities powered by electricity include air conditioning systems, fans, pumps, lights, and other plug loads. The thermal demand for space heating and hot water is met by gas furnace fueled by natural gas. Some types of buildings (e.g. medium office) use electricity to meet part of its heating demand.

$$E_{Conventional} = E_{Plug\ loads} + E_{Air\ Conditioning} \quad \textbf{Equation 2.3}$$

$$Th_{Conventional} = Th_{Heating} + Th_{Hot\ Water} \quad \textbf{Equation 2.4}$$

Where E stands for electrical energy (kWh), Th stands for thermal energy (kWh).

Equation 2.5 and Equation 2.6 determine the energy generation when buildings use the CCHP-RE-ESS. In this case, the air conditioning system is substituted by the absorption chiller that can convert heat into cooling power. The amount of heat needed by the absorption chiller is determined using the ratio of the coefficient of performance (COP) of the air conditioner and absorption chiller. The COP of the air conditioning units was assumed to be 3.8, and the COP of a double effect absorption chiller used is 1.42 [79]. The energy demand profiles for all building types and locations are shown in Appendix B.

$$E_{CCHP-RE-ESS} = E_{Plug\ loads} \quad \textbf{Equation 2.5}$$

$$\mathbf{Th_{CCHP-RE-ESS} = Th_{heating} + Th_{Hot\ Water} + \frac{COP_{Air\ Conditioner}}{COP_{Adsorption\ Chiller}}} \quad \textbf{Equation 2.6}$$

2.2.7 Parametric Models of the CCHP-RE-ESS

To account for nonlinear and varying performances of different components of the proposed CCHP-RE-ESS system, we developed submodule for three categories of commercially available technologies into the proposed energy generation system: (1) a microturbine for prime mover; (2) lithium-ion batteries for energy storage and (3) solar PVs for renewable energy.

2.2.7.1 Microturbine

Microturbines are small combustion turbines with outputs of 25 kW to 500 kW. This technology is comprised of a compressor, combustor, turbine, alternator, recuperator, and generator. Compared to other heat engine technologies for distributed energy generation, microturbines have several advantages include a compact size, less weight, greater efficiency, lower emissions, and fuel diversity. Hence, as a combustion-based technology, we choose microturbine for the prime mover of the CCHP-RE-ESS.

The Capstone air-cooled microturbines (Van Nuys, Los Angeles) were commercially available and were chosen for this study as they use air-cooling rather than water-cooling. The air-bearing design provides maintenance and fluid-free operation for the lifetime of the turbine. It also avoids the external cooling system for the turbine. The performance of the microturbine depends on factors such as ambient temperature, altitude, power output ratio. According to a manufacturer's data [80], a higher power output ratio results in higher efficiency and lower emissions. We used multiple non-linear regression to develop a model that can predict fuel consumption and emission for a C200 microturbine-based on manufacture data. Equation 2.7 shows the parametric regression equation for the microturbine. Equation 2.8 shows the objective function of the regression. Due to the lack of pressure data, the equation only estimates the fuel consumption based on ambient temperature and power output ratio under a standard atmosphere. The parameter value and objective function are shown in Table 2.6.

$$\mathbf{E} = \boldsymbol{\beta_1}^{(\mathbf{1}-\boldsymbol{PL})} * \boldsymbol{\beta_2} * \boldsymbol{T} \qquad \textbf{Equation 2.7}$$

$$\textbf{objective function} = \sqrt{\frac{1}{n-1}\sum[\frac{C_{data}-C_{sim}}{C_{sim}}]^2} \qquad \textbf{Equation 2.8}$$

Where E is fuel consumption (MJ), β is the regression coefficient, T is ambient temperature(K), PL is part-load ratio or power output ratio (%). Where n is the number of data points, and $C_{data}\ and\ C_{cal}$ (kg) are manufacture data and simulation data.

Table 2.6. Microturbine parametric model prediction.

Sizes	β_1	β_2	Objective function
200 kW turbine	**0.2202**	**7.5751**	**0.12**

2.2.7.2 Solar PVs

Solar energy is the cleanest and most abundant renewable energy source available everywhere. The Earth receives 174 petawatts (PW) of solar energy in the upper atmosphere. Approximately 22.5% of the radiation is going directly to Earth's surface while others are reflected, absorbed or scattered by the clouds. The annual total amount of solar energy reaching the surface of the Earth would be twice the amount of all non-renewable resource consumption.

Many factors (e.g., latitude, diurnal variation, climate, and geographic variation) are largely responsible for determining the effective solar radiation harvested by solar PVs. For the solar energy submodule, we incorporated a more accurate and technical rigorous PV performance model that was developed by Sandia National Laboratories [81]. The model includes 5 components: (1) weather and system design, (2) singe module DC output, (3) array DC output, (4) DC to AC conversion and (5) AC output. The final power generation and losses depend on parameters such as temperature, location, array orientation, time,

weather, etc. We used a fixed-tilt orientation for a solar array. The PV system was designed using polycrystalline silicon PV cells mounted at a 30-degree angle towards the south and a peak power factor of 0.2 kW/m^2. The detailed mathematical equation for the solar power model is shown in Appendix A. The unit size is 1.68m^2 per panel. According to the NABCEP PV resource guide [82], we assumed 80% of the roof area that has a suitable orientation can be used for mounting modules when room for maintenance, wiring paths, firefighter access [83] and aesthetic considerations are considered. The average power output for each square meter of the usable roof area is 0.2 kW [82]. We calculated the minimum required distance between PV arrays using a separation factor of 2 from the NABCEP PV resource guide [82]. The maximum useable roofing area for the PV is assumed to be 80% of the total roof area. The annual solar power generations for different climate zones are shown in Figure 2.4.

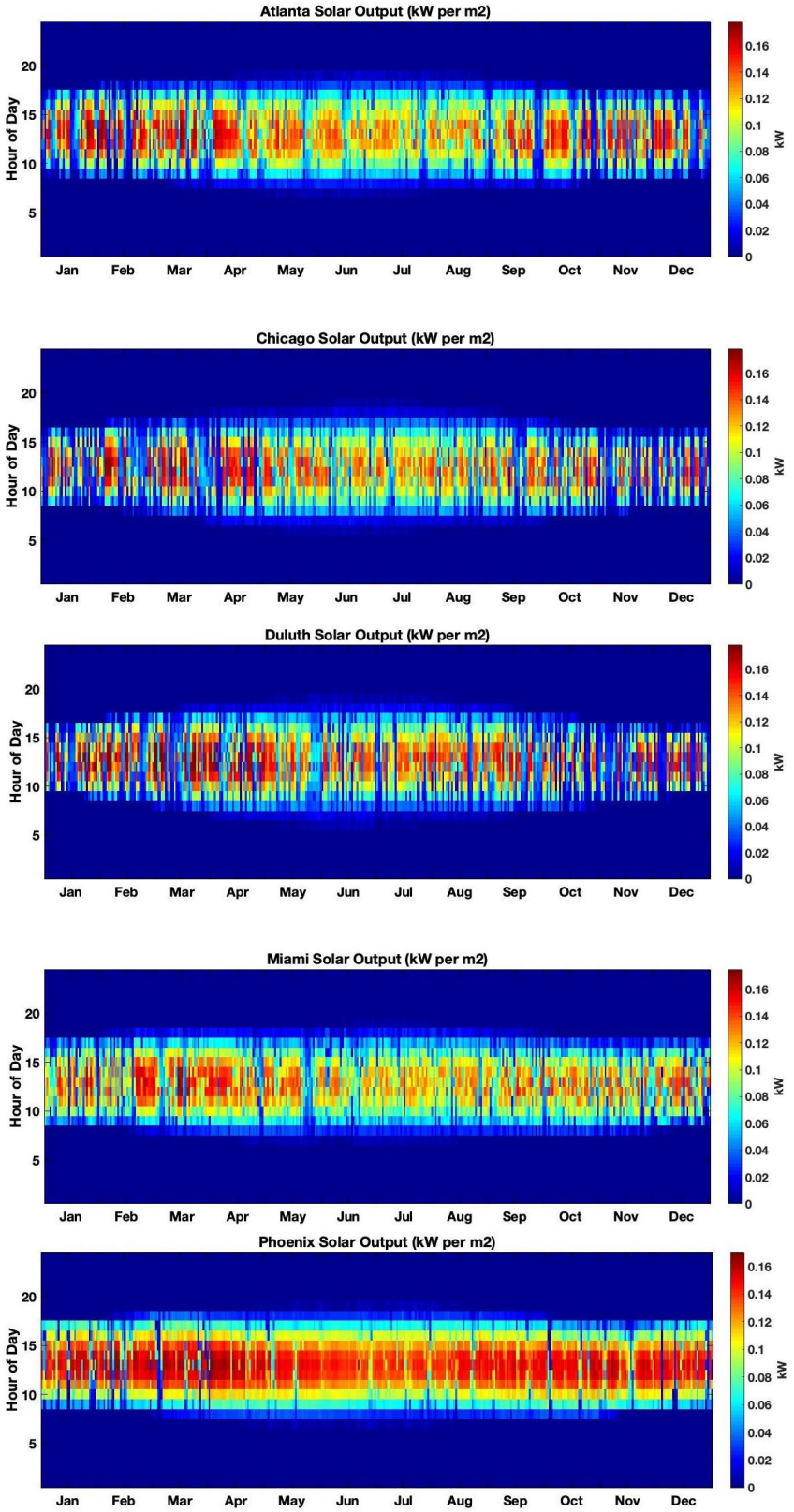

Figure 2.4. Annual solar PVs power simulation for five climate zones cities.

2.2.7.3 Lithium-ion Battery

For distributed energy generation adopting renewable energy, the primary challenge is variable or intermittent nature of renewable. The energy storage system (ESS) can capture energy produced at one time for use at a later time. For energy storage systems (ESS), the Li-ion batteries have been deployed in a wide range of energy-storage applications, ranging from a few kilowatt-hours in residential systems with rooftop photovoltaic arrays to multi-megawatt batteries for the provision of grid-level storage.

We choose Tesla Powerpack as the energy storage for the CCHP-RE-ESS and incorporated it into the parametric framework. The energy capacity for each power pack is 210 kWh (AC) with round-trip efficiency 90% [83]. The maximum power output is 50kW per power pack. One of the major lithium-ion battery disadvantages for consumer electronics is the aging of lithium-ion batteries in which the power storage and round-trip efficiency are reduced. This depends on the charging and discharging operation and the number of charge-discharge cycles that the battery has undergone. The battery in the proposed system is charged and discharged once per day. According to Tesla Powerwall 2 (2170 cell) warranty, there is a 70% capacity after 10 years [84]. We assumed EES technologies are replaced entirely every ten years and the battery performance deteriorates linearly for 10 years.

2.2.8 Economic and Environmental Trade-offs

The multi-disciplinary design optimization is performed to find the optimal sizes for solar PVs and batteries utilizing different environmental impact and economical cost. This optimization problem is a non-trivial multi-objective problem which means there exists a number of Pareto optimal solutions rather than a single one. To visualize the

problem, we used life cycle single score indicators, which can include several normalized and weighted impact categories and convert the optimization problem to a bi-objective problem. Every point on the tradeoff curve represents a situation of energy generation using different sizes of solar PVs and batteries. For each point, there are two objective functions: the environmental life cycle single score and the life cycle cost per functional unit. The Pareto font can be drawn on the objective plane. The meaning of the Pareto front is that elements that are not on the front are never the best choice because there is some element on the front which is better. Moreover, designs that are on the front are the best choices. By considering all of the potential solutions, we can focus on tradeoffs between LCC and LCA. In this research, we gave the environmental impact the highest priority.

2.2.9 Variability and Uncertainty

Unlike traditional life cycle assessment (LCA), our parametric LCA framework considers the environmental impact and economic cost based on the hourly variability of the energy dispatch and not on just a single average value for the year. It can explain how and why the result varies with system conditions (operation strategy) and external factors (ambient temperature, pressure, weather). The environmental and economic impacts depend on energy generation and demand that vary with numerous factors (e.g. weather, building type, sizes, etc.). In addition, the input data can have uncertainty. The single value of each input, such as product price, maintenance cost, emissions were determined from the literature or manufacturer's guide. A sensitivity analysis was conducted to understand the impacts of variations in key parameters including turbine emission, and prices for EIO-LCA.

For the conventional energy system, we also considered the variation in the energy mix and its influence on the impact reduction of the proposed system. For example, the current energy mix of Arizona is composed of natural gas (42.5%), coal (16.0%), nuclear (26.9%), hydro (6.0%), other renewables (7.8%) , whereas the energy mix of Georgia is composed of coal (67%), nuclear (21%), natural gas (10%), and hydro (2%) [85]. The difference in the energy mix (emissions) results in a difference in baseline condition when we compared the impact of the proposed system with conventional energy supply.

2.3 Results and Discussion

By using our parametric framework, we simulated the energy generation and supply of three commercial buildings at five major climate zones for the distributed CCHP-RE-ESS. The three commercial building types are small, medium and large office buildings. Five climate zones chosen are Atlanta Chicago, Duluth, Miami, and Phoenix in which most other cities' climate in the U.S. will look like these cities. The CCHP-RE-ESS energy generation technologies and components include Capstone microturbines, a heat recovery unit, an adsorption chiller, solar panels, and Tesla Powerpacks.

2.3.1 Environmental Life Cycle Impact and Economic Life Cycle Cost

By using our parametric framework, we simulated the energy generation and supply of a medium office in Atlanta for the proposed system. The global warming impact and water consumption of a medium office in Atlanta with different sizes of solar and energy storage are shown in Figure 2.5. Other impact categories, including acidification, eutrophication, ecotoxicity, ozone depletion, and fossil fuel depletion, are shown in Figure 2.6. As shown in Figure 2.5, compared to conventional energy generation in Atlanta, Georgia (32 kg CO_2 eq per ft^2 and 2.59-gal water per ft^2), the proposed distributed energy generation system can further decrease the global warming impact by 21-46%, the water consumption by 70%-98%. The proposed system also reduces the acidification and fossil fuel depletion impact by 52-93% and 67-91%, respectively. On the other hand, the ozone depletion, ecotoxicity, and eutrophication impact are higher than conventional energy supply. The ecotoxicity and eutrophication impact increases with solar and battery sizes since the impacts are generated during the product manufacturing stages.

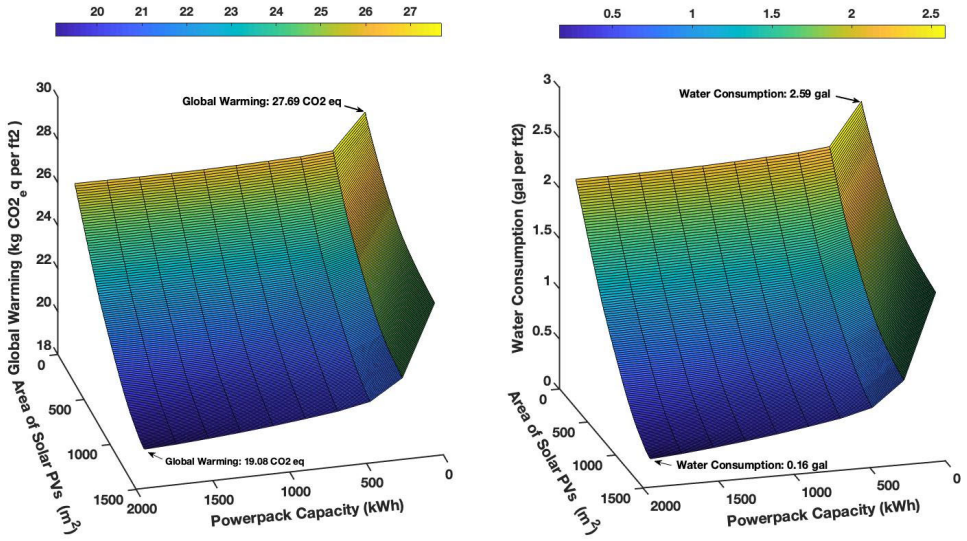

Figure 2.5. The global warming impact and water consumption.
The global warming impact and water consumption of the CCHP-RE-ESS system for a medium office in Atlanta. (For conventional energy, the global warming impact is 35 CO_2 eq per ft^2 and water consumption is 8.7 gal per ft^2.)

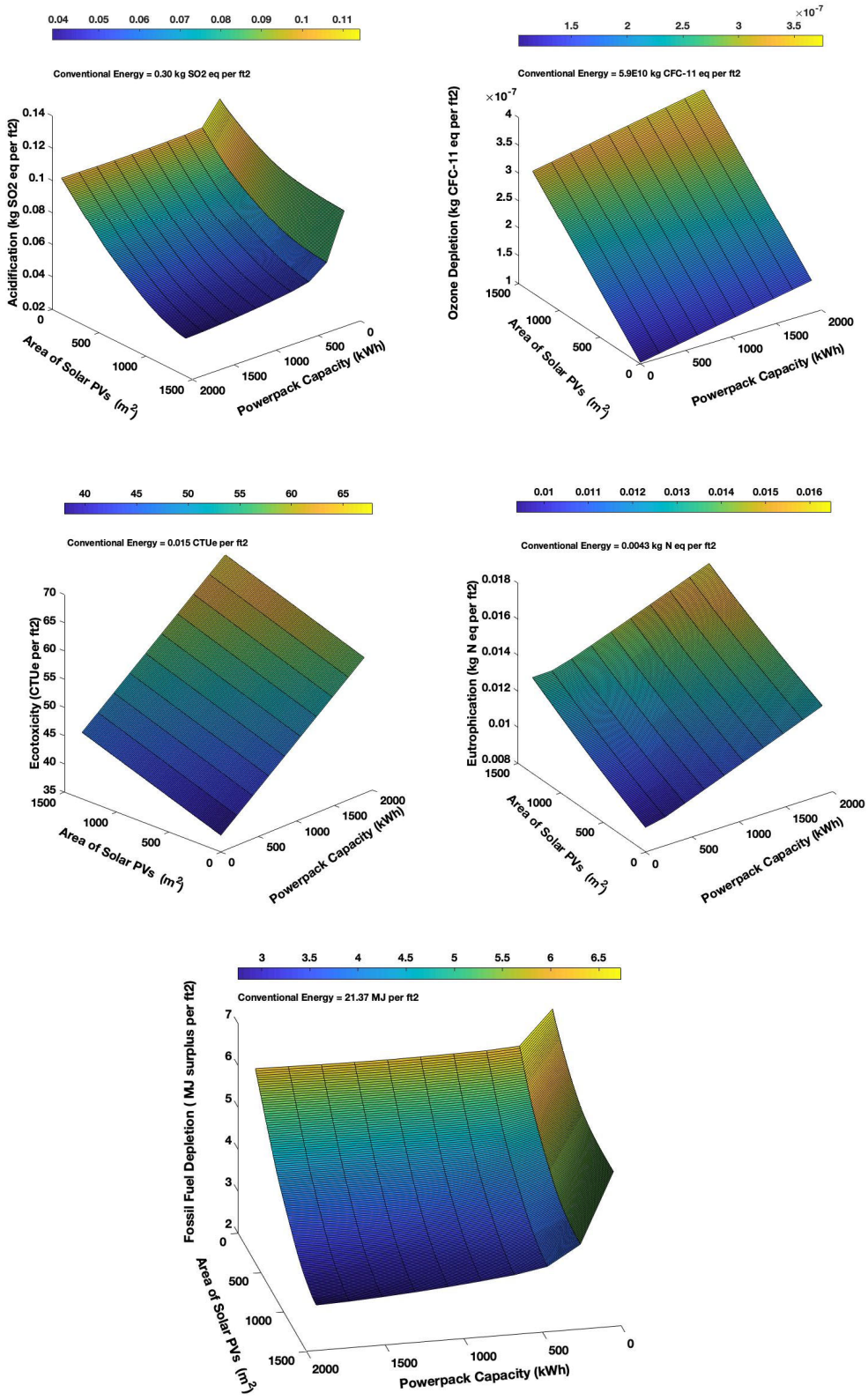

Figure 2.6. Environmental life cycle impact for a medium office in Atlanta.

The life cycle cost per functional unit is shown in Figure 2.7, the annual average price (electricity, heating, and cooling) for conventional energy supply is about 2.58 dollars per square feet as compared to $8 to $13 for the proposed system. The life cycle cost depends on how many solar panels and battery installed. Unlike most turbines for CCHP in the market, the maintenance cost of Capstone microturbine is just about 0.003 per kWh because of their air bearing technology. The higher marginal cost is useful for policymakers and other stakeholders to implement policy incentives. Admittedly, net metering can help to reduce the cost. However, in this case, selling energy back to the grid is not considered since Georgia Power did not offer a net energy metering tariff currently. Besides, the cost of the conventional energy system also varies with geospatial conditions.

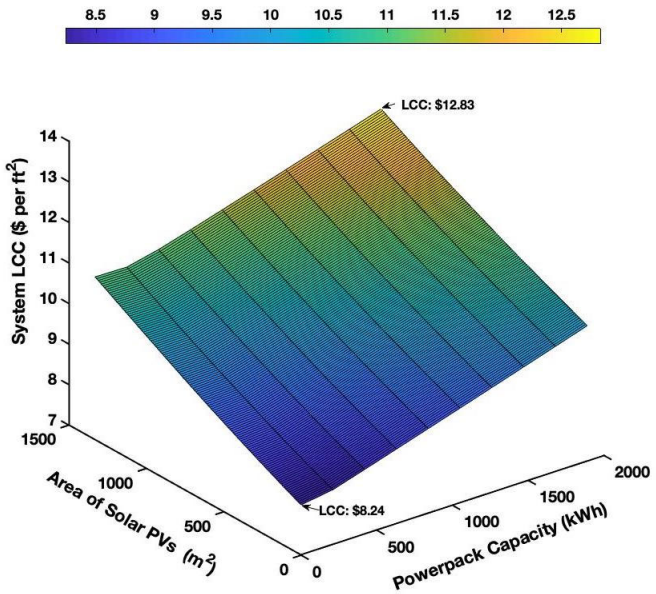

Figure 2.7. Life cycle cost of the proposed system for a medium office in Atlanta.

2.3.2 Economic and Environmental Trade-offs

As discussed, impacts and costs vary with PVs and batteries sizes. We created a Pareto front to find the optimal systems for hundreds of scenarios (building types and locations). The resulting Pareto front provides an approximation of all efficient solutions which can then be selected for detailed analyses. The Pareto front for Atlanta medium office is shown in Figure 2.8. The single score impact first reduces as the cost increases. After reaching its minimum, it starts to increase again which means the renewable system benefits have reached its maximum and increasing sizes will cause more impact because of the impacts of manufacturing. We choose the minimum environmental impact as our optimal solution. The corresponding sizes are 1300 m^2 of solar panels, 420 kWh battery or two battery packs. The optimal sizes for other system components for different building types and locations are shown in Table 2.7.

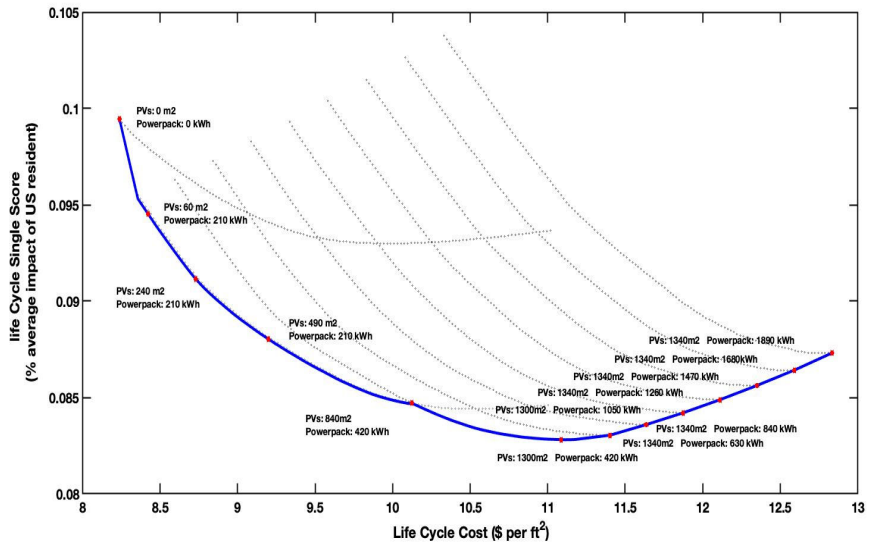

Figure 2.8. The Pareto front for different system sizes.

Table 2.7. Sizes of system components under the optimal case.

Location	Building	#of microturbine	#of Solar panels	Size of battery
Atlanta	Large Office	20×200kw	2946m^2	8×210kwh
Atlanta	Medium Office	2×200kw	910m^2	2×210kwh
Atlanta	Small Office	1×30kw	95m^2	1×210kwh
Chicago	Medium Office	2×200kw	933m^2	2×210kwh
Duluth	Medium Office	2×200kw	1147m^2	2×210kwh
Miami	Medium Office	2×200kw	293m^2	2×210kwh
Phoenix	Medium Office	3×200kw	935m^2	2×210kwh

2.3.3 Power Generation

Figure 2.9a shows the optimal scenario 14 days' power generation and energy demand of (from Wednesday, April 25th to Tuesday, May 8th) the proposed system for Atlanta medium office building. Figure 2.9 b shows the annual power generation from the grid with and without the CCHP-RE-ESS. The energy demand and corresponding generation of weekends are much lower than weekdays (Figure 2.9 a) since the studied building is an office that has less activity on the weekend. The battery system is charged during the day and discharges at night and before dawn. As shown in both Figure 2.9 a and b, at the end of April, the building requires a few electricity from the grid, and after April 27th, the building can be completely off-grid until early September according to the simulation result. This is because, in summer, the thermal demand is high (heating and cooling), by following thermal load, the electricity from microturbine is enough for daytime demand, and power from PV fully charge the battery. In total, the system can meet more than 90% of electricity demand for the building (turbine: 58%, solar and storage: 34%, and grid: 8%). Detailed electricity supply proportions of CCHP-RE-ESS system components for studied building types and locations are reported in Table 2.8.

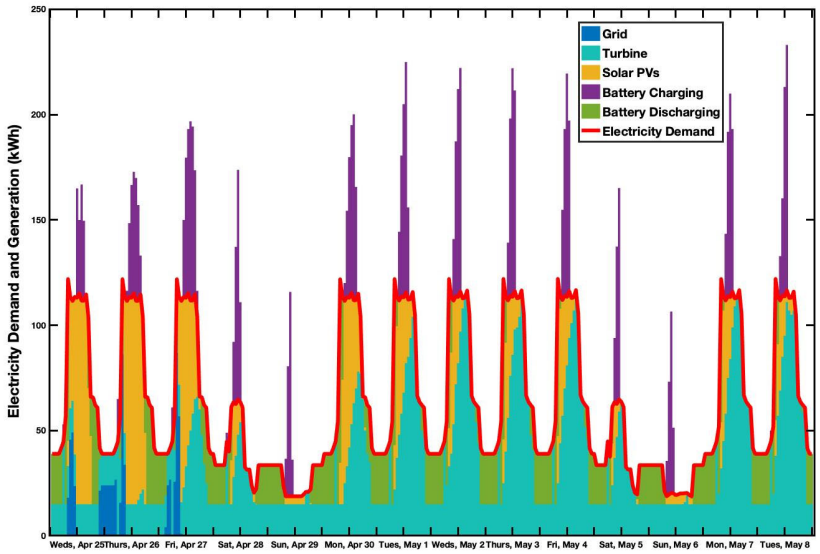

(a)

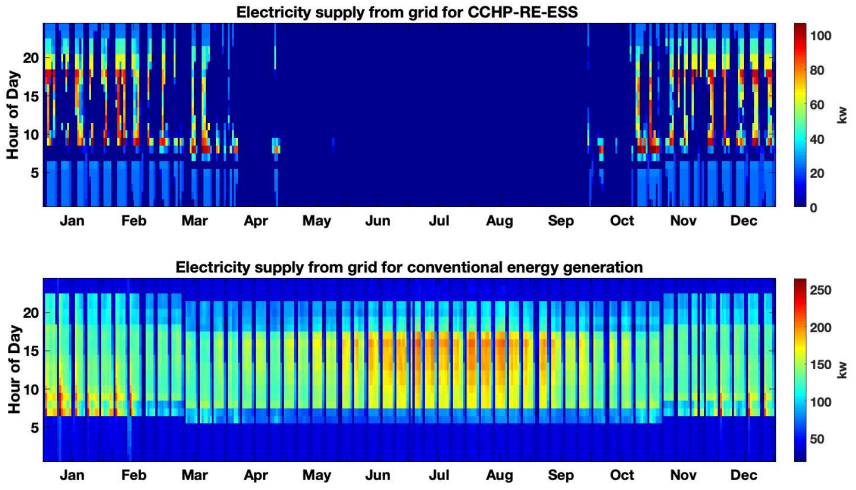

(b)

Figure 2.9. Electrical power generation for a medium office in Atlanta:
(a) 14 days (Wednesday, April 25th to Tuesday, May 8th) electrical power generation of the CCHP-RE-ESS system. (b) Annual electricity from gird (conventional energy generation and CCHP-RE-ESS scenarios).

Table 2.8. Electricity supply proportion for the CCHP-RE-ESS.

	Grid (%)	Turbine (%)	PVs and Storage (%)
Atlanta small office	**4.76**	**37.24**	**58**
Atlanta medium office	**7.73**	**57.83**	**34.44**
Atlanta large office	**5.22**	**75.84**	**18.94**
Chicago medium office	**13.52**	**49.13**	**37.35**
Duluth medium office	**6.09**	**45.06**	**48.85**
Miami medium office	**4.19**	**81.84**	**13.97**
Phoenix medium office	**5.53**	**66.80**	**27.67**

2.3.4 Building Types and Location

The optimal U.S. annual per capita environmental LCA single scores and LCC of the proposed system and local conventional energy generation are shown in Figure 2.10 and Figure 2.11. Figure 2.10 shows LCA single scores and LCC of a medium office in different weather zones. The single scores of CCHP-RE-ESS for medium offices are lower than the local conventional energy supply impact score except for Phoenix. There are not very much different for the single scores and cost of the proposed system for the medium office at Atlanta, Chicago, Duluth, and Miami. Phoenix medium office has the highest environmental single score and life cycle cost. According to Figure 2.11, for different building types in Atlanta, the large office has the lowest cost and the small office has the lowest single score. Compared to the single score of conventional energy generation, the medium office has the largest benefit by adopting CCHP-RE-ESS (30% reduction in overall impact).

On the other hand, the single score of CCHP-RE-ESS for the large office is nearly the same as the score of conventional energy generation. From these results, the majority

of the resulting impact and cost for our decentralized system is due to natural gas emissions from the turbine. We also conduct a sensitivity analysis of natural gas consumption and emission. According to the range shown in Figure 2.10 and Figure 2.11, the final impact can vary by about 20%. For each scenario, the specific environmental impacts under optimal situations are reported in Table 2.9. The environmental impacts for conventional energy generation in different states in Table 2.10.

Besides, the life cycle cost of CCHP-RE-ESS for the medium office in all cities is at least two times higher than conventional energy generation. The majority of the cost is due to the high capital cost of system components (from 50%-70%). Detailed cost proportions (investment, grid electricity, fuel, and maintenance cost) for LCC are reported in Table 2.11.

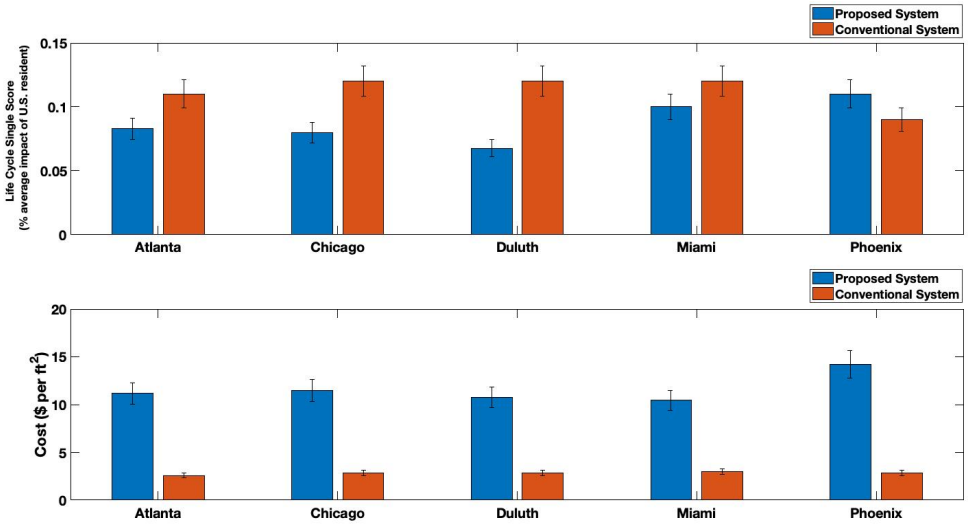

Figure 2.10. Comparison of the medium office buildings for different locations.

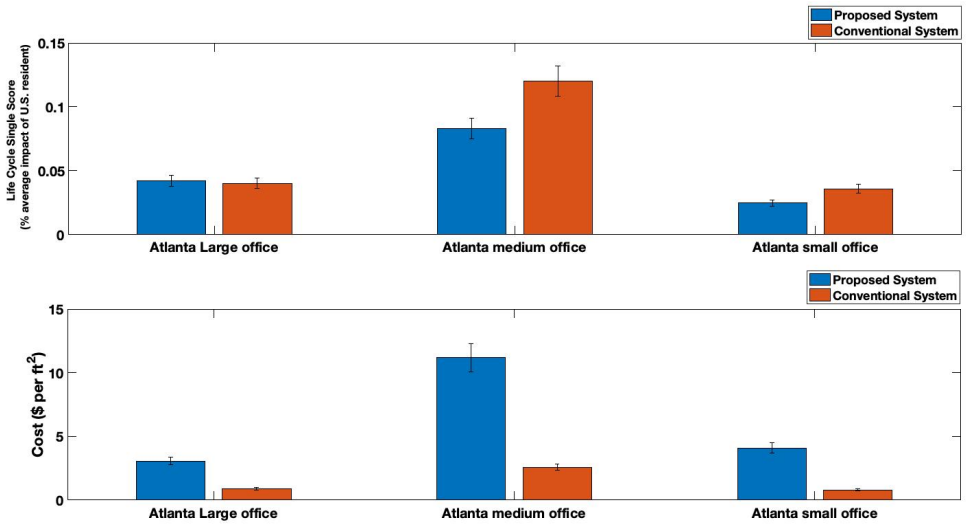

Figure 2.11. Comparison of different building types in Atlanta.

Table 2.9. The environmental life cycle impacts of the CCHP-RE-ESS.

	Global Warming (kg CO^2 eq)	Acidification (kg SO^2 eq)	Ozone Depletion (kg CFC-11 eq)	Ecotoxicity (CTUe)	Eutrophication (kg N eq)	Water (gal)	Fuel Depletion (MJ)
Atlanta small office	4.94	1.60e-3	1.27e-07	21.47	5.66e-3	0.105	1.09
Atlanta medium office	20.12	4.68e-2	3.32e-07	51.44	1.37e-2	0.474	3.22
Atlanta large office	12.76	1.74e-2	6.80e-08	13.86	3.48e-3	0.111	1.03
Chicago medium office	18.35	5.88e-2	3.33e-07	55.53	1.44e-2	0.829	2.94
Duluth medium office	15.33	5.11e-2	3.16e-07	48.15	1.28e-2	0.744	2.70
Miami medium office	30.60	4.40e-2	1.95e-07	46.11	1.13e-2	0.216	3.44
Phoenix medium office	28.40	4.82e-2	3.42e-07	50.38	1.69e-2	0.344	4.24

Table 2.10. The environmental life cycle impact of conventional energy.

	Global Warming (kg CO^2 eq)	Acidification (kg SO^2 eq)	Ozone Depletion (kg CFC-11 eq)	Ecotoxicity (CTUe)	Eutrophication (kg N eq)	Water (gal)	Fuel Depletion (MJ)
Atlanta small office	10.83	0.09	1.80e-10	4.5e-3	0.0014	2.7	10.58
Atlanta medium office	34.73	0.30	5.90e-10	0.02	0.0043	8.7	21.37
Atlanta large office	12.00	0.11	2.01e-10	5.1e-3	0.0015	9.3	9.26
Chicago medium office	39.61	0.34	7.40e-10	4.53	0.0050	9.1	23.04
Duluth medium office	37.07	0.33	7.40e-10	5.03	0.0047	9.4	36.03
Miami medium office	32.80	0.28	3.90e-10	28.67	0.0036	9.6	51.00
Phoenix medium office	23.85	0.21	2.33e-10	20.75	0.0024	9.7	41.40

Table 2.11. Cost proportion for the CCHP-RE-ESS.

Scenarios	Fuel (%)	Grid Electricity (%)	Capital Investment & Installation (%)	Maintenance (%)
Atlanta small office	23.97	1.23	70.28	4.52
Atlanta medium office	22.34	2.06	71.68	3.92
Atlanta large office	40.93	1.58	52.44	5.05
Chicago medium office	20.48	3.72	72.12	3.68
Duluth medium office	15.81	3.38	77.05	3.76
Miami medium office	45.36	1.16	50.01	3.47
Phoenix medium office	1.17	25.81	69.50	3.52

CHAPTER 3. THE OPTIMAL COMBINATION OF TECHNOLOGIES AND CORRESPONDING SIZE FOR THE CCHP-RE-ESS

3.1 Chapter Summary

This chapter aims to determine the best combination of technologies and their corresponding sizes for the distributed CCHP-RE-ESS system for various building types and climate zones. We added more technology submodules to the parametric LCA framework, such as solid oxide fuel cells, small wind turbines, and compressed air energy storage in this chapter. Combined with technologies discussed in the previous chapter (e.g., microturbine, solar PVs, Li-ion batteries, etc.), there are eight possible combinations of technologies for prime mover, renewable energy, and energy storage system of the CCHP-RE-ESS system. For each combination of technologies, there are millions of system components size combinations. The simulation shows that microturbine-solar PVs-lithium ion battery and fuel cells-solar PVs-lithium ion battery are two optimal combinations of technologies for all scenarios. For some situations (e.g., small and large offices in Miami), the optimal combination of technologies is only fuel cells integrated with solar PVs, and the energy storage system is not required. Overall, solar PVs and lithium-ion batteries are better than wind turbines and compressed-air energy storage according to the multi-disciplinary design optimization results. In terms of economic life cycle cost, the cost of the solid oxide fuel cell system is even higher than the microturbine system. The medium office is more benefited from the CCHP-RE-ESS system in terms of environmental life cycle impact. However, it has the highest average life cycle cost. The combination of

microturbine-solar PVs-lithium-ion battery is more cost-competitive and economical for the large office buildings and small office compared to conventional energy generation. Although technologies combination of fuel cells-wind turbine-battery is never selected, its sustainable performance is close to the optimal combination of technologies for Miami.

3.2 Methodology

3.2.1 The Wind Turbine

The wind is an important source of renewable energy. It is estimated that the global wind kinetic energy averaged approximately 1.5 MJ/m^2 over the period from 1979 to 2010. According to the U.S. Energy Information Administration (EIA), wind energy generation accounted for 6.5% of the nation's electricity supply in 2018. Until now, at least 83 countries are using the wind to power a portion of their electric power grids [86]. Different from solar energy, wind power can supply power 24/7, but it is also an intermittent energy source, which changes hourly, daily, and seasonally. However, annual variation is consistent from year to year. The wind speeds vary greatly across the United States and depend on water bodies, vegetation, and differences in terrain [87].

Total wind energy flowing through the imaginary surface with area A during the time t is shown in Equation 3.1 and power is shown in Equation 3.2. From equations, the wind power is thus proportional to wind speed to the power of 3.

$$\mathbf{E} = \frac{\mathbf{1}}{\mathbf{2}}\boldsymbol{mv^2} = \frac{\mathbf{1}}{\mathbf{2}}(\boldsymbol{Avtp}) = \frac{\mathbf{1}}{\mathbf{2}}\boldsymbol{t\rho v^3} \qquad \textbf{Equation 3.1}$$

$$\mathbf{P} = \frac{\boldsymbol{E}}{\boldsymbol{t}} = \frac{\mathbf{1}}{\mathbf{2}}\boldsymbol{A\rho v^3} \qquad \textbf{Equation 3.2}$$

Where m is the mass of air in kg; ρ is the density of air in kg/m^3; v is the wind speed in m/s; A is the swept area of blades in m^2; t is the time in seconds.

3.2.1.1 Wind Turbine and Categories

A wind turbine can convert the kinetic energy of wind into electricity. Wind turbines can fall into two basic groups: horizontal-axis and vertical-axis. The horizontal-

axis wind turbines have three blades. The vertical-axis turbines have a set of blades that spins around a vertical axis, which is omnidirectional and can run without orienting the turbines toward the wind direction. Although vertical designs can produce electricity for any wind direction and operate at lower wind speeds, they are much less efficient as compared to the horizontal axis because of the additional drag that is created when their blades rotate [88]. Hence, in this research, we choose the horizontal-axis wind turbines into the simulation framework. According to Betz's law, the maximal efficiency of the wind turbine is 59.3% of the kinetic energy of air. Further inefficiencies can come from gearbox losses, power generator and converter losses, etc.

3.2.1.2 Wind Speed Profile and Data Acquisition

According to Equation 3.2, wind power is proportional to the third power of the wind speed. The power from the wind turbine largely depends on wind speed. We used the TMY3 dataset produced by NREL's Electric Systems Center for wind speed [89]. This dataset contains hourly based wind speed data for 1020 locations in the U.S. The wind speed varies at a different height, but the TMY3 dataset only contains wind speed for a specific height. Hence, we used the Power Law (Equation 3.3) approach to extrapolates and estimate the wind speed to a certain height [90]. We assumed the wind speed is the same in overall the rotor area due to the small wind turbine diameter. In practice, it has been found that α varies with the terrain. The larger the exponent, the larger the vertical gradient in the wind speed. The wind shear exponent parameter for the urban area is 0.25 [91].

$$v_2 = v_1 \times \left(\frac{h_2}{h_1}\right)^{\alpha} \qquad \textbf{Equation 3.3}$$

Where v is the wind speed in m/s and h is the height in m, α is wind shear exponent

3.2.1.3 Wind Turbine Simulation

We choose a commercially available horizontal-axis wind turbine SD6 (SD Wind Energy, Ltd.) of parametric simulation. This turbine is qualified by the Small Wind Certification Council (SWCC), which provides independent, accredited certification of small wind turbines and consumer information. The detailed product summary report (including experimental data) is provided in Appendix B. The parameters are shown in Table 3.1 below. The mathematical formulation of the turbine is shown below (Equation 3.4, Equation 3.5, and Equation 3.6). The electricity produced by the wind turbine mainly depends on the power coefficient (C_p). The coefficient of power is the most important variable that varies with wind speed and different turbine types and blade design. We employed a third-order polynomial regression and developed a function for C_p.

Besides, the power efficiency of the wind turbine is also affected by generator and gear losses (N_{Loss}). N_{Loss} can be calculated from the manufacturer guide. We assumed a reference air density of 1.225 kg per cubic meter. The wind turbine is installed on the flat roof of the building with a height of 9 meters. The height of the small, medium and large office is 4.5, 12, and 48 meters, respectively. The annual power simulations of the wind turbine at different locations are shown in Figure 3.1 below.

$$\textbf{Power} = \frac{1}{2} \times \rho \times A \times v^3 \times C_p \times (1 - N_{Loss}) \qquad \textbf{Equation 3.4}$$

$$A_{Horizontal-axis} = \pi \times (\frac{D^2}{2}) \qquad \textbf{Equation 3.5}$$

$$C_p = \frac{Electricy\ produced\ by\ wind\ turbine}{Total\ Energy\ available\ in\ the\ wind} = \beta_3 \times v^3 + \beta_2 \times v^2 + \beta_1 \times v + \beta_0 \qquad \textbf{Equation 3.6}$$

Where P is power generated in W, v is the velocity of the wind in m/s, ρ is the density of the wind in kg/m^3, A is the swept area m^2, C_p is the power coefficient, N_{Loss} is efficiency loss of generator and gearbox, D is the rotor diameter in m, and H is the rotor height in m.

Table 3.1. Wind turbine parameters.

Product Model	**SD6 (240VAC, 1-phase, 60Hz)**
Manufacturer	**SD Wind Energy, Ltd.**
Rotor Diameter	**5.6m**
Swept Area	**24.63m^2**
Tower Height	**9m**
Peak Power	**6.1kW@17m/s**

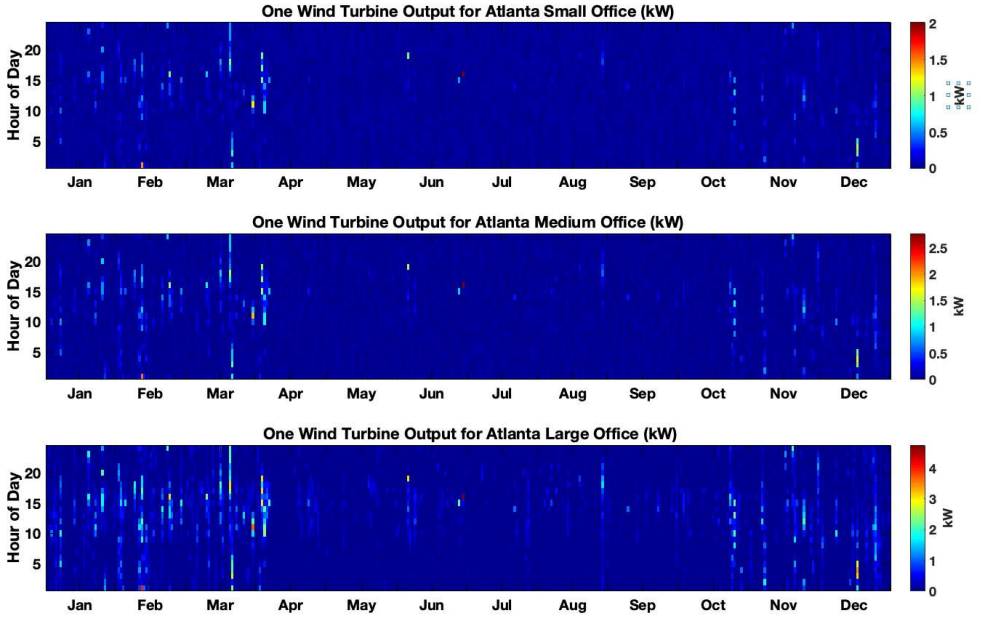
One Wind Turbine Output for Atlanta Small Office (kW)
One Wind Turbine Output for Atlanta Medium Office (kW)
One Wind Turbine Output for Atlanta Large Office (kW)
Hour of Day
Jan
Feb
Mar
Apr
May
Jun
Jul
Aug
Sep
Oct
Nov
Dec
kW

(a)

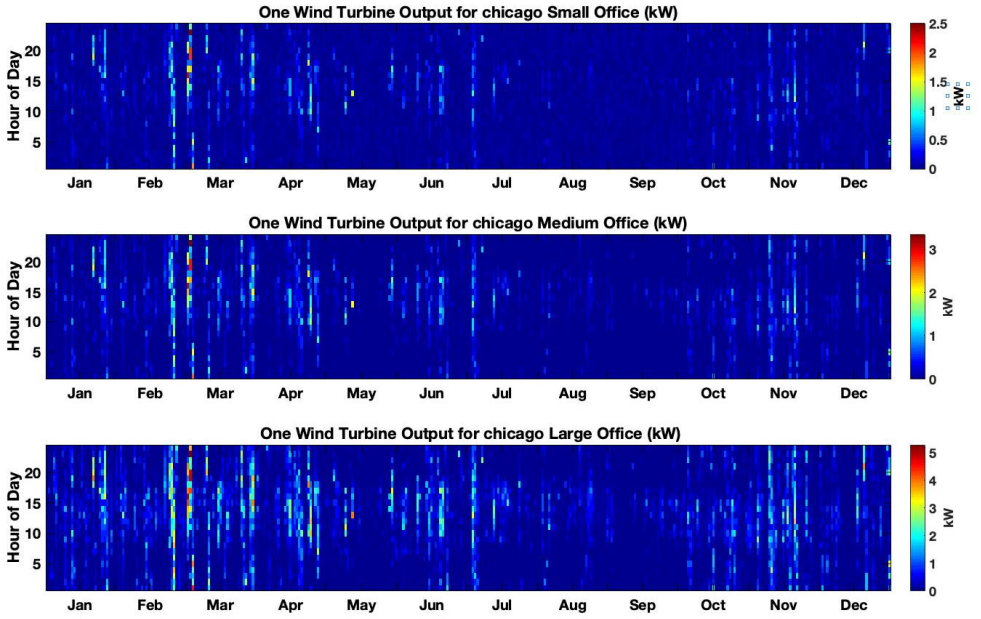
One Wind Turbine Output for chicago Small Office (kW)
One Wind Turbine Output for chicago Medium Office (kW)
One Wind Turbine Output for chicago Large Office (kW)
Hour of Day
Jan
Feb
Mar
Apr
May
Jun
Jul
Aug
Sep
Oct
Nov
Dec
kW

(b)

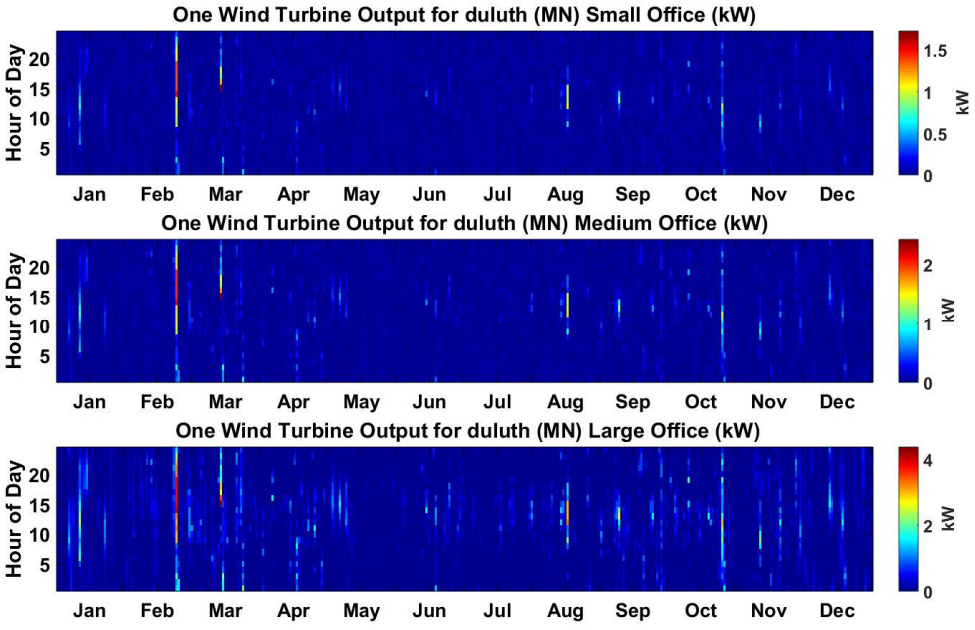
One Wind Turbine Output for duluth (MN) Small Office (kW)
Hour of Day
20
15
10
5
Jan Feb Mar Apr May Jun Jul Aug Sep Oct Nov Dec
1.5
1
0.5
0
kW
One Wind Turbine Output for duluth (MN) Medium Office (kW)
Hour of Day
20
15
10
5
Jan Feb Mar Apr May Jun Jul Aug Sep Oct Nov Dec
2
1
0
kW
One Wind Turbine Output for duluth (MN) Large Office (kW)
Hour of Day
20
15
10
5
Jan Feb Mar Apr May Jun Jul Aug Sep Oct Nov Dec
4
2
0
kW

(c)

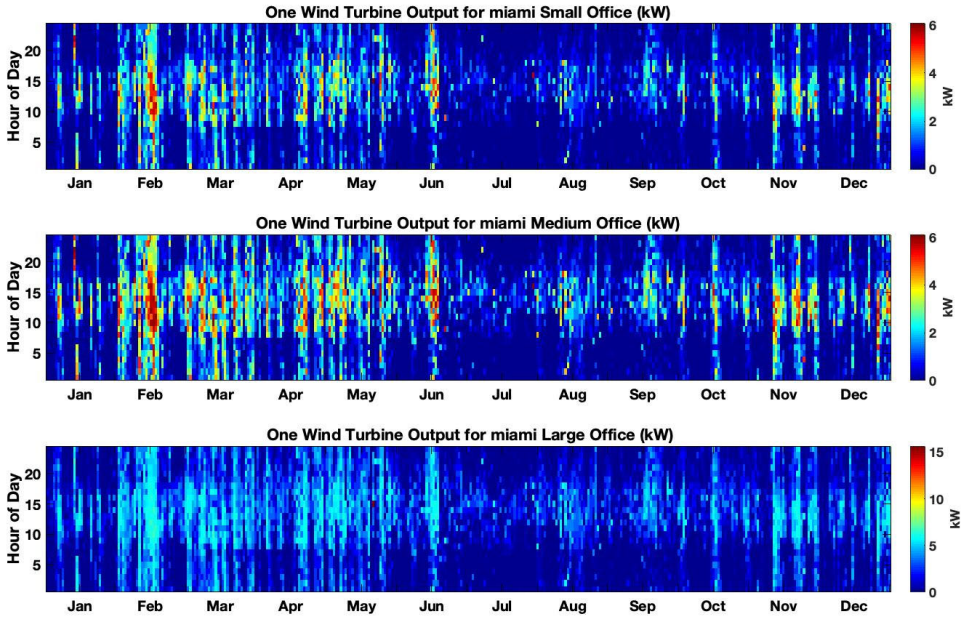
One Wind Turbine Output for miami Small Office (kW)
Hour of Day
20
15
10
5
Jan Feb Mar Apr May Jun Jul Aug Sep Oct Nov Dec
6
4
2
0
kW
One Wind Turbine Output for miami Medium Office (kW)
Hour of Day
20
15
10
5
Jan Feb Mar Apr May Jun Jul Aug Sep Oct Nov Dec
6
4
2
0
kW
One Wind Turbine Output for miami Large Office (kW)
Hour of Day
20
15
10
5
Jan Feb Mar Apr May Jun Jul Aug Sep Oct Nov Dec
15
10
5
0
kW

(d)

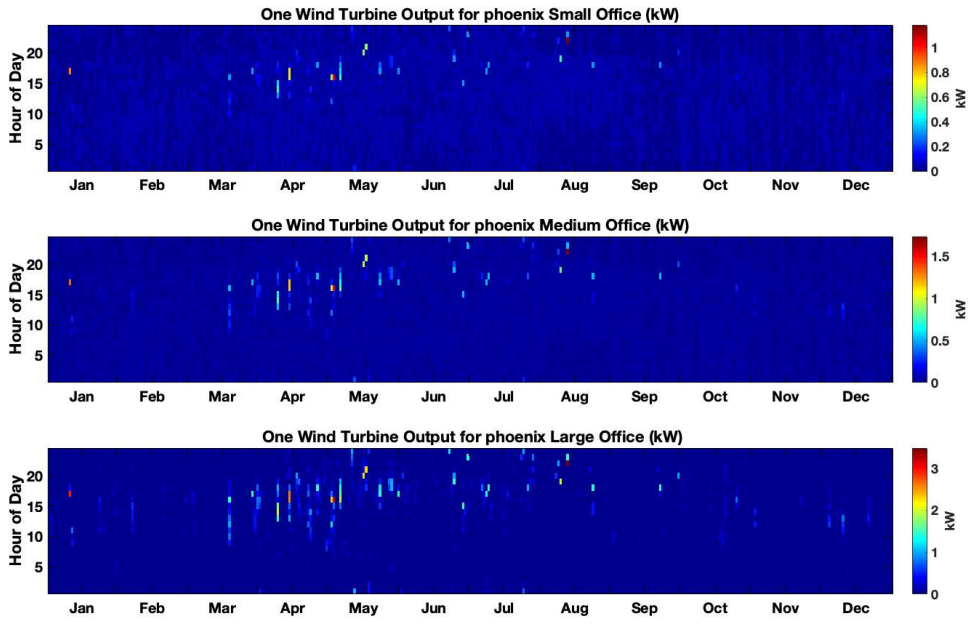

(e)

Figure 3.1. Wind turbine simulation.

For wind turbine installation, the accepted turbine separation distances in the industry have generally been 5 – 8 rotor diameters [92]. We used a wind turbine separation of 6 rotor diameter (manufacturer-recommended) to retain significant speed when entering the next. The roof area and shape are from the DOE commercial prototype building models [77]. The roof space and maximum capacity for installation for office buildings are shown in Table 3.2. The life cycle impact inventory of small wind turbine manufacturing stage is listed in Appendix B. We assumed the wind turbine has a 20-year lifetime since the analysis of more than 3000 wind turbines older than ten years in Denmark has an average less than 1% of production decrease. The related cost of the wind turbine is shown in Table 3.3 [93].

Table 3.2. The maximum number of turbines for installation.

	Length (m)	Width (m)	Maximum number of turbines
Small office	**27.686**	**18.457**	**2**
Medium office	**49.905**	**33.27**	**5**
Large office	**76.092**	**50.728**	**8**

Table 3.3. The cost inventory of wind turbine.

Cost	Cost/kw
Capital and installation	**500**
maintenance	**48**

3.2.2 The Fuel Cells

According to the Catalog of CHP technologies by the U.S. Environmental Protection Agency [94], fuel cell technology can generate electricity through chemical reactions rather than other combustion-based distributed prime mover technologies such as microturbine, steam turbine, and gas turbine, etc. Compared to combustion-based technologies, fuel cells can operate at higher efficiencies. The electrical efficiency of fuel cells is generally higher and between 40–60%.

For combined heat and power (CHP) applications, four primary types of fuel cells can be used as prime movers include phosphoric acid (PAFC), molten carbonate (MCFC), solid oxide (SOFC), and proton exchange membrane (PEMFC). Currently, there are 126 fuel cell installations with a total of about 83.6 MW capacity in the United States that are configured for CHP operation [95]. Although fuel cells use hydrogen as the fuel, most technologies use steam reforming of natural gas to produce hydrogen.

3.2.2.1 Solid Oxide Fuel Cells Simulation

In this research, we studied and modeled the solid oxide fuel cells (SOFC) because they have high efficiency, stability and reliability, and high operating temperature. The all-solid-state ceramic construction makes SOFC highly stable and reliable. The high operating temperature makes the internal reforming process possible, which is endothermic and energy-consuming. The SOFC has become a trend in the U.S. as the fuel cell technology [96].

Fuel Cell Simulation

Since the detailed manufacture data of SOFC are not available. We used a data-validated SOFC stack model developed by Chinappini et al. [97] for the electricity and thermal energy generation. The SOFC stack model has a power capacity of 25-250 kW. A turndown ratio of 0.3 is assumed, which means the fuel cells will not run at less than 30% of its rated power. A schematic of the model is given in Figure 3.2. As shown, the fuel cell systems are composed of three primary subsystems: 1) the fuel cell stack that produces direct current electricity; 2) the reformer that converts natural gas into hydrogen; and 3) the inverter that converts direct current to alternating current. The efficiency of the inverter is typically between 92 to 96 percent.

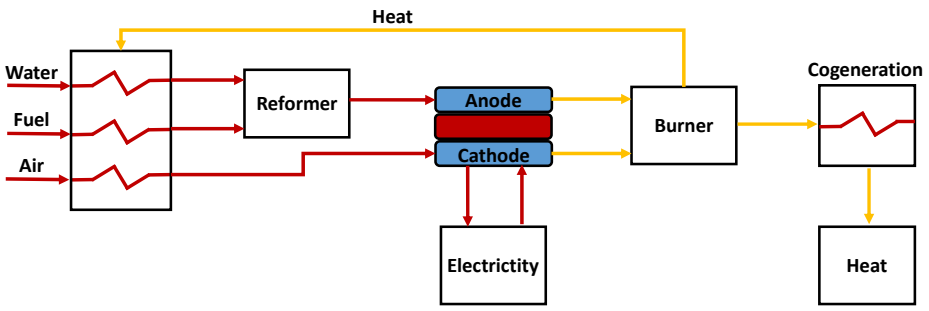

Figure 3.2. The solid oxide fuel cell system configuration.

The electrical and thermal power output of the SOFC depends on three parameters: the load factor, the operating temperature, and the fuel utilization factor. According to commercial product information [98], we used the highest available operating temperature at 1160 K (proportional to electrical and thermal efficiency), with the highest fuel utilization factor of 80%. The simulation results of electrical efficiency and thermal efficiency versus the partial-load ratio are shown in Figure 3.3. Since the SOFC model predicts kW output (performance do no vary with turbine size), we assumed there are three sizes 35kW, 65kW, and 200kW, which are similar to microturbine. We used the CHP-RE-ESS system because the fuel cell has a high power to heat energy generation ratio. Consequently, the cooling demand can be met using electricity, and the SOFC-based system does not require the adsorption chiller to turn heat to cooling. In this case, the energy demand profile for building installed with fuel cells have same electrical demand as conventional energy from the grid (i.e., power is used for plug load and cooling, and the waste heat for hot water and

heating just like a boiler or furnace. See Figure 3.5.). The detailed energy demand profile for fuel cells system for different building and locations are shown in Appendix B.

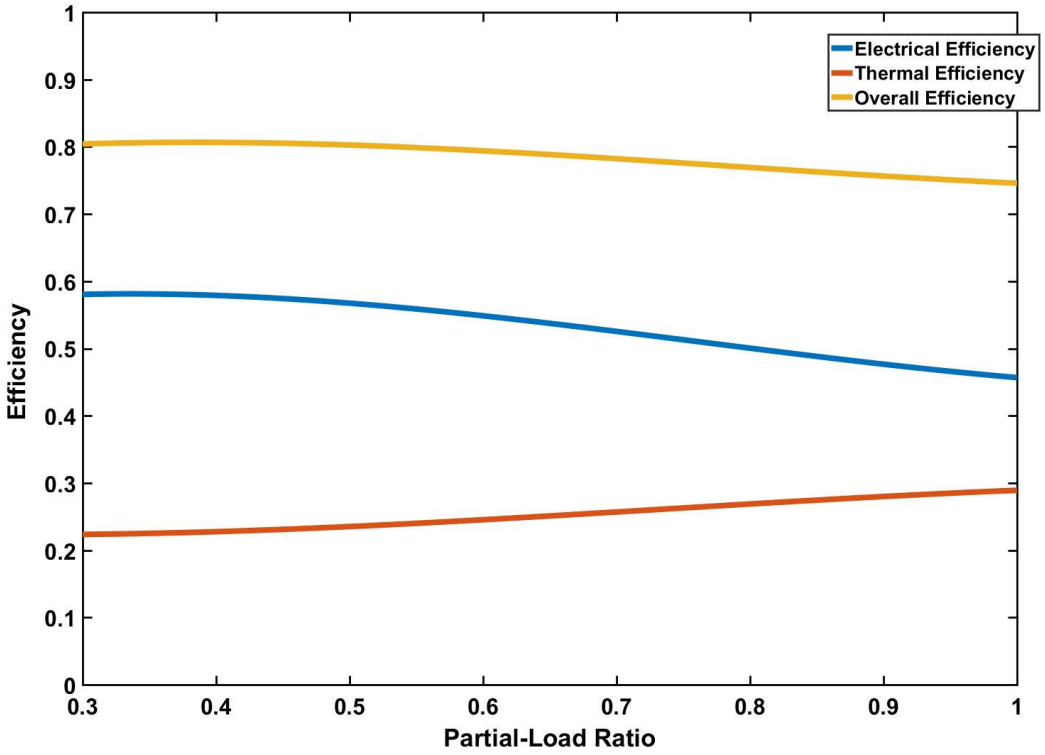

Figure 3.3. The electrical and thermal efficiency of SOFC versus the partial-load ratio.

The life cycle impact inventory for SOFCs during the manufacturing stage is listed in Appendix B. During the operational stage, fuel cells generally have very low emissions. The NO_x, SO_2, CO, VOC emissions for SOFC are negligible. The CO_2 emission of the system is based on model fuel input and fuel utilization rate. In terms of economic cost, the capital cost and maintenance cost are shown in Table 3.4 [3]. The maintenance costs for the fuel cell system depend on the size and maturity of the equipment. Typical expenses include labor, ancillary replacement parts, catalyst replacement (3-5 years), stack replacement (3-5years).

Table 3.4. The cost inventory of SOFC.

Installed Cost components	Fuel cell system
Fuel Cell Type	SOFC
Total Package Cost ($/kW)	$ 23,000
O&M Costs ($/MWh)	$ 55
Fuel cost ($)	varies with location

3.2.3 The Compressed Air Energy Storage

The decentralized Compressed-air energy storage (CAES) is another energy storage technology for small-scale and distributed energy generation. The CAES is a kind of physical battery as opposed to a chemical battery such as lithium-ion. It stores energy via the compressor and recovers energy via air expansion. The CAES does not require rare metals or toxic materials like the electrochemical batteries, and the hardware is easily recyclable when scraped. Besides, chemical batteries store only about two to ten times the energy that is required to manufacture them [99]. The CAES has a longer lifespan since the storage capacity of CAES does not decay and has an almost infinite number of charge and discharge cycles.

There are three types of CAES systems, and they depend on how the system deals with air storage: adiabatic, diabatic, isothermal, or near-isothermal [100]. The adiabatic compressed air energy storage (A-CAES) technology is the most common, commercially available, and research focused technology [100]. Compared to conventional CAES, the ACAES system has higher round-trip efficiency since the heat in the compression process is recovered and used for expansion [101]. According to DOE global energy storage database [102], there are three decentralized A-CAES under construction, contracted and operational

with power 5000kW (10 MWh storage capacity), 1750kW (7 MWh storage capacity), and 660kW (1 MWh storage capacity), respectively.

3.2.3.1 Adiabatic CAES Simulation

Adiabatic storage keeps the heat produced in the air compression stage and returns it to the air when it expands to generate power. Compression creates heat while expansion removes heat. The loss of heat can affect the round-trip efficiency. The heating and cooling storage for the system can help improve storage efficiency as the heat of compression is reused during the discharging process. The working process is shown in Figure 3.4.

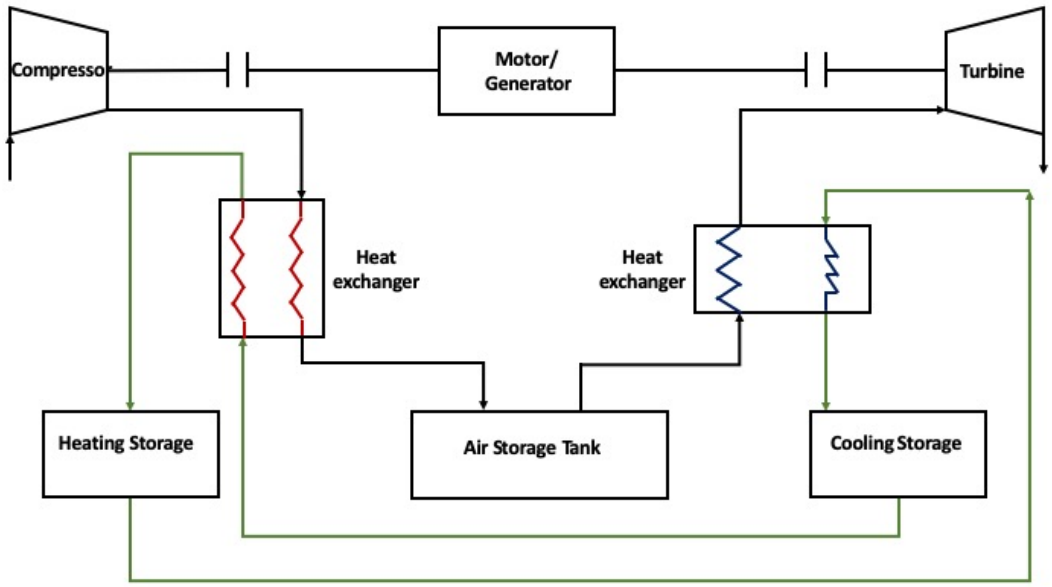

Figure 3.4. ACAES system configuration.

We used a multi-scale adiabatic compressed air energy storage model developed by Xing Luo et al. [103]. The model includes: (1) a four-stage air compression unit formed by three Low-Pressure and one High-Pressure compressor; (2) a four-stage air expansion unit consists of one High-Pressure and three Low-Pressure turbines; (3) a controlled volume air storage reservoir(s) has been chosen as the controlled volume boundary for

thermodynamic process analysis; (4) a heat storage unit and a heat recovery unit for air expansion; and, (5) a set of water pump for heat exchanger.

The fundamental equations for the whole system are the balance of the mass and energy in and out of the system components [104]. The following two equations are the fundamental governing equations for modeling the system. Figure 3.7 is the mass balance equation, and Equation 3.8 is the first law of thermodynamics. It is assumed that both heat energy storage and cold energy storage are adiabatic.

$$\frac{dm}{dt} = \dot{m}_{in} - \dot{m}_{out} + m_{created} \qquad \textbf{Equation 3.7}$$

$$\Delta U = Q - W \qquad \textbf{Equation 3.8}$$

Where $\dot{m}$ is the mass of the flow, ΔU is the internal energy of a closed system, Q is the heat supplied to the system, W is the work down to the system.

For the whole system, the model assumes the airflow is a steady flow and no air leakage from the system components, which means the input mass flow rate of the compressors equals the output mass flow rate. In this case, the following Equation 3.9 can be derived from Equation 3.7 and 3.8.

$$\dot{m}_{in}\left(U_{in} + \frac{V_{in}^2}{2} + H_{in}\right) + \dot{Q} + \dot{W} = \dot{m}_{out}\left(U_{out} + \frac{V_{out}^2}{2} + H_{out}\right) \qquad \textbf{Equation 3.9}$$

Where *Q* is the heat input to the system, *W* is work done to the system, *U* is the specific enthalpy, *H* is the height, and *V* is the velocity.

There is no fuel combustion to heat the air in the air expansion process for the turbine. A heat recovery unit and thermal storage system are designed to recovery heat produced during the air compression process. For capital and maintenance costs concerns,

the heat storage reservoir is designed to be adiabatic while the cooling storage reservoir is non-adiabatic. The constant volume of air storage is also non-adiabatic for cost reasons. The system can be scaled up and down. The system charging and discharging time and capacity depend on storage reservoir volume and compressor and turbine rating. The model parameters setting is shown in Table 3.5 below.

There is no built-in life cycle impact inventory for the A-CAES system life cycle inventory in the current LCA database, so we used Evert 's [105] system inventory (Table 3.6) and evaluated the product's environmental impact on a per kW basis. For all inventories, it was assumed that the power rating is scaled linearly. Detailed environmental impact is shown in Appendix B. The ACAES cost inventory is from the Energy Storage Technology and Cost Characterization Report from U.S. DOE [106] and is shown in Table 3.7.

Table 3.5. ACAES system parameters.

Parameters	**Value**	**Unit**
Ambient (environment) temperature	**293.15**	**K**
Ambient (environment) pressure	**1.013**	**bar**
Charge–discharge time ratio	**2**	**None**
Stage numbers of air compression & expansion	**4 stages to both**	
High- & low-pressure air compressors (series connection)		
Isentropic efficiency to compressors	**80**	**%**
The pressure ratio of each stage	**2.75**	**None**
High- & low-pressure air turbines (series connection)		
Isentropic efficiency to air turbines	**80**	**%**
The expansion ratio of each stage	**2.55**	**None**

Table 3.6. Inventory of 100kW ACAES (800kWh storage capacity).

Inventory	sizes
Air Compressor	140kW
Gas turbine	100kW
Thermal Storage	64000L
construction	NA

Table 3.7. The cost inventory of ACAES.

Installed Cost components	CAES System
CAES Type	Adiabatic
Total Package Cost ($/kW)	$ 1,669
O&M Costs ($/MWh)	$ 16.7
Fuel cost ($)	None

3.2.4 Building Energy Demand Profile

As stated in the previous chapter, the building's heating, cooling, and electrical energy demands for the conventional energy system and the CCHP-RE-ESS system are simulated using the Energy Plus software developed by the U.S. DOE. For the conventional energy system, the building's electrical demand is met entirely by the power grid. The building heat demand is met by building heating equipment (electrical or gas furnace). The cooling demand is met by the air conditioning system powered by electricity. For the CCHP-RE-ESS using microturbine as the prime mover, the cooling demand is met by absorption chiller, which converts heat energy into cooling energy since microturbines produce more heat than electricity (high heat-to-power ratio). On the other hand, for CCHP-RE-ESS using SOFC as the prime mover, the air conditioning system is powered by electricity, because the fuel cell has a high power to heat energy generation ratio. In this case, the energy demand profile for building installed with fuel cells have the same

electrical demand as conventional energy from the grid. Figure 3.5 shows all the building energy demand profiles of commercial office (small, medium, and large) in Atlanta. The building energy demand profiles for other building types and cities are shown in Appendix B.

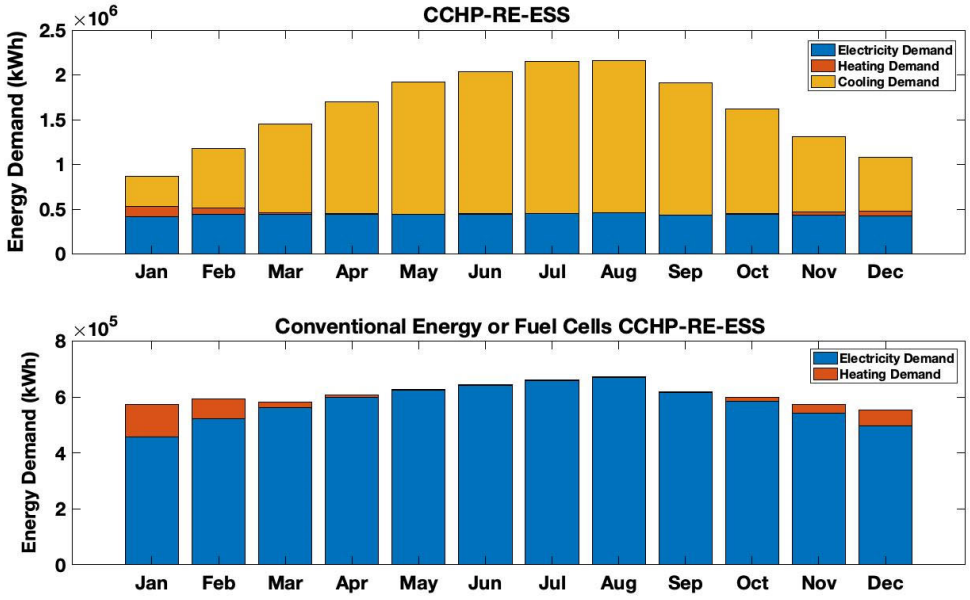
CCHP-RE-ESS
×10^6
Energy Demand (kWh)
Electricity Demand
Heating Demand
Cooling Demand
Jan
Feb
Mar
Apr
May
Jun
Jul
Aug
Sep
Oct
Nov
Dec
Conventional Energy or Fuel Cells CCHP-RE-ESS
×10^5
Energy Demand (kWh)
Electricity Demand
Heating Demand

(a)

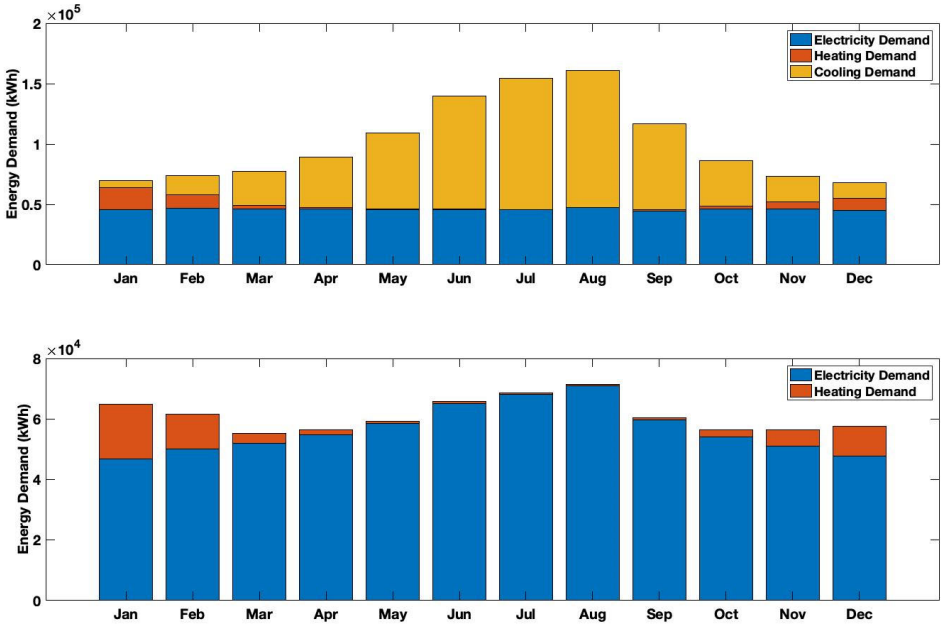
×10^5
Energy Demand (kWh)
Electricity Demand
Heating Demand
Cooling Demand
Jan
Feb
Mar
Apr
May
Jun
Jul
Aug
Sep
Oct
Nov
Dec
×10^4
Energy Demand (kWh)
Electricity Demand
Heating Demand

(b)

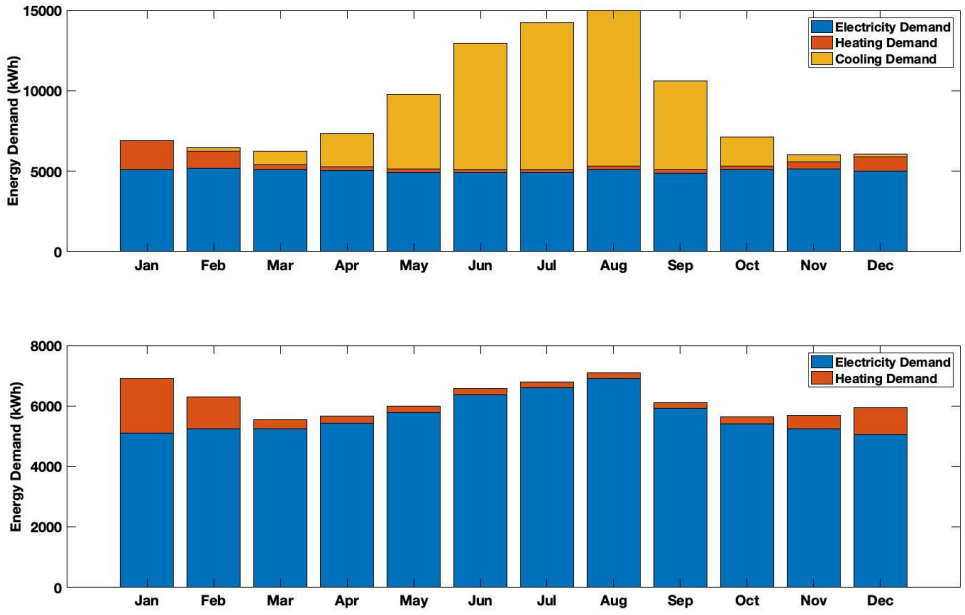

(c)

Figure 3.5. The energy demand profiles of commercial office in Atlanta. (a)Demand profile for a large office building in Atlanta. (b) Demand profile for a medium office building in Atlanta (c) Demand profile for a small office building in Atlanta

3.2.5 Multi-Disciplinary Design Optimization Framework

By adding different technologies into the parametric LCA framework, the model has six technologies: two for prime movers (microturbine and fuel cells), two for renewables (solar power and small wind turbine), and two for energy storage (lithium-ion battery and compressed air energy storage). We adopted the multi-disciplinary design optimization method and determined the Pareto front for the optimal combination of technologies and corresponding sizes for different scenarios. The two dependent variables are LCA results (environmental sustainability single score) and economic costs (life cycle cost). We gave environmental impact the highest priority. The flow chart for the simulations are shown in Figure 3.6.

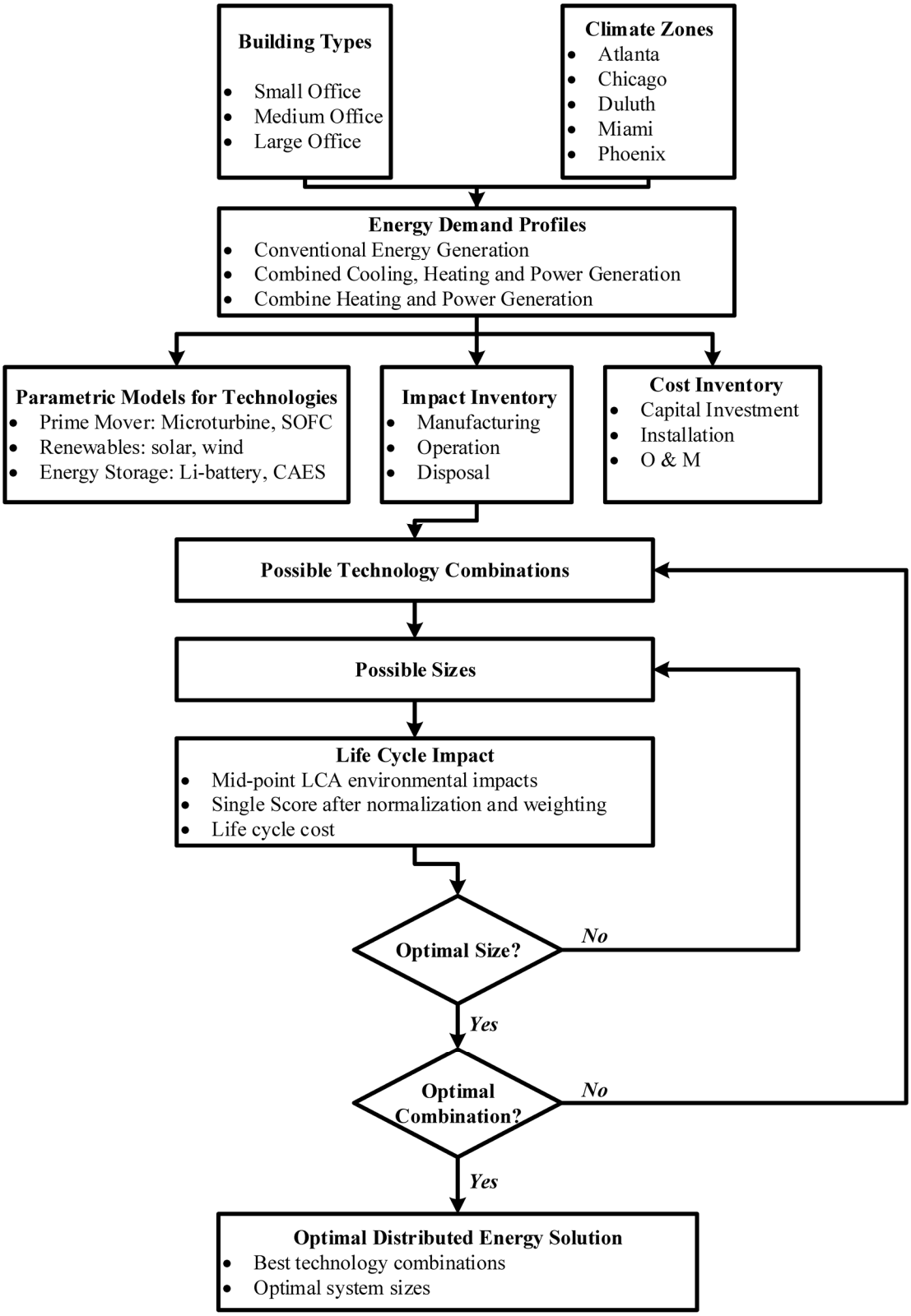

Figure 3.6. The multi-disciplinary design optimization flow chart.

3.3 Results and Discussion

3.3.1 Optimal Combination of Technologies

After billions of simulations, the life cycle single scores and costs of eight possible combinations of technologies are plot below for each building type and location shown in Figure 3.7. The best technology combinations for each building type and location are shown in Table 3.8. Results show there are two possible optimal combinations for different scenarios: SOFC-Solar PVs-Li-ion batteries (FSB) and Microturbine-Solar PVs-Li-ion batteries (MSB). This means the synergy of solar energy and Li-ion batteries performs better than small wind turbines and compressed air energy storage in terms of life cycle impact. In some scenarios, no energy storage system is required (only prime mover and renewable energy), which avoid extra investment and save cost. Although the synergy of wind and compressed air energy has never been the best life cycle technology, they show their potential in Phoenix and Miami, in which the LCA single score is close to the optimal case.

Admittedly, the building energy demand in this study is based on the simulation results. However, by adopting the parametric LCA framework, every building with its unique building energy demand can find its customizable combination of technologies and system size. According to Figure 3.7, the life cycle cost of the system largely depends on which prime mover is adopted. The cost of the SOFC-based CCHP-RE-ESS system is much higher than the microturbine-based CCHP-RE-ESS system.

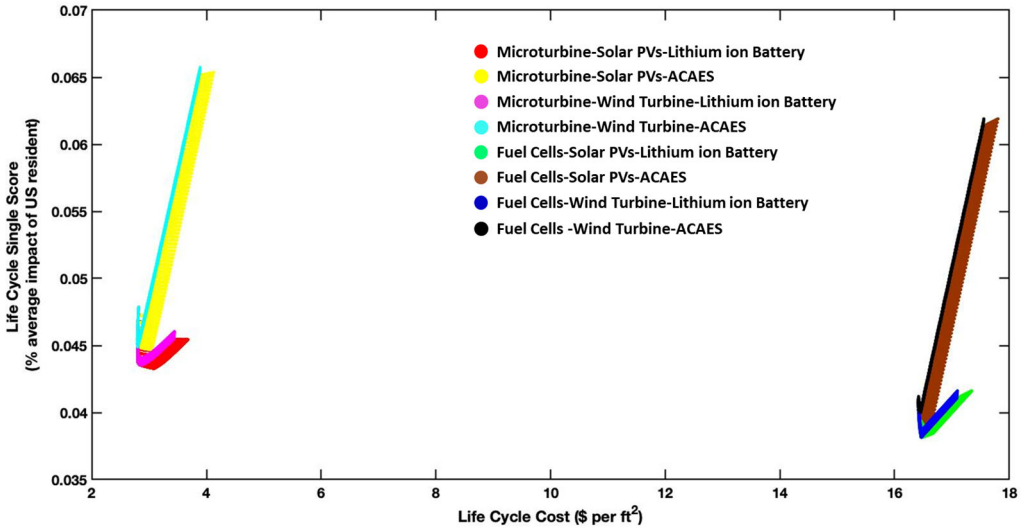

Atlanta Large Office

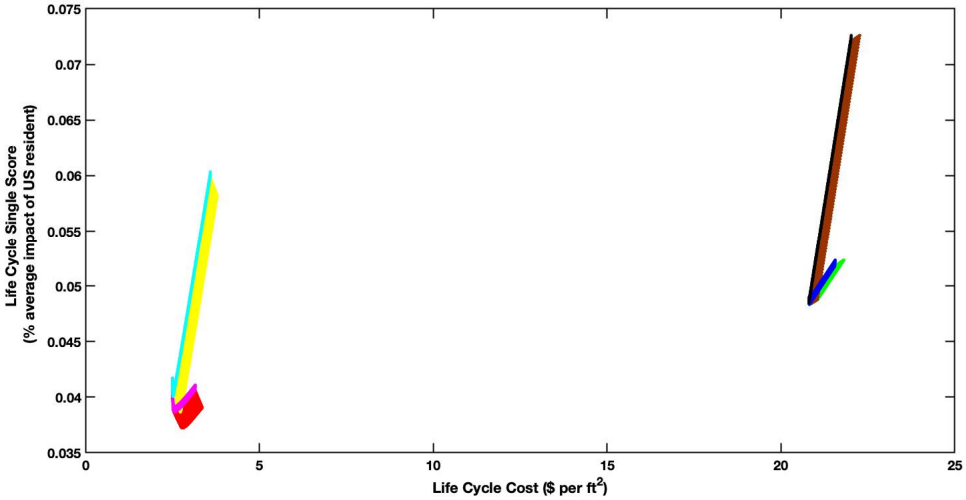

Chicago Large Office

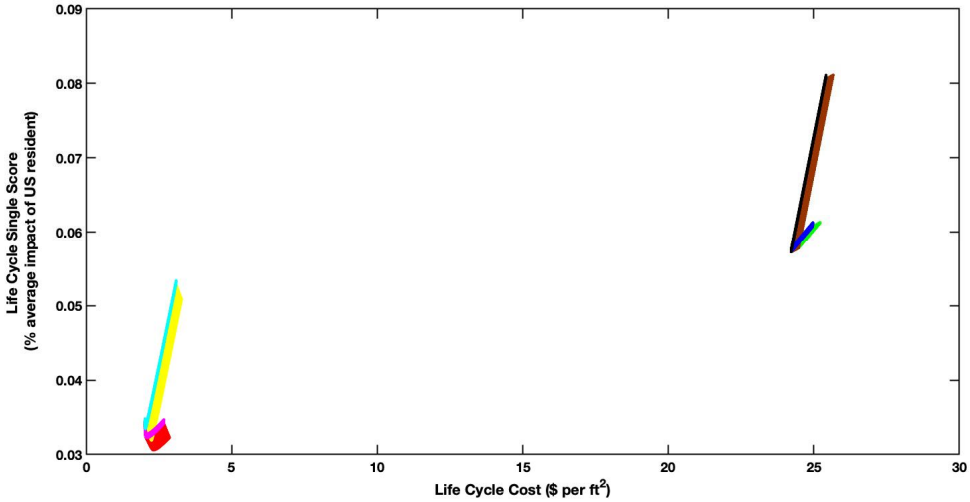

Duluth Large Office

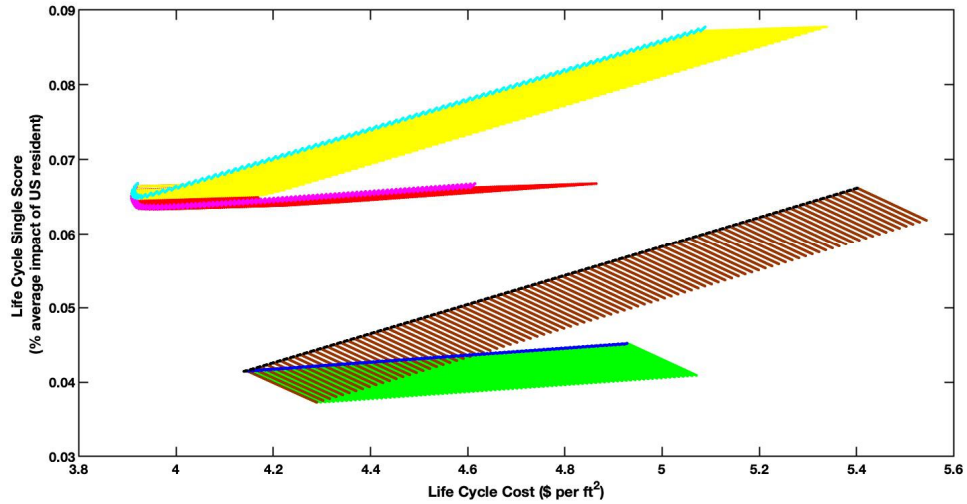

Miami Large Office

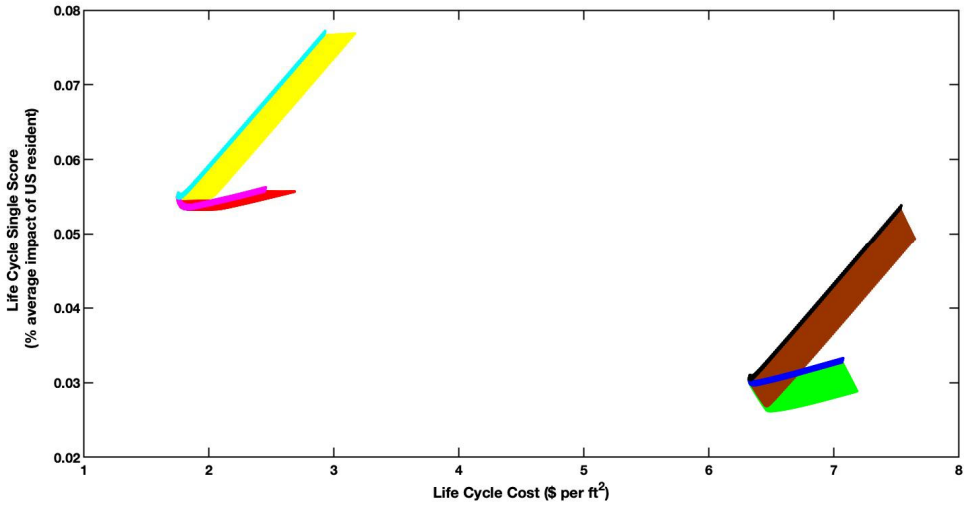

Phoenix Large Office

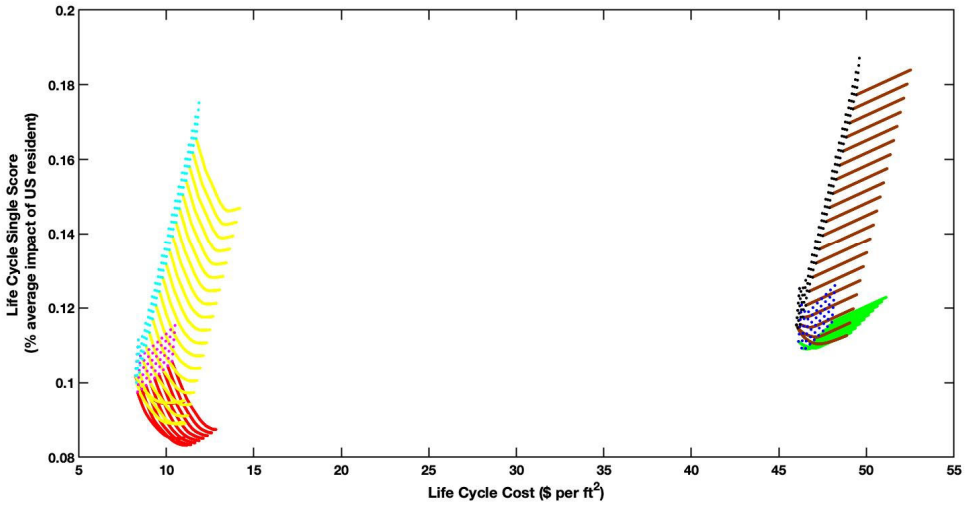

Atlanta Medium Office

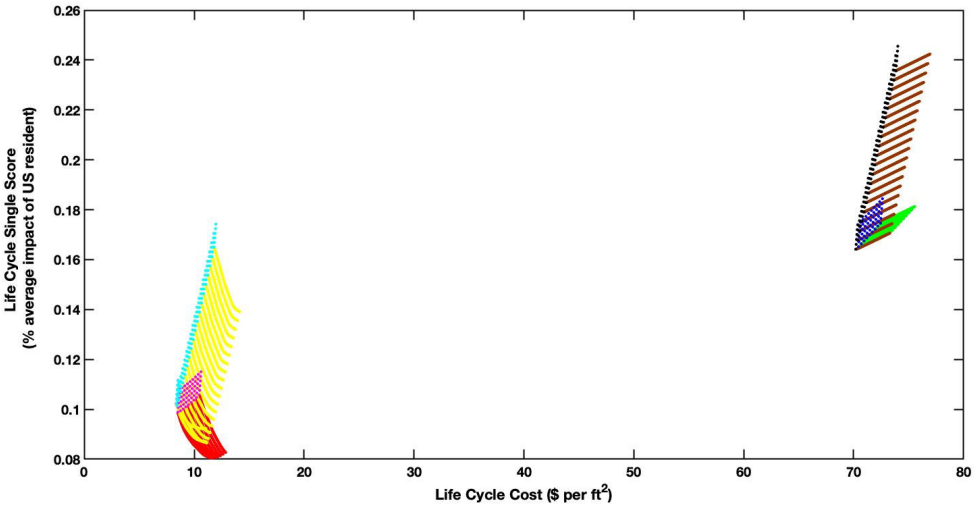

Chicago Medium Office

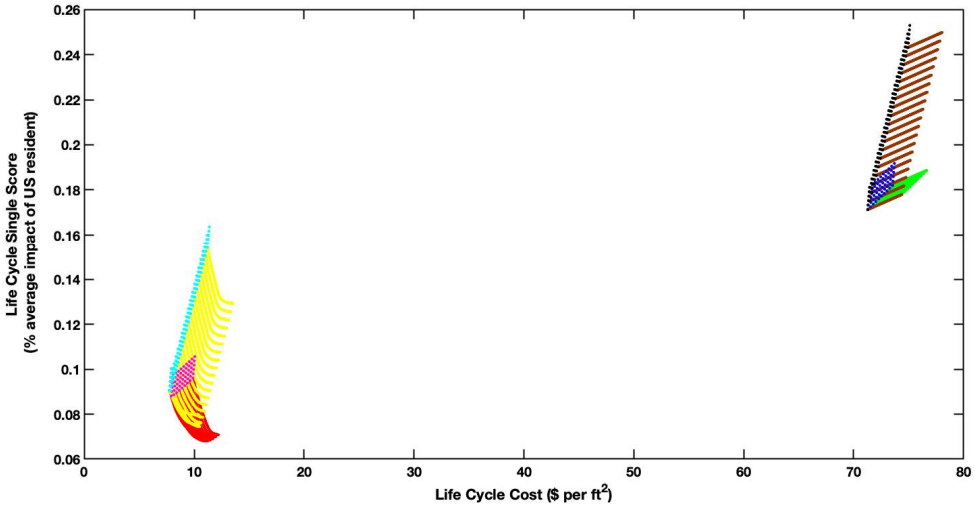

Duluth Medium Office

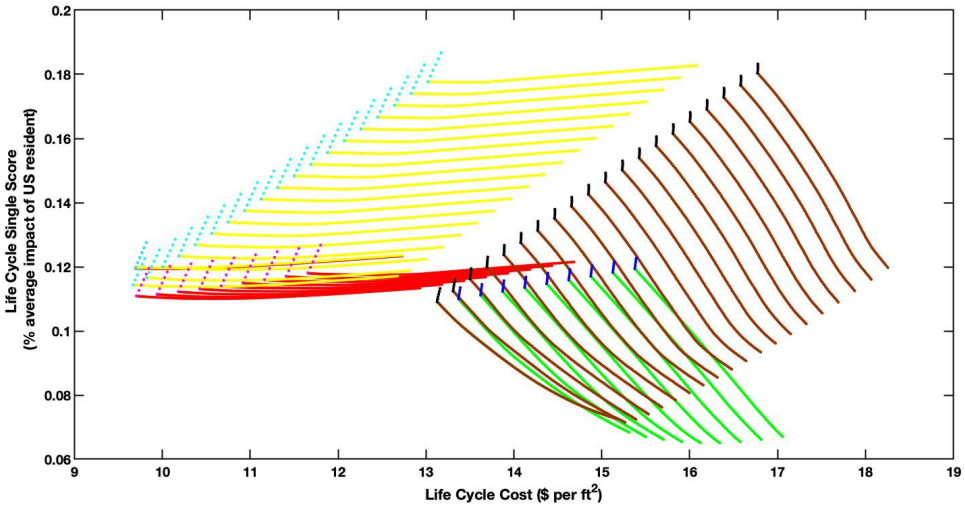

Miami Medium Office

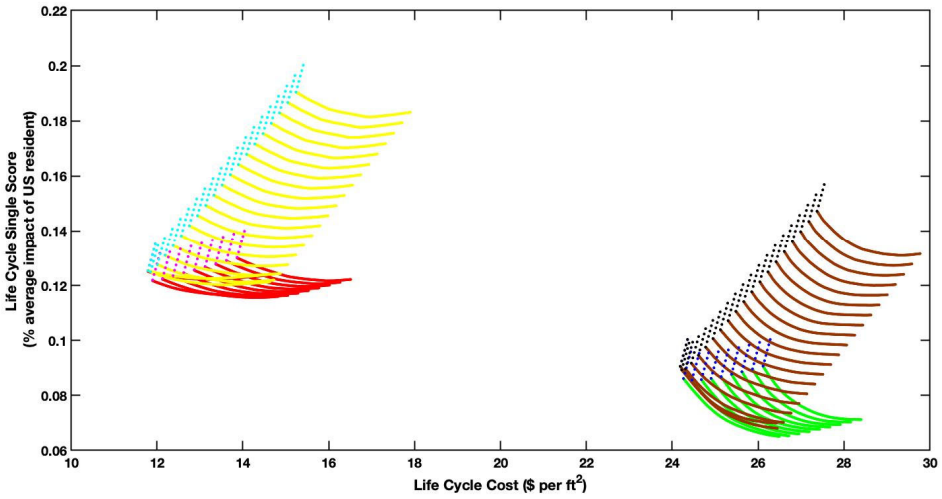

Phoenix Medium Office

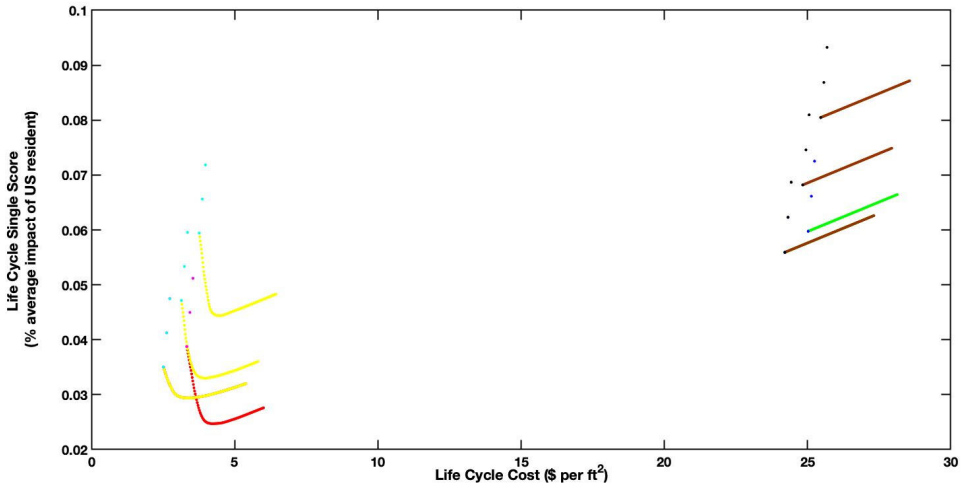

Atlanta Small Office

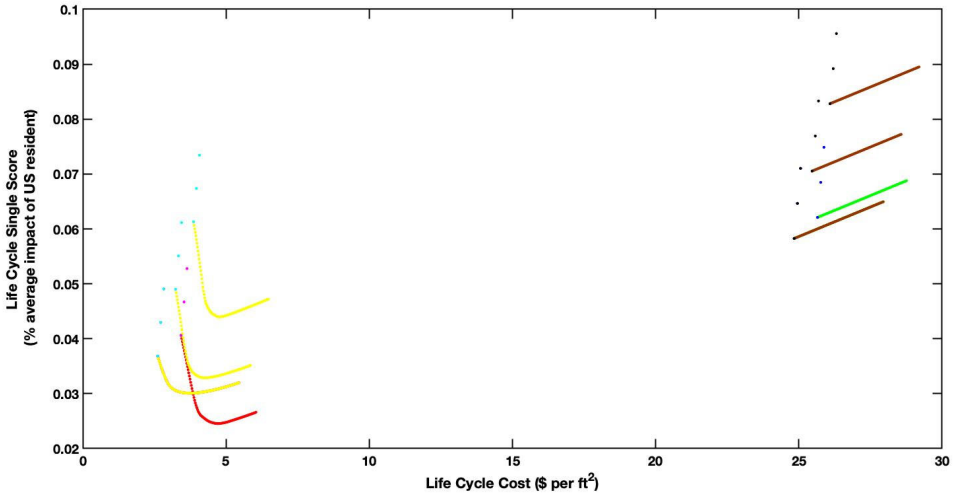

Chicago Small Office

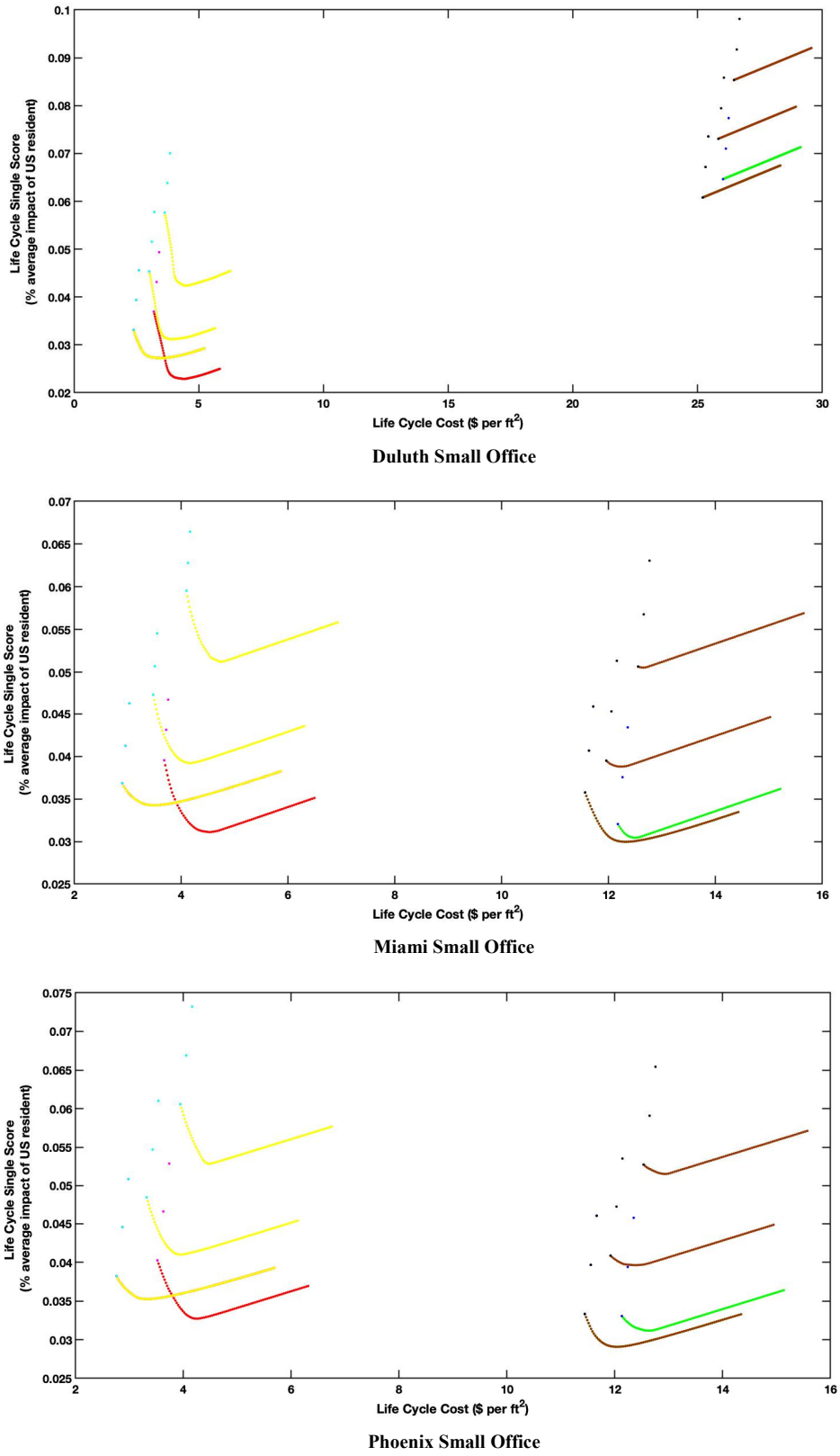

Figure 3.7. The impact of all possible technologies combinations and sizes.

Table 3.8. The best technologies combinations and corresponding sizes

Scenarios	Prime Mover	Size (kWh)	Renewable Energy	Size	Energy Storage	Size (kWh)
Atlanta Small Office	Microturbine	30	Solar PVs	170	Battery	210
Chicago Small Office	Microturbine	30	Solar PVs	230	Battery	210
Duluth Small Office	Microturbine	30	Solar PVs	220	Battery	210
Miami Small Office	SOFC	30	Solar PVs	130	None	0
Phoenix Small Office	SOFC	30	Solar PVs	105	None	0
Atlanta Medium Office	Microturbine	400	Solar PVs	1330	Battery	420
Chicago Medium Office	Microturbine	400	Solar PVs	1330	Battery	630
Duluth Medium Office	Microturbine	400	Solar PVs	1330	Battery	840
Miami Medium Office	SOFC	95	Solar PVs	1330	Battery	1260
Phoenix Medium Office	SOFC	200	Solar PVs	1330	Battery	210
Atlanta Large Office	SOFC	4000	None	0	Battery	3150
Chicago Large Office	Microturbine	2800	Solar PVs	3100	Battery	3570
Duluth Large Office	Microturbine	2400	Solar PVs	3100	Battery	2780
Miami Large Office	SOFC	800	Solar PVs	3100	None	0
Phoenix Large Office	SOFC	1400	Solar PVs	3100	Battery	1890

3.3.2 The Optimal LCA Single Scores and LCC for Different Scenarios

The optimal US annual per capita environmental LCA single scores and life cycle costs for different building energy profiles are shown in Figure 3.8 and Figure 3.9. All monetary values are in constant 2019 dollars in net present value over 20 years of system lifetime, at a 7% discount rate [107]. The life cycle impact single score (in terms of % annual impact of US resident) of CCHP-RE-ESS is less than conventional energy. For different building types, the medium offices have a larger single score than small offices and large offices. However, the medium office has more life cycle impact reduction by adopting the CCHP-RE-ESS system. The single scores of each building type for different cities are similar. Buildings in Phoenix have lower impacts (LCA single scores) compared to buildings in other cities. The single scores of large offices are lower than in small offices and medium offices. Detailed impact categories for conventional and CCHP-RE-ESS are reported in Table 3.9 and Table 3.10.

In terms of life cycle cost, the cost of CCHP-RE-ESS is higher than conventional energy. For Miami small office, Phoenix small office, Miami medium office, Phoenix medium office, Atlanta large office, Miami large office, and Phoenix large office, the LCC is much higher because they adopt SOFC-based CCHP-RE-ESS system. On average, the LCC of medium office is higher than the small office and large office. The distributed CCHP-RE-ESS system LCC for large office is the most economical and close to the cost of conventional energy, especially for the Chicago and Duluth large office with a microturbine system. Detailed LCC and cost categories are reported in Figure 3.10 and Table 3.11.

In total, for most of the situations, the CCHP-RE-ESS system can meet more than 90% of electricity demand for the building. Detailed electricity supply proportions of CCHP-RE-ESS system components for studied building types and locations are reported in Figure 3.11 and Table 3.12. However, for the large offices in Duluth (30% from the grid), Miami (64% from the grid), and Phoenix (39% from the grid), getting more electricity from local grid (with local energy mix) is a better trade-off option as compared to other scenarios (buildings and locations).

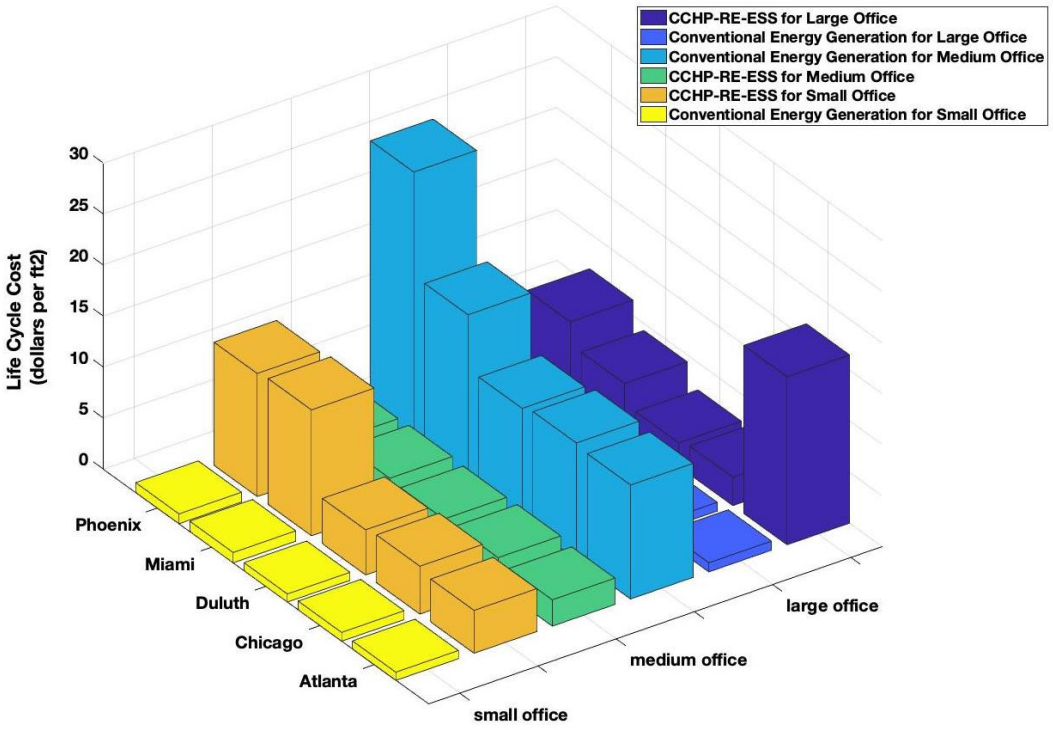

Figure 3.8. The life cycle cost for optimal scenarios.

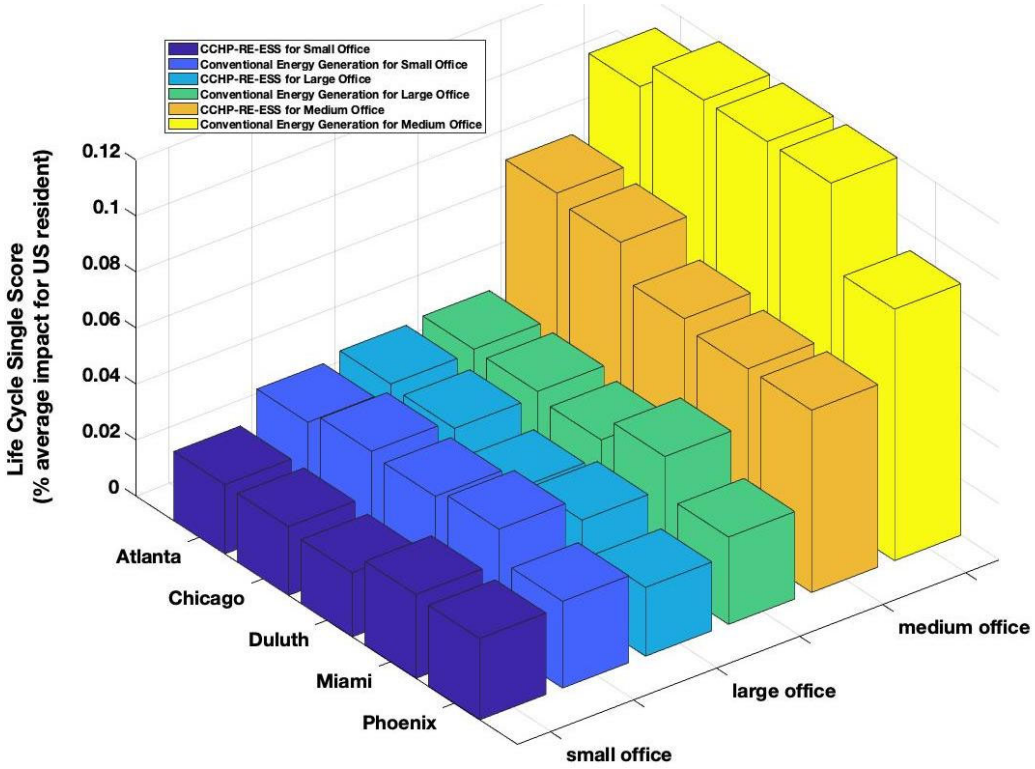

Figure 3.9. The life cycle single score for optimal scenarios.

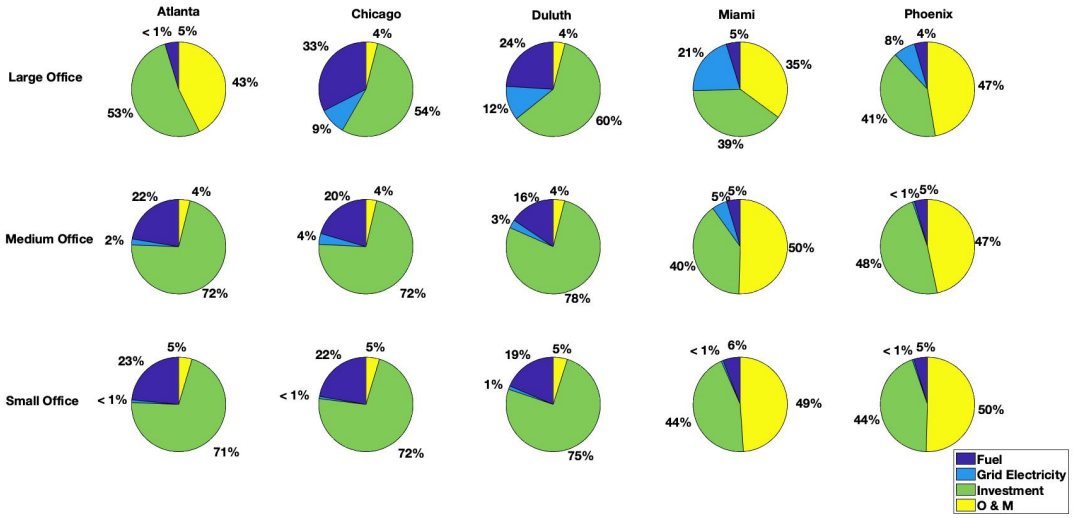

Figure 3.10. The cost proportions for optimal scenarios.

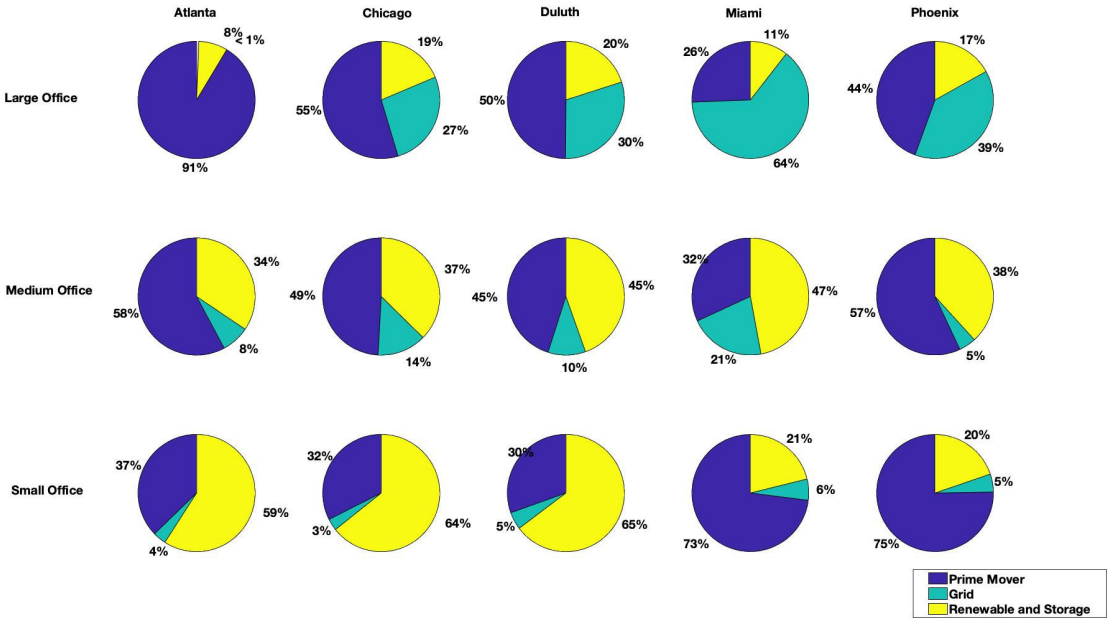

Figure 3.11. The electricity dispatch proportions for optimal scenarios.

Table 3.9. The CCHP-RE-ESS environmental life cycle impacts for optimal scenarios.

Scenarios	Global Warming (kg CO_2 eq)	Acidification (kg SO_2 eq)	Ozone Depletion (kg CFC-11 eq)	Ecotoxicity (CTUe)	Eutrophication (kg N eq)	Water (gal)	Fuel Depletion (MJ)	Single Score	Cost (dollar)
Atlanta Small Office	4.8922	0.0156	1.3497e-7	21.791	0.0058	0.08	21.0785	2.4711e-4	4.2045
Chicago Small Office	4.5755	0.0157	1.6644e-7	23.291	0.0064	0.072	1.0631	2.4546e-4	4.6935
Duluth Small Office	4.4167	0.0162	1.5689e-7	20.728	0.0059	0.1057	1.0505	2.2887e-4	4.4260
Miami Small Office	8.5661	0.0248	1.3326e-6	1.768	0.0033	0.1767	0.8962	2.9968e-4	12.3366
Phoenix Small Office	8.2773	0.0215	1.3314e-6	10.475	0.0030	0.1497	1.3340	2.9082e-4	12.0575
Atlanta Medium Office	20.2520	0.0480	3.3230e-7	51.440	0.0133	0.4739	3.3908	8.3323e-4	11.1767
Chicago Medium Office	18.5930	0.0609	3.3330e-7	55.560	0.0144	0.8289	2.9896	8.0595e-4	11.4562
Duluth Medium Office	15.1270	0.0493	3.2280e-7	50.460	0.0132	0.6377	2.6652	6.8146e-4	11.0053
Miami Medium Office	15.3260	0.0802	1.5140e-6	36.510	0.0095	1.8724	11.6779	6.5059e-4	16.3440
Phoenix Medium Office	17.6430	0.0489	2.8430e-6	28.220	0.0087	0.4118	3.5414	6.5096e-4	26.4970
Atlanta Large Office	11.1466	0.0248	1.8480e-6	12.858	0.0029	1.225 e-4	0.7419	3.7930e-4	16.4700
Chicago Large Office	10.4700	0.0311	5.9560e-8	14.56	0.0036	0.5419	1.151	3.6890e-4	2.7750
Duluth Large Office	8.4010	0.0300	5.2640e-8	13.02	0.0032	6.602	1.113	3.0290 e-4	2.3050
Miami Large Office	10.0410	0.0698	3.9130e-7	9.825	0.0018	2.113	11.919	3.3780e-4	4.2900
Phoenix Large Office	7.1580	0.0361	6.7930e-7	8.265	0.0019	1.185	5.548	2.4560e-4	6.4970

Table 3.10. The conventional energy environmental life cycle impacts.

Scenarios	Global Warming (kg CO_2 eq)	Acidification (kg SO_2 eq)	Ozone Depletion (kg CFC-11 eq)	Ecotoxicity (CTUe)	Eutrophication (kg N eq)	Water (gal)	Fuel Depletion (MJ)	Single Score	Cost (dollar)
Atlanta Small Office	10.8266	0.0913	1.7989e-10	0.0045	0.0014	2.6523	10.58	3.5630e-4	0.8017
Chicago Small Office	11.9020	0.0956	2.0911e-10	1.2746	0.0015	2.5511	18.26	4.0077e-4	0.8630
Duluth Small Office	10.6955	0.0863	1.922e-10	1.2972	0.0013	2.4282	26.82	3.8838e-4	0.7896
Miami Small Office	11.1932	0.0925	1.3203e-10	9.6986	0.0013	3.2367	18.80	4.1927e-4	1.0146
Phoenix Small Office	8.0853	0.0683	7.7431e-11	6.8876	8.3558e-4	3.2140	16.36	3.0974e-4	0.9586
Atlanta Medium Office	34.7402	0.2990	5.9008e-10	0.0149	2.4491e-4	8.7202	21.36	0.0011	2.5821
Chicago Medium Office	39.6076	0.3367	7.3909e-10	4.5308	0.0051	9.0686	23.04	0.0012	2.8763
Duluth Medium Office	37.0690	0.3291	7.1749e-10	5.0272	0.0049	9.4098	36.02	0.0012	2.8139
Miami Medium Office	32.7959	0.2732	3.8955e-10	0.0035	0.0035	9.5694	50.97	0.0012	2.9732
Phoenix Medium Office	23.8536	0.2051	2.3251e-10	0.0024	0.0024	9.6843	41.40	8.9797e-4	2.8537
Atlanta Large Office	12.0300	0.1026	2.0240e-10	0.0051	0.0014	2.989	9.25	3.896e-4	0.8923
Chicago Large Office	11.7900	0.0950	2.1150e-10	1.2920	0.0014	2.486	14.23	3.871e-4	0.8552
Duluth Large Office	10.2400	0.0846	1.8808e-10	1.2780	0.0013	2.391	21.89	3.623e-4	0.7613
Miami Large Office	12.1300	0.1010	1.4420e-10	10.6060	0.0014	3.540	18.87	4.509e-4	1.0998
Phoenix Large Office	8.1900	0.0696	7.8960e-11	7.6310	8.266e-4	3.282	15.70	3.118e-4	0.9744

Table 3.11 The cost proportions for optimal scenarios.

Scenarios	Fuel (%)	Grid Electricity (%)	Capital Investment & Installation (%)	Maintenance (%)	LCC
Atlanta Small Office	23.45	0.92	71.03	4.59	4.81
Chicago Small Office	22.26	0.79	72.28	4.67	5.33
Duluth Small Office	18.63	1.16	75.33	4.87	4.95
Miami Small Office	5.99	0.64	44.42	48.95	16.25
Phoenix Small Office	4.76	0.52	44.27	50.44	15.89
Atlanta Medium Office	22.34	2.06	71.68	3.91	12.74
Chicago Medium Office	20.48	3.72	72.12	3.68	13.03
Duluth Medium Office	15.55	2.85	77.68	3.92	12.18
Miami Medium Office	4.66	5.26	39.64	50.43	20.81
Phoenix Medium Office	4.52	0.66	48.16	46.66	34.46
Atlanta Large Office	4.71	3.10e-4	52.59	42.70	21.91
Chicago Large Office	32.53	9.16	54.28	4.03	3.46
Duluth Large Office	24.00	11.77	60.15	4.08	2.79
Miami Large Office	4.83	20.71	39.37	35.10	5.97
Phoenix Large Office	4.48	7.52	40.64	47.35	8.75

Table 3.12. The electricity dispatch proportions for optimal scenarios.

Scenarios	Prime Mover (%)	Grid Electricity (%)	Renewable and energy storage (%)
Atlanta Small Office	0.3724	0.0365	0.5911
Chicago Small Office	0.3246	0.0324	0.6430
Duluth Small Office	0.3047	0.0480	0.6473
Miami Small Office	0.7302	0.0584	0.2113
Phoenix Small Office	0.7528	0.0498	0.1973
Atlanta Medium Office	0.5783	0.0773	0.3444
Chicago Medium Office	0.4913	0.1352	0.3735
Duluth Medium Office	0.4506	0.1038	0.4456
Miami Medium Office	0.3188	0.2104	0.4708
Phoenix Medium Office	0.5703	0.0474	0.3824
Atlanta Large Office	0.9139	4.381e-5	0.0801
Chicago Large Office	0.5464	0.2671	0.1865
Duluth Large Office	0.4988	0.3006	0.2006
Miami Large Office	0.2560	0.6386	0.1054
Phoenix Large Office	0.4445	0.3864	0.1691

CHAPTER 4. SOCIAL COST AND POLICY INCENTIVES

4.1 Chapter Summary

This chapter examines the social cost of the CCHP-RE-ESS system and evaluates the cost-saving potential of US renewable energy policy incentives. We used the The Air Pollution Emission Experiments and Policy analysis APEEP model to estimate the social damage costs of air pollutants emission in 3110 counties in the US. Different regions have different social costs of emission damage; consequently, the damage or social cost of each emission varies with local conditions. Although the CCHP-RE-ESS can reduce impact, its emissions are closer to the users or cities, which may suffer higher unit social damage costs. For conventional energy generation, power plants are scattered in different regions, and their energy-related emission social damages are allocated to other regions rather than the local area. We used plant data from the eGRID dataset and simulated all 8000 power plants and corresponding regional emissions damage costs in a more accurate way. Results show that the social cost for conventional energy is about 2-3 times higher than the CCHP-RE-ESS. Accordingly, since the cost of CCHP-RE-ESS is higher than conventional energy, we added policy incentive submodules including investment tax credit, accelerated depreciation, 100-percent bonus depreciation, and a low-interest loan to evaluate the cost-saving potential of these policies. Our simulations show that there is an average of about 40% cost reduction for the CCHP-RE-ESS system by current US renewable policy incentives. Tax credit and 100% bonus depreciation contribute to the all percentage of savings, while the low-interest loan increased the LCC by about 30%. By adopting these policies, the CCHP-RE-ESS cost for large office can be reduced to a competitive LCC as

compared to conventional energy generation. Although the reduced LCC for the small and medium office is still higher than conventional energy generation, the LCC differences can give local policymaker ideas about how to provide further incentives based on the local CCHP-RE-ESS performance. Besides, if the social cost is considered, the resulted LCC of 50% of distributed energy generation scenarios are cost-competitive as compared to conventional energy generation.

4.2 Methodology

4.2.1 Social Cost of Emissions

Energy-related emissions can cause devastating impacts and damages [108]. These impacts can cost individuals, families, businesses, and governments hundreds of billions of dollars through rising health care costs, increased food prices, increased taxes, and more [109]. The social cost of emission is a measure of the economic harm from those damages. In economics, the social cost is called an externality. The externality is defined as the cost or benefit that affects a party who did not choose to incur that cost or benefit [110]. Externalities can be both positive or negative. In the energy production industry, a negative externality or cost occurs since fossil fuel energy produces fails to consider the social cost of emissions from power production (most often relating to fossil fuel combustion). In this research, we examined the negative externalities caused by air emission of the energy generation

4.2.1.1 The Regional Social Cost of Emissions

We used the Air Pollution Emissions Experiments and Policy (APEEP) model [111] to evaluate the monetized emissions damage cost. We also considered the social cost of carbon emissions or carbon equivalent, which is $42 per metric ton CO_2 [112]. APEEP is designed to calculate the marginal damages emissions on a dollar-per-ton basis. Damages include adverse effects on human health, reduced yields of crops, harvest timing, reductions in visibility, enhanced depreciation of human-made materials and damages due to lost recreation services. The APEEP has nearly 10,000 emission sources in the United States. There are six pollutant emissions measured by the U.S. Environmental Protection Agency, including sulfur dioxide (SO_2), volatile organic compounds (VOC_s), nitrogen

oxides (NO_x), fine particulate matter ($PM_{2.5}$), coarse particulate matter (PM_{10}), and ammonia (NH_3).

There are four types of emissions sources simulated by the APEEP model: ground-level area sources (including mobile and non-point sources), low-point sources (effective height of less than 250 meters), mid-point level sources (effective height between 250 and 500 meters), and high-point sources (effective height greater than 500 meters). The model evaluates the social cost based on 3110 area sources or counties. APEEP aggregates emissions from ground-level area sources, low point sources, and mid-level point sources in each of the 3110 counties in the lower 48 states. Also, high point sources are treated at the plant level (conventional energy). For distributed CCHP-RE-ESS system, the emissions are treated as the low-point sources.

To evaluate damages of six air pollutants, the model first calculates total damages from all reported emissions. Then the model adds one ton of one pollutant at one source to baseline emissions and reevaluates the monetized damages. The difference between the two calculations is the marginal damages. Secondary pollutants are also considered, such as fine particulate matter and ozone (formed by six air pollutants). We used the AP3 version of the APEEP model, and all dollar values reported in AP3 2018 U.S. dollars. We then converted this into 2019 dollars. According to the Bureau of Labor Statistics, (the consumer price index) the 2019 prices are 2.25% higher than average prices throughout 2018 [113].

We used the ArcGIS [114] to plot and visualize the regional simulations (social cost for different emissions). Figure 4.1 shows the marginal cost of six pollutants for the U.S. mainland. For each city, we averaged the damage cost of its counties. The detailed damages

for six pollutants in Atlanta, Chicago, Duluth, Miami, and Phoenix are reported in Table 4.1.

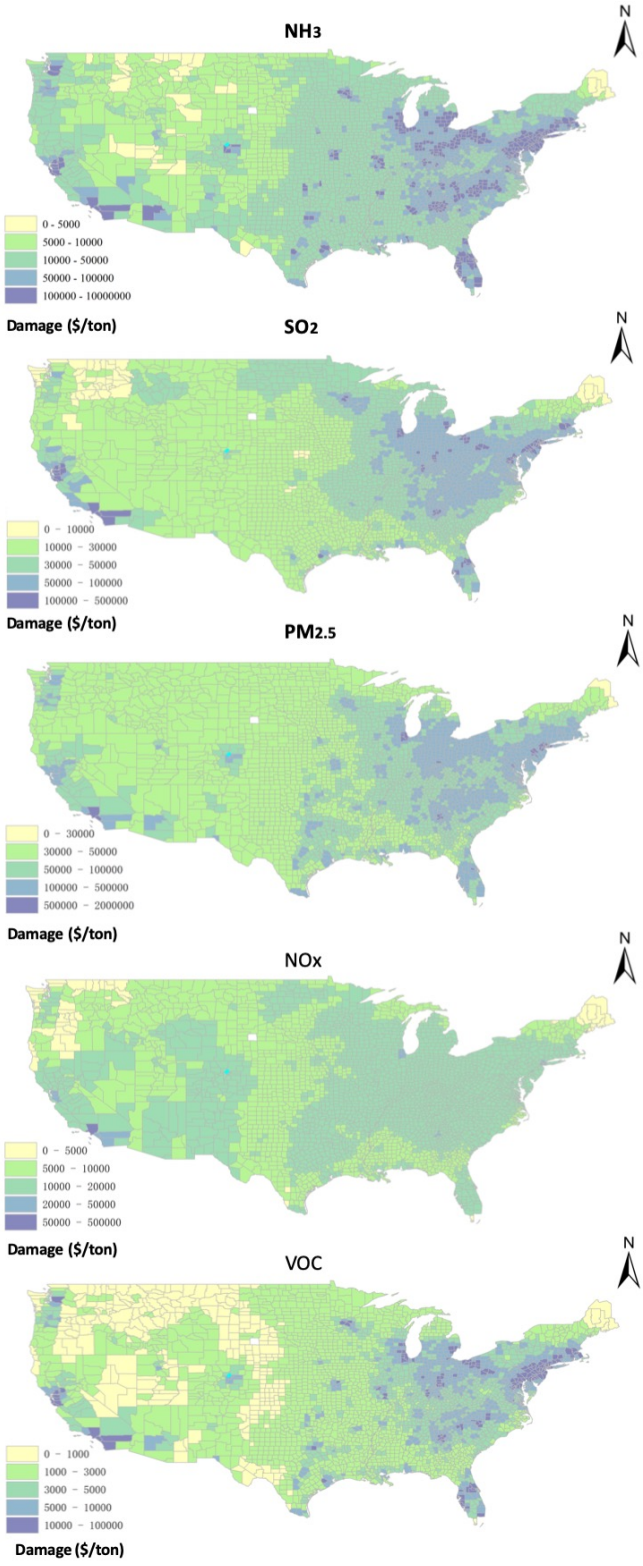

Figure 4.1. The regional social cost for pollutants.

Table 4.1. The social cost of emissions.

Cities	Counties Name	NH_3 ($/kg)	SO_2 ($/kg)	$PM_{2.5}$ ($/kg)	NO_x ($/kg)	VOC ($/kg)
Atlanta	Fulton, Dekalb	484	147	582	53	26
Chicago	Cook, DuPage	696	173	798	63	36
Duluth	St Louis	12	40	32	10	1
Miami	Dude	136	63	194	20	9
Phoenix	Maricopa	102	44	150	33	7

4.2.1.2 The Social Cost of Grid Electricity

For gird electricity, different power transmission regions have different energy mixes. To calculate the social cost of grid emission, we used the emission date from The Emissions & Generation Resource Integrated Database (eGRID) [115]. The eGRID is a comprehensive source of data on the air pollutant emissions of almost all power plants generated in the United States. The emissions in eGRID include carbon dioxide, nitrogen oxides, sulfur dioxide, and carbon dioxide equivalent (i.e., for methane and nitrous oxide). The eGRID data also include plant location in the various counties.

The power generation and distribution are not based on strict geographical boundaries, and it is based on the transmission system. Hence, we used the NERC region for electricity impact from each region. The NERC region refers to a region designated by the North American Electric Reliability Corporation (NERC). NERC defines the Bulk-Power System as the electric power generation facilities combined with the high-voltage

transmission system, which together create and transport electricity around North America. The ten NERC region map, names, and their acronyms for eGRID are displayed in Appendix B. The cities and corresponding NERCs region are shown in Table 4.2.

Table 4.2. Cities and corresponding NERC regions.

Cities	NERC Region
Atlanta	SERC
Chicago	RFC
Duluth	MISO
Miami	FRCC
Phoenix	WECC

For convention energy generation, which is centralized and far from end-users, the transmission over long distances creates power losses. eGRID output emission rates do not account for any line losses between the points of consumption and the points of generation. According to eGRID, they estimate grid gross loss percentages for each U.S. interconnect power grid, and the average loss is 4.48%.

The social cost of NERC region emission is calculated in dollar per-kilowatt hour base by Equation 4.1. The damage cost of each pollutant is the overall damage cost of this pollutant of all power plants in this region divided by the overall electricity generated. To incorporate the eGRID data into APEEP, we used the AP2 version of the model, and all social costs are reported in year 2000 dollars. The 2019 dollar is 49.11% higher than 2000 based on inflation data and we converted the social costs of emission into 2019 dollars. The social cost of each city grid is reported in Table 4.3 in $ per kWh base.

$$\boldsymbol{MD_{i,r} = \frac{\sum E_{i,j,r} \times SC_{i,j,r}}{\sum P_{i,j,r}} \times (1 + PT_{loss})}$$ **Equation 4.1**

Where $MD_{i,r}$ is the marginal damage cost of i-th pollutant in r-th NREC region, $E_{i,j,r}$ is the emission (kg) of i-th pollutant emission of j-th power plant in the r-th region. $SC_{i,j,r}$ is the social cost (dollar) of i-th pollutant emission of j-th power plant in the r-th region. $P_{i,j,r}$ overall electricity generation of i-th pollutant emission of the j-th power plant in the r-th region. PT_{loss} is the average power of US transmission loss.

Table 4.3. The social cost of grid electricity.

Cities	**CO_2 ($/kWh)**	**NH_3 ($/kWh)**	**SO_2 ($/kWh)**	**NO_x ($/kWh)**	**$PM_{2.5}$ ($/kWh)**	**VOC ($/kWh)**
Atlanta	0.0392	NA	0.0577	0.0019	0.0025	NA
Chicago	0.0532	NA	0.0695	0.0026	0.0061	NA
Duluth	0.0405	NA	0.0754	0.0038	0.0041	NA
Miami	0.0351	NA	0.0425	0.00085	0.0036	NA
Phoenix	0.0289	NA	0.0056	0.0024	0.00076	NA

4.2.2 Current Policy Incentives

We reviewed all the US market-based policies for the development of clean energy. In the U.S., most energy policy incentives take the form of financial incentives. Examples include tax breaks, tax reductions, tax exemptions, rebates, loans, and specific funding. In the following session, we evaluated the cost-saving potential of investment tax credit,

bonus depreciation and low-interest loan for the distributed CCHP-RE-ESS with various technologies combinations.

4.2.2.1 Investment Tax Credit

The tax credit is one of the leading methods to stimulate renewable energy development. On the consumer side, the Investment Tax Credit (ITC) reduces federal income taxes for qualified tax-paying owners based on dollars of capital investment in businesses or consumers can receive a 30% tax credit on renewable energy systems, called the energy investment tax credit (ITC). To be more specific, the ITC can provide: (1) 30% tax credit for solar, (2) $1,500 per 0.5 kW for fuel cells and wind; (3) 10% tax credit for microturbines ($200 per kW) and CHP systems. The IRS states that battery storage systems are eligible for this credit when a solar electric generation system charges the batteries. For this work, we assumed that the investor has the investor have enough tax load to absorb the tax credit and deduction.

4.2.2.2 Accelerated Depreciation Schedule and 100% Bonus Depreciation

Depreciation is an accounting method of allocating the cost of a tangible or physical asset over its useful life or life expectancy. Depreciation in the U.S. tax code allows companies to claim the loss of asset value as a noncash expense, which may be deducted from taxable income and this decreases the annual income tax. The depreciation per year formula is shown in Equation 4.2 below. The method of depreciation in the U.S. is known as the Modified Accelerated Cost Recovery System (MACRS). MACRS sets the time period over, which an asset is depreciated and the percent of depreciation per year. A nonrenewable power facility typically falls into either the 15- or 20-year depreciation

schedule; however, with accelerated depreciation, the assets of a renewable energy facility may be placed on the five-year schedule where tax benefits occur earlier in the project lifetime.

$$\textbf{Depreciation Per Yea Formula} = \frac{(\textbf{Cost of Asset} - \textbf{Salvage Value})}{\textbf{Useful Life of Asset}} \quad \textbf{Equation 4.2}$$

Under the federal tax code, renewable energy systems and the CHP system qualify for a 5-year Modified Accelerated Cost-Recovery System (MACRS) depreciation schedule. The Modified Accelerated Cost Recovery System (MACRS), established in 1986, is a method of depreciation in which a business' investments in certain tangible property are recovered, for tax purposes, over a specified time period through annual deductions. This is favorable to investors because of the time value of money that is associated with inflation, where an after-tax dollar is worth more today than in the future. Since its establishment in 1986, MACRS has assigned a five-year useful life to most renewable energy technologies including solar, wind, geothermal, fuel cells, combined heat and power (CHP), microturbines, renewable energy generation technologies that are part of small electric power facilities and certain biomass-fueled technologies.

The Tax Cuts and Jobs Act of 2017 [116] increased bonus depreciation to 100% for these technologies that were acquired and placed in service after September 27, 2017, and before January 1, 2023. In addition, the 100 percent bonus depreciation can be deducted in the first year. Accelerated depreciation can make a large difference in income tax since federal income tax rates for corporations run at about 35% (before 2018), and 21 percent (after 2018) reduced by the Tax Cuts and Jobs Act in 2018 [117]. We assumed that all tax benefits would be used by the investor.

4.2.2.3 Low-Cost Debt Financing

The distributed energy generation is capital intensive, and investors often feel the risk to invest in such capital intensive technologies. Making low-cost financing available is a good way of promoting CCHP-RE-ESS by reducing the risk and reducing centralized conventional energy production methods. However, the cost of debt or interest is a significant portion of the investment cost. A key goal of financing is to reduce monthly payments so that energy savings can cover all or most of the payment. One way to achieve this is to lengthen the loan term (20-year loan). The other major factor is whether the program can provide a low-interest rate. A low rate can not only reduce the loan payment cost but also help customers feel that they are getting a cheaper deal. Rates over 7 percent to 8 percent appear to hurt a program's success.

Financing CCHP-RE-ESS projects via capital raised through public markets (public capital) offers the potential to substantially increase the availability and lower the cost of investment that is critical to continued growth. The public capital vehicles generally include Asset-backed securities (ABSs), which are comprised of payments on assets such as mortgages, auto loans, and student debt, investment pools such as master limited partnerships (MLPs), real estate investment trusts (REITs) [118]. We assumed that the CCHP-RE-ESS project is qualified to get the lowest available interest loan such as a 3% interest rate and a 20-year debt term (by ABS). The loan usually requires monthly payoff. Equation 4.3 calculates the monthly repayment on the loan.

$$\boldsymbol{M = \frac{P \times (\frac{r}{12}) \times (1 + \frac{r}{12})^{12 \times t}}{(1 + \frac{r}{12})^{12 \times t} - 1}} \qquad \textbf{Equation 4.3}$$

Where M is a monthly payment, P is the amount of load, r is the interest, t is the time of loan in years.

4.2.3 The After-policy Life Cycle Cost

Equation 4.4 calculates the LCC after policy incentives. The after-policy life cycle cost is equal to the sum of the annual loan payment, fuel price, and operational cost minus the tax credit and bonus deprecation saving. All monetary values are in constant 2019 dollars in present net worth over 20 years of system lifetime and a 7% discount rate [107]. We assumed all tax credit, and deprecation saving is deducted in the first year, and the company can absorb these savings.

$$\boldsymbol{LCC = \sum \frac{M \times 12 + F + O}{(1 + r)^{i} \times 20} - TC_{savings} - MCAR_{savings}} \qquad \textbf{Equation 4.4}$$

Where LCC is the annual life cycle cost, M is the monthly payment of the loan, F is the annual payment of fuel price, O is the annual operational cost, TC is tax credit saving, and MCAR is accelerated depreciation savings. All are expressed in dollars per ft^2.

4.3 Results and Discussion

4.3.1 Social Cost Comparison

The social cost of CCHP-RE-ESS for different scenarios (building types and locations) are shown in Figure 4.2 below. The social cost of CCHP-RE-ESS with their optimal technologies combination and their corresponding sizes is much lower than the social cost of conventional energy. The small office and medium offices have more than 60 percent higher social cost reduction by adopting the CCHP-RE-ESS system. The social cost reduction for large offices varies with building locations (i.e., 30-80% reduction). For each building type, the lowest social cost of the CCHP-RE-ESS is the large office in Atlanta, medium office in Phoenix, and a small office in Duluth, respectively. The large office in Atlanta has the lowest social cost compared to the large office in other locations.

Although market-based regulations do not currently include social cost, and our rationale for estimation of the social cost is to show the potential economic impact of considering it. In the U.S., there are about 5.6 million commercial buildings that have 87 billion square feet of floor space, and this number will is expected to reach 126.1 billion square feet by 2050 [119]. If we assumed the annual social cost of conventional energy is one dollar more than distributed energy (per ft^2) according to the simulation results, the CCHP-RE-ESS system can reduce social damage by at least 100 billion dollars in the future.

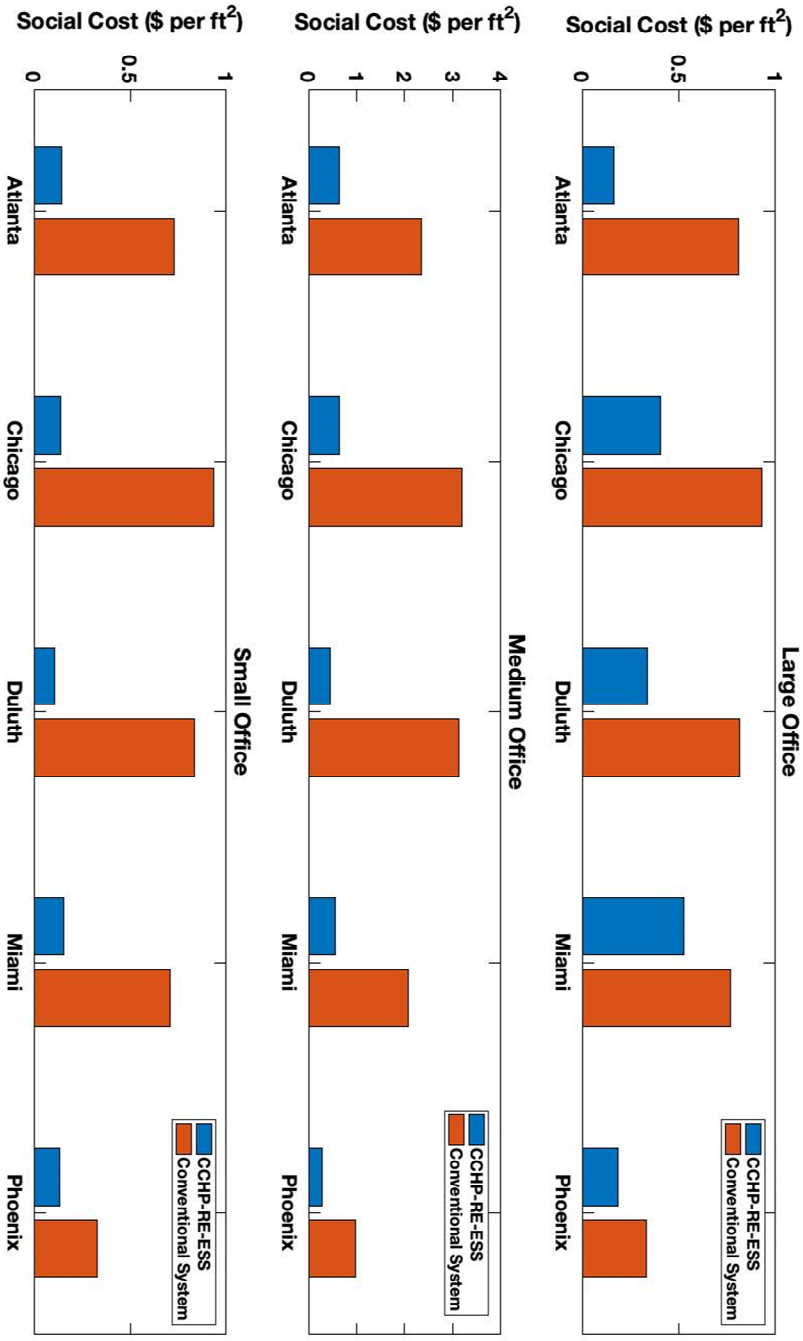

Figure 4.2. The social cost for CCHP-RE-ESS versus conventional energy.

4.3.2 Cost Savings Potential

As shown in Figure 4.3 below, current policy incentives (include tax credit, MACRS, and 100% bonus depreciation) can reduce the CCHP-RE-ESS cost by 20-60%. For the small and large office with a microturbine-based CCHP-RE-ESS system, the after-incentive cost is competitive to conventional energy generation. On the other hand, the after-incentive cost of the fuel cell-based system is still much higher than conventional energy generation, which means more aggressive policies are required to fuel cell-based system cost-competitive. For the medium office, the after-incentive cost is the highest among the three commercial building types, and it is still higher than conventional energy generation for both microturbine-based and fuel cell-based systems. The detailed cost reduction of policy incentives is shown in Table 4.4 and Table 4.5 below. The depreciation accounts for about 60-80% of overall cost savings. On the other hand, the long-term 3% interest loan can increase the overall LCC by 18-28%.

As stated in section 4.1, the social cost of the conventional energy system is much higher than the distributed CCHP-RE-ESS. Figure 4.4 shows the combined LCC (the social cost and after-policy LCC) for different energy generation systems. As shown, the resulted combined LCC for large office in Duluth and medium office in Chicago for CCHP-RE-ESS is equivalent to combined LCC of conventional energy generation. The CCHP-RE-ESS combined LCCs for Chicago large office, Atlanta medium office, Atlanta small office, Chicago small office and Duluth small office are only slightly (less than 10%) higher than conventional energy supply. However, the combined LCC for the fuel cell system is still higher due to the high capital cost.

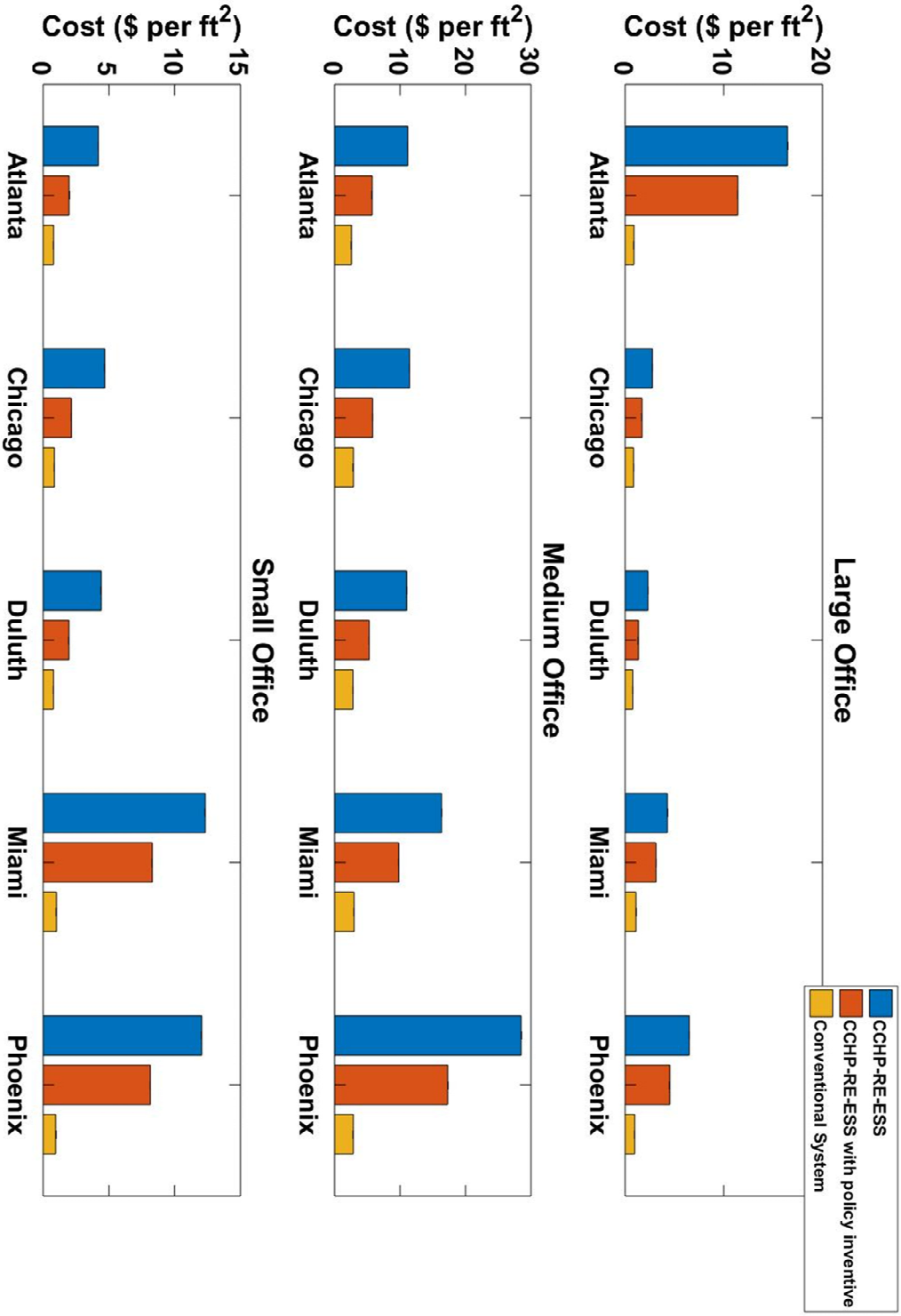

Figure 4.3. The after-policy life cycle cost.

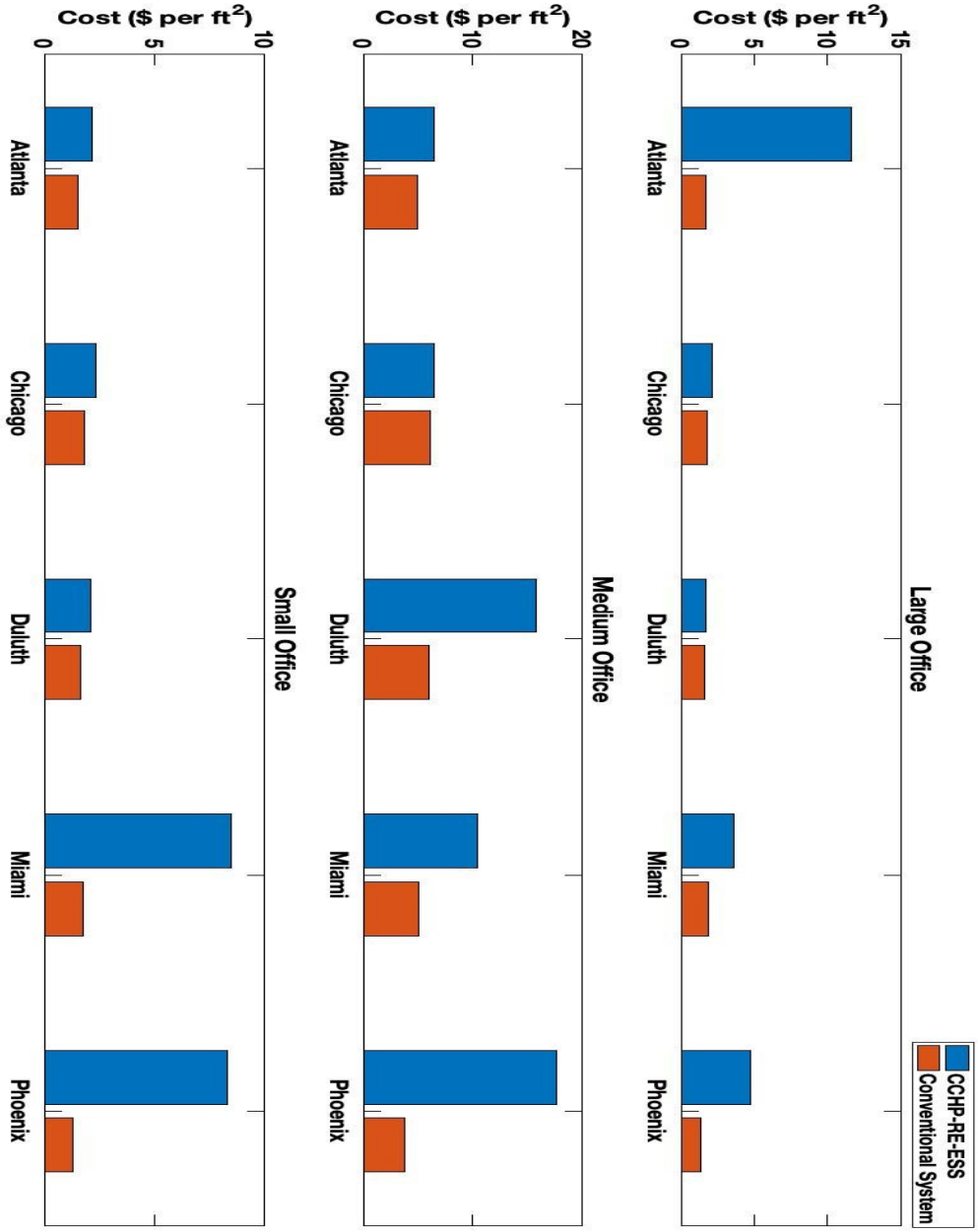

Figure 4.4. The after-policy LCC combined with the social cost.

Table 4.4. The cost saving proportions.

Scenarios	Tax credit (%)	depreciation (%)
Atlanta Small Office	38.37	61.63
Chicago Small Office	39.53	60.47
Duluth Small Office	39.49	60.51
Miami Small Office	20.25	79.75
Phoenix Small Office	19.17	80.83
Atlanta Medium Office	28.23	71.77
Chicago Medium Office	29.26	70.74
Duluth Medium Office	30.23	69.77
Miami Medium Office	33.66	6634
Phoenix Medium Office	23.63	76.37
Atlanta Large Office	14.58	85.42
Chicago Large Office	21.26	78.74
Duluth Large Office	2305	76.95
Miami Large Office	19.67	80.33
Phoenix Large Office	18.76	81.24

Table 4.5. The low-interest loans impact on life cycle cost.

Scenarios	Loan (%)
Atlanta Small Office	0.2689
Chicago Small Office	0.2719
Duluth Small Office	0.2792
Miami Small Office	0.1937
Phoenix Small Office	0.1932
Atlanta Medium Office	0.2795
Chicago Medium Office	0.2715
Duluth Medium Office	0.2847
Miami Medium Office	0.2126
Phoenix Medium Office	0.2009
Atlanta Large Office	0.1880
Chicago Large Office	0.2241
Duluth Large Office	0.2407
Miami Large Office	0.1616
Phoenix Large Office	0.1811

CHAPTER 5. CONCLUSIONS AND FUTURE WORK

5.1 Major Conclusion

In this research, we developed a parametric life cycle assessment framework that can evaluate and find the environmental and economic trade-offs of CCHP-RE-ESS. The model can find the best combination of technologies and their corresponding sizes. The parametric LCA framework illustrates how LCA impacts and costs change. The input parameters are adjustable and allow the needs of scenario-specific (specific technology, size, location, temperature, policy, etc.). By using the parametric LCA framework, we evaluated the distributed energy for various trigeneration technologies at various geographic regions and conventional energy environmental and economic impact. We also evaluated the social cost of the CCHP-RE-ESS system compared to conventional energy via the APEEP model and ArcGIS. Besides, we evaluated the policy incentive cost-saving potentials under current corporate accounting standards. Based on simulation results, key findings are:

- The parametric LCA framework is more accurate than conventional LCA and shows how and why the impact change with the inputs.
- With the help of MDO, we can find the best combination of technologies and their corresponding sizes for distributed CCHP-RE-ESS based on various energy demand profiles.

- The distributed CCHP-RE-ESS energy generation can primarily reduce the environmental impact as compared to the conventional energy system. However, the life cycle cost is higher, especially for fuel cell-based system.

- The social cost of conventional energy is much higher than of CCHP-RE-ESS.

- Although current green energy policies can primarily reduce the cost of distributed CCHP-RE-ESS, for most situations, the life cycle cost is still higher especially for SOFC based CCHP-RE-ESS. However, if the social cost of energy-related emissions is considered, 50% of building energy supply scenarios for the distributed CCHP-RE-ESS are cost-competitive as compared to conventional energy.

Overall, the distributed CCHP-RE-ESS is a more efficient and environmentally friendly way to meet the increasing urban energy demand. The parametric model developed by this research can help users find the optimal techno-economic distributed energy solutions. It can also help policymakers understand the effectiveness of current clean energy policies and issue more reasonable and customizable incentives in the local areas.

5.2 Future Work

1. **Integrating hybrid operation strategy switching between following electrical load and following the thermal load**

   In some scenarios, the thermal demand (cooling and heating) is high during summertime, follow thermal load will cause electricity being generated. Adopting the hybrid operational strategy and thermal storage will help deal with this problem.

2. **Additional tri-generation technologies**

   Other system configurations could be used to produce heat and electrical energy. For example, PV thermal hybrid systems and geothermal for heating production. Electrical vehicle for electrical energy storage and cost-saving (vehicle to grid).

3. **Integration of technologies and their synergy effect**

   In this research, we only evaluate one technology for each system component (prime mover, renewable energy, and energy storage). The integration of technologies may have better benefits. For example, the integration of microturbine and fuel cells can adjust heat to power ratio. The integration of solar and wind can increase renewable penetration and reliability.

4. **The network effect of the distributed energy**

   The distributed energy generation system simulated in this research is only for matching the energy demand of a single building. Future research studies can evaluate the network effect when different distributed energy generation are connected together for 100 percent off-grid. The decentralized and distributed network can be evaluated for resiliency and reliability of energy supply.

APPENDIX A： APPENDIX FOR CHAPTER 2

A.1 The eGRID states emission.

Table A1. Emissions inventory for conventional energy generation.

	State annual NO_x total output emission rate (lb/MWh)	State ozone season NO_x total output emission rate (lb/MWh)	State annual SO_2 total output emission rate (lb/MWh)
Georgia	0.446	0.334	0.359
Minnesota	0.670	0.661	0.582
Florida	0.546	0.560	0.374
Arizona	0.625	0.603	0.238
Illinois	0.357	0.395	0.954
	State annual CO_2 total output emission rate (lb/MWh)	State annual CH_4 total output emission rate (lb/MWh)	State annual N_2O total output emission rate (lb/MWh)
Georgia	1,001.754	0.086	0.013
Minnesota	1,012.670	0.123	0.018
Florida	1,024.205	0.077	0.010
Arizona	932.225	0.067	0.011
Illinois	811.318	0.048	0.012

Table A2. States energy mix.

	State annual coal generation (MWh)	State annual oil generation (MWh)	State annual gas generation (MWh)
Georgia	37,890,475	211,845	52,862,465
Minnesota	23,206,289	30,705	8,929,398
Florida	39,429,468	2,820,303	158,459,723
Arizona	30,403,392	51,595	34,182,808
Illinois	59,337,802	69,503	17,480,439
	State annual nuclear generation (MWh)	State annual hydro generation (MWh)	State annual biomass generation (MWh)
Georgia	34,480,662	1,901,511	4,573,416
Minnesota	13,860,816	1,208,502	2,182,426
Florida	29,320,022	174,551	6,098,942
Arizona	32,377,477	7,226,393	214,378
Illinois	98,607,038	132,834	467,012
	State annual wind generation (MWh)	State annual solar generation (MWh)	State annual geothermal generation (MWh)
Georgia	0	880,923	0
Minnesota	10,491,209	10,107	0
Florida	0	223,983	0
Arizona	541,582	3,737,659	0
Illinois	10,663,434	48,810	0

	State annual other fossil generation (MWh)	State annual other unknown/ purchased fuel generation (MWh)	
Georgia	**97,549**	**3,429**	
Minnesota	**0**	**117,023**	
Florida	**23,790**	**1,675,646**	
Arizona	**0**	**0**	
Illinois	**207,080**	**423,431**	

Table A.3. Impact inventory for system components.

Impact Category	Unit	Multi-Si PV cell (per m^2)	Microturbine (per kW)	Li-ion battery cell (per kg)	Adsorption Chiller (per kW)	Inverter (per kW)
Ozone depletion	**kg CFC-11 eq**	**4.7693E-05**	**1.89967E-05**	**6.3636E-07**	**3.72917E-05**	**6.6561E-06**
Global warming	**kg CO_2 eq**	**173.953458**	**190.3087847**	**6.41465413**	**271.2705182**	**31.1787285**
Smog	**kg O_3 eq**	**9.79148779**	**11.59496839**	**0.56887029**	**19.82413536**	**2.00151049**
Acidification	**kg SO_2 eq**	**1.01633508**	**1.678366186**	**0.10303713**	**3.164068861**	**0.34095161**
Eutrophication	**kg N eq**	**1.07595406**	**1.567197925**	**0.14962786**	**4.461569199**	**0.58419795**
Ecotoxicity	**CTUe**	**1709.27264**	**8487.352687**	**826.128015**	**22743.04756**	**3226.82907**
Fossil fuel depletion	**MJ surplus**	**172.826352**	**165.3910461**	**7.55189103**	**238.0838595**	**43.0615754**

A.2 The solar PVs mathematical model

The plane of the incident (POA) is the effective irradiance on the plane of array, it is dependent upon sun position, irradiance components, solar array orientation, etc. Mathematically, POA (A1) irradiance is:

$$\boldsymbol{E_{POA} = E_b + E_g + E_d} \qquad \textbf{(A1)}$$

Where E_b (kW/m^2) is the POA beam component, E_g (kW/m^2) is the POA ground-reflected component, and E_d (kW/m^2) is the POA sky-diffuse component.

The plane of array (POA) beam component of irradiance is calculated by adjusting the direct normal irradiance (DNI*)* by the angle of incidence (AOI) in the following equation (Equation A2 and Equation A3):

$$\mathbf{E_b = DNI \times \cos(AOI)} \qquad \textbf{(A2)}$$

$$\mathbf{AOI = \cos - 1[\cos(\theta z)\cos(\theta_T) + \sin(\theta z)\sin(\theta_T)\cos(\theta_A - \theta_A, array)]} \qquad \textbf{(A3)}$$

Where θ_A and θ_z are the solar azimuth and zenith angles, respectively. θ_T and $\theta_{A,\,array}$ are the tilt and azimuth angles of the array, respectively.

Eg is calculated as a function of the irradiance on the ground or global horizontal irradiance (GHI), the reflectivity of the ground surface, known as albedo, and the tilt angle of the surface, $\theta_{T,surf}$(A4):

$$\mathbf{Eg = GHI \times albedo \times \frac{(1 - \cos(\theta_{T,surf}))}{2}} \qquad \textbf{(A4)}$$

The PV DC power model is shown in A5. There are two variables: effective irradiance and PV cell temperature. Effective irradiance is the total plane of array (POA) irradiance adjusted for the angle of incidence. In a general sense, it can be thought of as the irradiance that is "available" to the PV array for power conversion.

$$P_{mp} = \frac{E_e}{E_0} P_{mp0}[1 + \gamma(T_c - T_0)] \qquad \textbf{(A5)}$$

Where E_0 and T_0 are reference irradiance(1000W/m^2)and reference temperature (25℃), respectively. γ is the temperature correction for maximum power (P_{mp}).

APPENDIX B：APPENDIX FOR CHAPTER 3

B.1 Energy Demand Profiles for Different Building Types and Locations

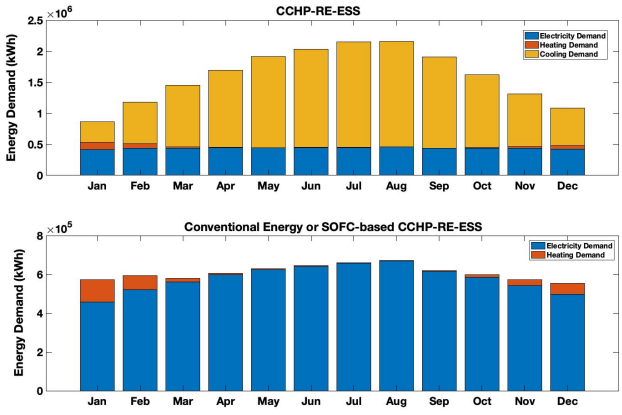

Large office

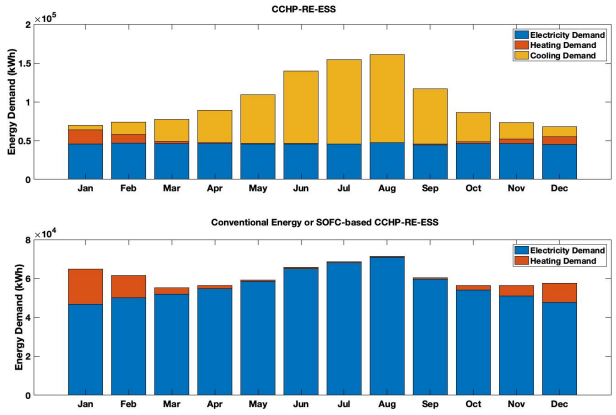

Medium office

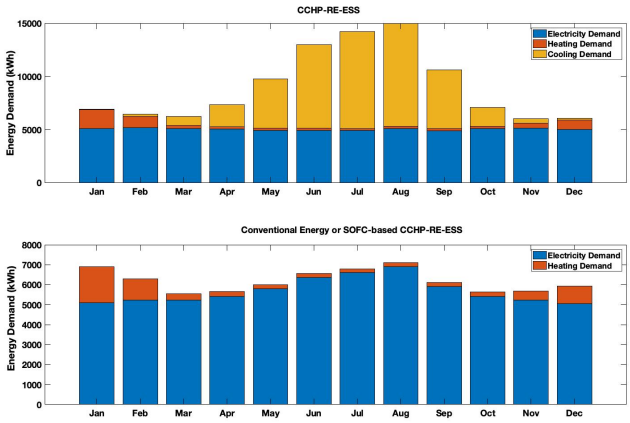

Small office

Figure B.1. The office energy demand profile in Atlanta.

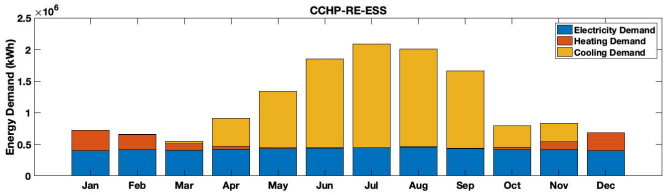

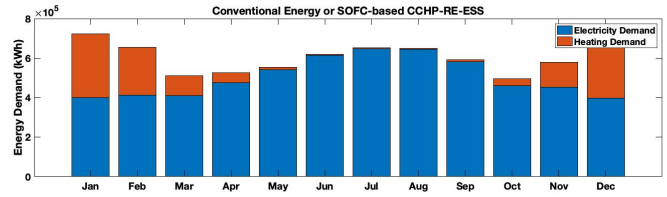

Large office

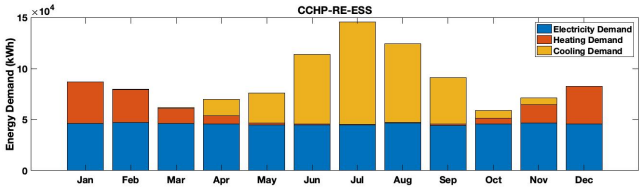

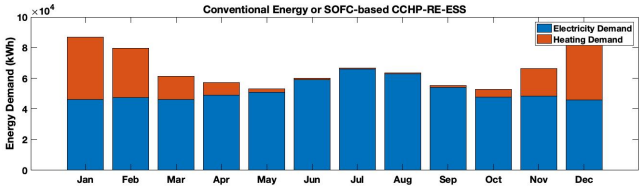

Medium office

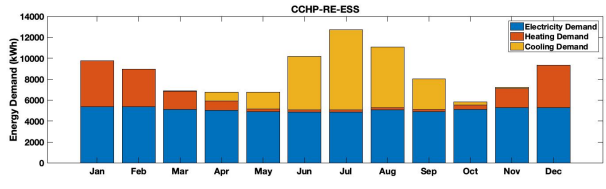

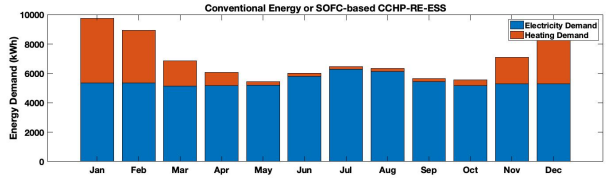

Small office

Figure B.2. The office energy demand profile in Chicago.

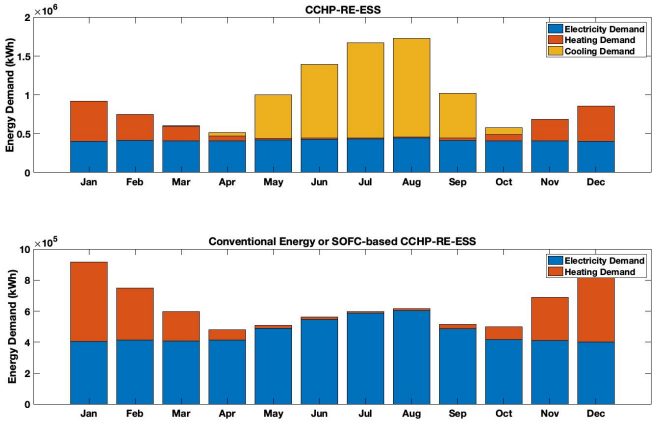

Large office

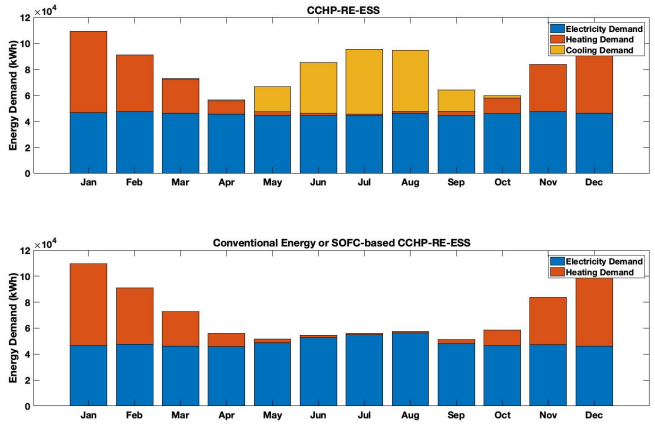

Medium office

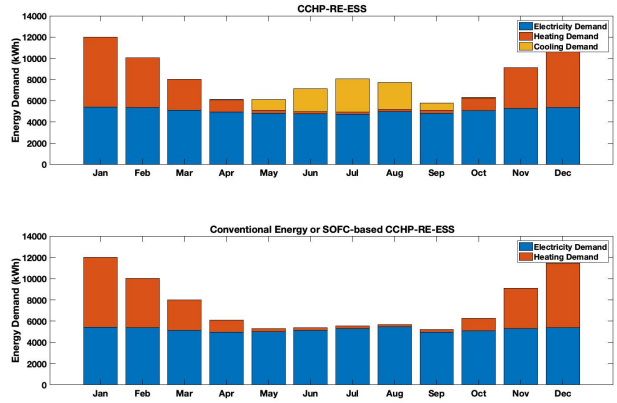

Small office

Figure B.3. The office energy demand profile in Duluth.

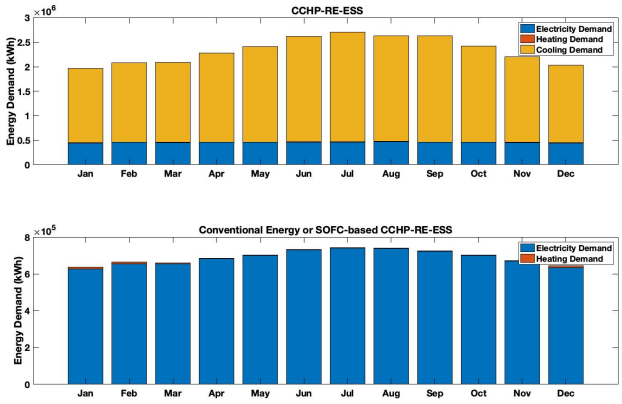

Large office

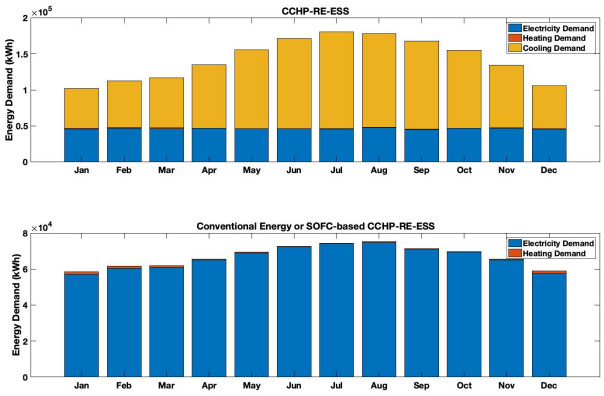

Medium office

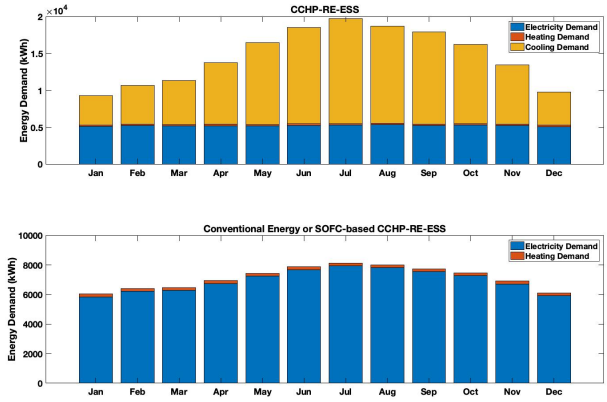

Small office

Figure B.4. The office energy demand profile in Miami.

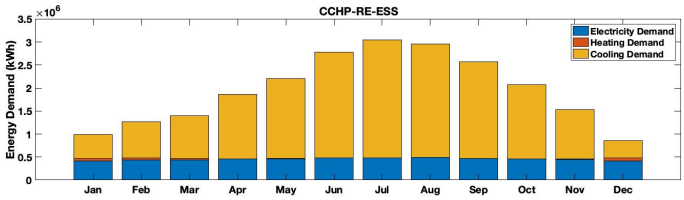

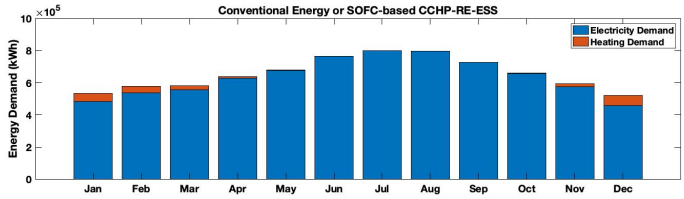

Large office

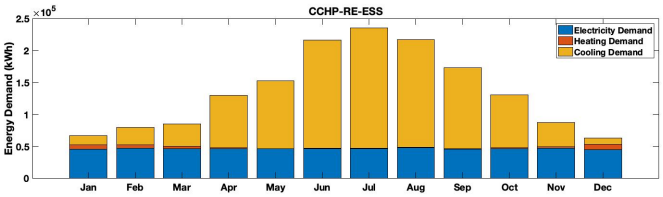

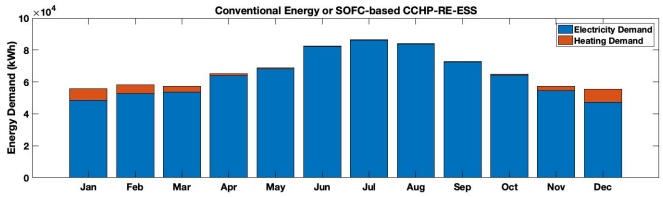

Medium office

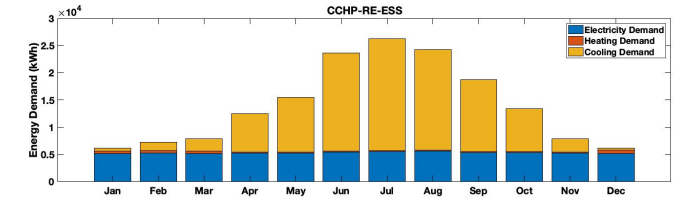

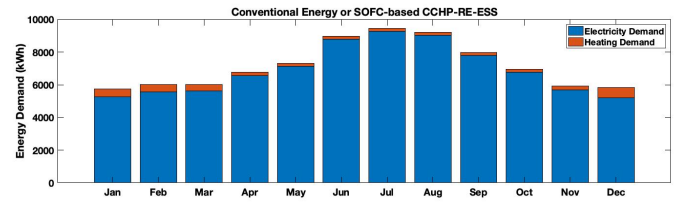

Small office

Figure B.5. The office energy demand profile in Phoenix.

B.2 Small Wind Turbine Product Summary

Manufacturer: SD Wind Energy, Ltd.

Wind Turbine Model: SD6 (240 VAC, 1-phase, 60 Hz)

Certification Number: SWCC-11-04

The above-identified Small Wind Turbine is certified under the ICC– SWCC Small Wind Turbine Certification Program to be in conformance with the AWEA Small Wind Turbine Performance and Safety Standard (AWEA 9.1–2009). For the ICC-SWCC Certificate visit: www.smallwindcertification.org. This report summarizes the results of testing and certification of the SD Wind Energy SD6 turbine in accordance with AWEA Standard 9.1-2009. The KW6 is a 3-blade, downwind, horizontal axis wind turbine with a swept area of 23.7 m^2 . The tested and certified system was comprised of the KW6 turbine on a 9 m (29.5 ft) monopole tower, an SMA Wind Interface and Aurora Power One 6 kW grid tie inverter. Power Performance, Duration and Safety & Function testing were conducted by TUV-NEL at their Myres Hill test site in East Kilbride, Scotland.

Power Performance testing was conducted from February 1, 2011 to February 7, 2011. Duration testing was conducted from February 1, 2011 to August 2, 2011. Acoustic testing was performed on June 16, 2011 by Sgurr Energy in Lumb, Lancashire, UK. This turbine has been granted certification to the Microgeneration Certification Scheme by TUV-NEL (Certification number TUV 0008).

B.2.1 Turbine Ratings

The DS3000 performance testing was conducted in accordance with Section 2 of AWEA Standard 9.1-2009. The resulting turbine ratings tabulated graphical Annual Energy Production (AEP), and graphical and tabulated power curve are given below.

Table B.1. DS3000 performance rating.

AWEA Rated Annual Energy @ 5m/s	8950 kWh
AWEA Rated Sound Level	43.1 dB(A)
AWEA Rated Power @ 11m/s	5.2kW
Peak Power @ 17m/s	5.1kW

B.2.2 Power Curve

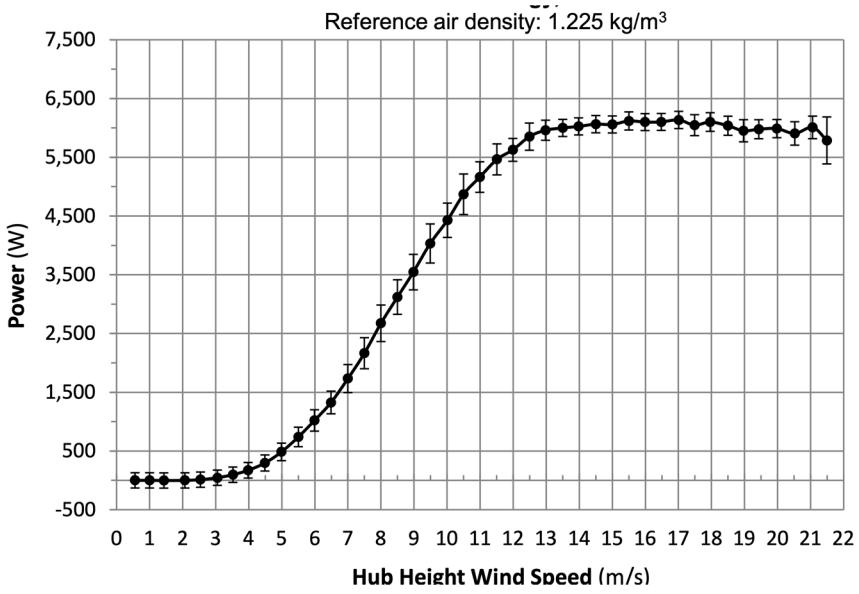

Figure B.6. The hub height wind speed.

B.3 Impact Inventory for System Components

Table B.2. Environmental impact inventory for system components.

Impact Category	Unit	ACAES (per kW)	SOFC (per kW)	Wind Turbine (per kW)
Ozone depletion	kg CFC-11 eq	5.47613E-05	0.00011699	2.86659E-05
Global warming	kg CO2 eq	595.4473794	1080.64492	325.9784596
Smog	kg O3 eq	37.70151085	70.7958747	20.3369757
Acidification	kg SO2 eq	4.288458065	10.2716508	1.513628856
Eutrophication	kg N eq	4.611485616	6.85118767	2.002571315
Carcinogenics	CTUh	0.000435136	0.00041937	0.000242828
Non carcinogenics	CTUh	0.000919907	0.00105426	0.000331913
Respiratory effects	kg PM2.5 eq	1.029161025	1.61281738	0.435591676
Ecotoxicity	CTUe	24442.10708	36136.6436	79602.3376
Fossil fuel depletion	MJ surplus	490.0025011	1059.19254	249.2472089

APPENDIX C: APPENDIX FOR CHAPTER 4

C.1 NERC Region

Figure C.1. The NERC region map.

Table C.1. The NERC region acronym and names for eGRID.

NERC Region	NERC Name
ASCC	Alaska Systems Coordinating Council
FRCC	Florida Reliability Coordinating Council
HICC	Hawaiian Islands Coordinating Council
MRO	Midwest Reliability Organization
NPCC	Northeast Power Coordinating Council
RFC	Reliability First Corporation
SERC	SERC Reliability Corporation
SPP	Southwest Power Pool
TRE	Texas Regional Entity
WECC	Western Electricity Coordinating Council

C.2 Federal Clean Energy Policy

C.2.1 Investment Tax Credit

- Implementing Sector:
  - Federal
- Category:
  - Financial Incentive
- State:
  - Federal
- Incentive Type:
  - Corporate Tax Credit
- Administrator:
  - U.S. Internal Revenue Service
- Expiration Date:
  - Varies by technology, see below
- Eligible Renewable/Other Technologies:
  - Solar Water Heat, Solar Space Heat, Geothermal Electric, Solar Thermal Electric, Solar Thermal Process Heat, Solar Photovoltaics, Wind (All), Geothermal Heat Pumps, Municipal Solid Waste, Combined Heat & Power, Fuel Cells using Non-Renewable Fuels, Tidal, Wind (Small), Geothermal Direct-Use, Fuel Cells using Renewable Fuels, Microturbines
- Applicable Sectors:
  - Commercial, Industrial, Investor-Owned Utility, Cooperative Utilities, Agricultural

- Incentive Amount:
  - 30% for solar, fuel cells, wind
  - 10% for geothermal, microturbines and CHP
- Maximum Incentive:
  - Fuel cells: $1,500 per 0.5 kW
  - Microturbines: $200 per kW
  - Small wind turbines placed in service 10/4/08 - 12/31/08: $4,000
    Small wind turbines placed in service after 12/31/08: no limit
    All other eligible technologies: no limit
- Eligible System Size:
  - Small wind turbines: 100 kW or less
  - Fuel cells: 0.5 kW or greater
  - Microturbines: 2 MW or less
  - CHP: 50 MW or less*
- Equipment Requirements:
  - Fuel cells, microturbines and CHP systems must meet specific energy-efficiency criteria

    Small wind turbines must meet the performance and quality standards set forth by either the American Wind Energy Association Small Wind Turbine Performance and Safety Standard 9.1-2009 (AWEA), or the International Electrotechnical Commission 61400-1, 61400-12, and 61400-11 (IEC)
  - ***Note: The Consolidated Appropriations Act, signed in December 2015, included several amendments to this credit which applied only to solar technologies and***

PTC-eligible technologies. However, the Bipartisan Budget Act of 2018 reinstated this tax credit for the remaining technologies that have historically been eligible for the credit.

- Name:
  - 26 USC § 48
- Name:
  - Instructions for IRS Form 3468
- Name:
  - IRS Form 3468
- Name:
  - H.R. 1892 (Bipartisan Budget Act of 2018)
- Date Enacted:
  - 02/09/2018

C.2.2 MACRS + 100 Tax Bonus

- Implementing Sector:
  - Federal
- Category:
  - Financial Incentive
- State:
  - Federal
- Incentive Type:

- Corporate Depreciation

- Administrator:
  - U.S. Internal Revenue Service
- Start Date:
  - 01/26/1986
- Eligible Renewable/Other Technologies:
  - Solar Water Heat, Solar Space Heat, Geothermal Electric, Solar Thermal Electric, Solar Thermal Process Heat, Solar Photovoltaics, Wind (All), Biomass, Geothermal Heat Pumps, Municipal Solid Waste, Combined Heat & Power, Fuel Cells using Non-Renewable Fuels, Landfill Gas, Tidal, Wave, Ocean Thermal, Wind (Small), Geothermal Direct-Use, Anaerobic Digestion, Fuel Cells using Renewable Fuels, Microturbines
- Applicable Sectors:
  - Commercial, Industrial, Agricultural
  - ***Note: The Tax Cuts and Jobs Act of 2017 increased bonus depreciation to 100% for qualified property acquired and placed in service after September 27, 2017 and before January 1, 2023.*** Under the federal Modified Accelerated Cost-Recovery System (MACRS), businesses may recover investments in certain property through depreciation deductions. The MACRS establishes a set of class lives for various types of property, ranging from three to 50 years, over which the property may be depreciated. A number of renewable energy technologies are classified as five-year property (26 USC § 168(e)(3)(B)(vi)) under the MACRS,

which refers to 26 USC § 48(a)(3)(A), often known as the energy investment tax credit or ITC to define eligible property. Such property currently includes*:

- a variety of solar-electric and solar-thermal technologies
- fuel cells and microturbines
- geothermal electric
- direct-use geothermal and geothermal heat pumps
- small wind (100 kW or less)
- combined heat and power (CHP)
- the provision which defines ITC technologies as eligible also adds the general term "wind" as an eligible technology, extending the five-year schedule to large wind facilities as well.

- Name:
  - 26 USC § 168
- Effective Date:
  - 1986

- Name
  - 26 USC § 48

- Name:
  - The Tax Cuts and Jobs Act of 2017
- Date Enacted:
  - 12/22/2017

APPENDIX D: MATLAB CODE

D.1 Main Simulation

```
% Multi-disciplinary Design Optimization

clear;
clc;

% MSB: microturbine solar batteries
% MSC: microturbine solar CAES
% MWB: microturbine wind batteries
% MWC: microturbine wind CAES
% FSB: SOFC solar batteries
% FSC: SOFC solar CAES
% FWB: SOFC wind batteries
% FWC: SOFC wind CAES

                  run initiation % read building energy demand, weather data, solar and
wind output, etc.


                   disp('microturbine-solar-battery is running (1)')

                   run parametric_simulation_MSB    % parametric simulation

                   save('Results/microturbine-solar-battery for atlanta medium office
Result(1)')    %save


                  run initiation
                   disp('microturbine-solar-CAES is running  (2)')

                   run parametric_simulation_MSC


                   save('Results/microturbine-solar-CAES for atlanta medium office
Result(2)')

                   run initiation
                   disp('microturbine-wind-battery is running  (3)')

                   run parametric_simulation_MWB


                   save('Results/microturbine-wind-battery for atlanta medium office
Result(3)')

                  run initiation
                   disp('microturbine-wind-CAES is running  (4)')
```

```
                    run parametric_simulation_MWC


                    save('Results/microturbine-wind-CAES for atlanta medium office
Result(4)')

                    run initiation
                    disp('fuelcell-solar-battery is running  (5)')

                    run parametric_simulation_FSB


                    save('Results/fuelcell-solar-battery  for atlanta medium office
Result(5)')

                    run initiation
                    disp('fuelcell-solar-CAES is running (6)')

                     run parametric_simulation_FSC

                    save('Results/fuelcell-solar-CAES for atlanta medium office
Result(6)')

                    run initiation
                    disp('fuelcell-wind-battery is running  (7)')

                    run  parametric_simulation_FWB


                    save('Results/fuelcell-wind-battery for atlanta medium office
Result(7)')

                    run initiation
                    disp('fuelcell-wind-CAES is running (8)')

                    run  parametric_simulation_FWC


                    save('Results/fuelcell-wind-CAES for atlanta medium office
Result(8)')
```

Published with MATLAB® R2016b

D.2 Initiation for Simulation

```
% Initiation

clear;
clc;

% 1. building local weather

% 1.1 load building energy demand


%   load('duluth_new_medium_office_demand.mat') ;
%  load('atlanta_new_large_office_demand.mat')
 load('atlanta_new_medium_office_demand.mat')
% load('atlanta_new_small_office_demand.mat')
%  load('chicago_new_medium_office_demand.mat')
%  load('miami_new_medium_office_demand.mat')
%  load('pheonix_new_medium_office_demand.mat')

% office charaterization
medium_office_area_ft2 = 17878.86;
medium_office_roof_area_m2 = 1660;
floor_area_ft2=medium_office_area_ft2;
roof_area_m2 = medium_office_roof_area_m2;

% large_office_area_ft2 = 498588;  %building type
% large_office_roof_area_m2 = 3860;
%
% floor_area_ft2=large_office_area_ft2;
% roof_area_m2 = large_office_roof_area_m2;

% small_office_area_ft2 = 5500.36;
% small_office_roof_area_m2 = 511;
%
% floor_area_ft2=small_office_area_ft2;
% roof_area_m2 = small_office_roof_area_m2;


% 1.2 load solar and wind

load('atlanta_solar_power.mat')  ;
%  load('duluth_solar_power.mat')  ;
%  load('chicago_solar_power.mat')  ;
% load('miami_solar_power.mat')  ;
%  load('phoenix_solar_power.mat')  ;


load('atlanta_wind_power.mat')  ;
% load('duluth_wind_power.mat')  ;
% load('chicago_wind_power.mat')  ;
```

```
% load('miami_wind_power.mat')  ;
% load('phoenix_wind_power.mat')  ;

One_hour_wind_power_kW=wind_power_atlanta_mediumoffice_kW;  % change wind for different
building type

% 2. Emission Impact Inventory

load('Traci_inventory.mat');

load EIO02.mat;

load('grid_and_turbine_emission.mat')

run simapro_system_impact_inventory
run grid_impact_inventory

grid_Global_Warming_Air_impact = nosystem_Global_Warming_Air_impact_atlanta;
grid_Acidification_Air_impact = nosystem_Acidification_Air_impact_atlanta;
grid_HH_Particulate_Air_impact = nosystem_HH_Particulate_Air_impact_atlanta;
grid_Eutrophication_Air_impact = nosystem_Eutrophication_Air_impact_atlanta;
grid_Eutrophication_Water_impact=nosystem_Eutrophication_Water_impact_atlanta;
grid_Ozone_Depletion_Air_impact=  nosystem_Ozone_Depletion_Air_impact_atlanta;
grid_Smog_Air_impact = nosystem_Smog_Air_impact_atlanta;
grid_Ecotox_impact = nosystem_Ecotox_impact_atlanta;
grid_fuel_depletion_impact = nosystem_fuel_depletion_impact_atlanta;
grid_HumanHCancer_impact = nosystem_HumanHCancer_impact_atlanta;
grid_HumanHNonCancer_impact = nosystem_HumanHNonCancer_impact_atlanta;
grid_water_consuption_gal = nosystem_water_consuption_gal_atlanta;

run electricity_and_gas_price

eletricity_unit_price = atlanta_electricity_price;
nature_gas_unit_price = atlanta_naturegas_pirce;

% 3. Annual Operation Simulation for CCHP-RE-ESS

load('capston_turbine_output.mat')
load('fuel_cell_output.mat')
run find_max_demand_and_output.m
run choose_max_microturbine_size;
run choose_max_fuelcell_size;

% 4. Choose turbine size based on following the thermal load

run choose_max_battery_size;

run choose_max_CAES_size;
```

Published with MATLAB® R2016b

D.3 Parametric Simulation: An Example of SOFC-Solar PVs-Li-ion Batteries

```
op = 0;
os = 0;
for op = 0:10:round(0.8*roof_area_m2/10)*10 % solar PVs sizes

    for os = 0:210:round(battery_max_capacity_kWh/210)*210 % bateries sizes

              disp([op os])

      run following_hourly_thermal_load_FSB   % following the thermal load

      run calculate_operation_emission_and_water_FC % emission in operation

      run Calculate_productandOM_EIO_FSB % impact in manufacturing stage

      run LCIA_FSB  % evaluate the environmental impact

      run LCC_FSB  % evaluate the economic cost

    end


end
```

Published with MATLAB® R2016b

D.4 LCC: An Example of SOFC-Solar PVs-Li-ion Batteries

```
oc = 0; %no chiller for fuel cell
oe = max(thermal_demand_FC_kWh);

%Maintanance and Operation

%Turbine
% https://www.energy.gov/sites/prod/files/2016/09/f33/CHP-Microturbines_0.pdf
% 1.2cent/kWh
maintanance_price_machine = sum(current_turbine_elec_FC_kW)*55*10E-3;

%Solar and storage
% file:///Users/junchenyan/Downloads/7556-52022-1-PB.pdf 10$per kwper year
 maintanance_price_solar_and_energy_storage = round(os/210)*50*10+op*3;

annual_total_maintenance_cost =
maintanance_price_machine+maintanance_price_solar_and_energy_storage;


% Capital Cost
% Energy Storage
energy_storage_unit_price_dollar = 400;
energy_storage_price = os * energy_storage_unit_price_dollar ;

% Solar Panel  3$per watt
solar_panel_unit_price_dollar = 3;
solar_price = op * 200* solar_panel_unit_price_dollar ;

%AC/DC Inverter 1$per watt
%'Electronic capacitor, resistor, coil, transformer, and other inductor manufacturing '
inverter_unit_price_dollar = 1;
inverter_price=op * 200*inverter_unit_price_dollar;

% Adsorption Chiller
adsorption_chiller_price_dollar = 1800*0.284; %dollar per kw
adsorption_chiller_price = adsorption_chiller_price_dollar*oc;

% Microturbine
% microturbine_price_dollar

 microturbine_price = fuelcell_price_dollar;

%Heat Recovery Unit or Heat Exchanger


Heat_recovery_price_dollar = 764/80; %dollarper kw

heat_recovery_price = Heat_recovery_price_dollar*oe;

total_product_price =
energy_storage_price+solar_price+inverter_price+adsorption_chiller_price+microturbine_pri
```

```
ce+heat_recovery_price;

% fuel price   Georgia $1.3/therm   therm is 100000BTU

annual_total_fuel_price = sum(current_fuel_input_FC_kW)* nature_gas_unit_price/293.0711;

% electricity price Georgia

annual_total_electricity_pirce = eletricity_unit_price*sum(current_grid_elec_kW);

% annual cost per ft2
system_LCC(op/10+1,os/210+1) = annual_total_electricity_pirce/floor_area_ft2 +
annual_total_maintenance_cost/floor_area_ft2 +
total_product_price/(20*floor_area_ft2)+annual_total_fuel_price/floor_area_ft2;
system_LCC_buffer(op/10+1,os/210+1) = system_LCC(op/10+1,os/210+1)-
total_product_price/(20*floor_area_ft2);
system_LCC_NPV(op/10+1,os/210+1) = total_product_price/(20*floor_area_ft2) + pvvar([ -
system_LCC_buffer(op/10+1,os/210+1) -system_LCC_buffer(op/10+1,os/210+1) -
system_LCC_buffer(op/10+1,os/210+1) -system_LCC_buffer(op/10+1,os/210+1) -
system_LCC_buffer(op/10+1,os/210+1) -system_LCC_buffer(op/10+1,os/210+1) -
system_LCC_buffer(op/10+1,os/210+1) -system_LCC_buffer(op/10+1,os/210+1) -
system_LCC_buffer(op/10+1,os/210+1) -system_LCC_buffer(op/10+1,os/210+1) -
system_LCC_buffer(op/10+1,os/210+1) -system_LCC_buffer(op/10+1,os/210+1) -
system_LCC_buffer(op/10+1,os/210+1) -system_LCC_buffer(op/10+1,os/210+1) -
system_LCC_buffer(op/10+1,os/210+1) -system_LCC_buffer(op/10+1,os/210+1) -
system_LCC_buffer(op/10+1,os/210+1) -system_LCC_buffer(op/10+1,os/210+1) -
system_LCC_buffer(op/10+1,os/210+1) -system_LCC_buffer(op/10+1,os/210+1)],0.07)/-20;
```

Published with MATLAB® R2016b

D.5 LCIA: An Example of SOFC-Solar PVs-Li-ion Batteries

```
%LCIA

cchp_emission = zeros(8,1);
cchp_emission(1) = unit_emissions_turbine_CO2_kgperft2;
cchp_emission(2) = unit_emissions_turbine_NOx_kgperft2;
cchp_emission(6) =  unit_emissions_turbine_VOC_kgperft2;
cchp_impact = lca_impact_matrix' * cchp_emission;
system_total_lca_impact = cchp_impact;

%Annual impact per ft2
system_Global_Warming_Air_impact =
system_total_lca_impact(1)+maintanance_EIO_GW_impact+product_EIO_GW_impact+
grid_Global_Warming_Air_impact*sum(current_grid_elec_kW)/floor_area_ft2+
aquisition_Global_Warming_Air_impact*sum(current_fuel_input_FC_kW)/floor_area_ft2;
system_Acidification_Air_impact =
system_total_lca_impact(2)+maintanance_EIO_AcidAir_impact+product_EIO_AcidAir_impact+grid
_Acidification_Air_impact*sum(current_grid_elec_kW)/floor_area_ft2+aquisition_Acidificati
on_Air_impact*sum(current_fuel_input_FC_kW)/floor_area_ft2;
system_HH_Particulate_Air_impact =
system_total_lca_impact(3)+maintanance_EIO_HHParticle_impcat+product_EIO_HHParticle_impca
t+grid_HH_Particulate_Air_impact*sum(current_grid_elec_kW)/floor_area_ft2+aquisition_HH_P
articulate_Air_impact*sum(current_fuel_input_FC_kW)/floor_area_ft2;
system_Eutrophication_Air_impact =
system_total_lca_impact(4)+maintanance_EIO_EutroAir_impact+product_EIO_EutroAir_impact+gr
id_Eutrophication_Air_impact*sum(current_grid_elec_kW)/floor_area_ft2+aquisition_Eutrophi
cation_Air_impact*sum(current_fuel_input_FC_kW)/floor_area_ft2;
system_Eutrophication_Water_impact =
system_total_lca_impact(5)+maintanance_EIO_EutroWat_impact+product_EIO_EutroWat_impact+gr
id_Eutrophication_Water_impact*sum(current_grid_elec_kW)/floor_area_ft2+aquisition_Eutrop
hication_Water_impact*sum(current_fuel_input_FC_kW)/floor_area_ft2;
system_Ozone_Depletion_Air_impact=
system_total_lca_impact(6)+maintanance_EIO_OzoneDep_impact+product_EIO_OzoneDep_impact+gr
id_Ozone_Depletion_Air_impact*sum(current_grid_elec_kW)/floor_area_ft2+aquisition_Ozone_D
epletion_Air_impact*sum(current_fuel_input_FC_kW)/floor_area_ft2;
system_Smog_Air_impact =
system_total_lca_impact(7)+maintanance_EIO_SmogAir_impact+product_EIO_SmogAir_impact+grid
_Smog_Air_impact*sum(current_grid_elec_kW)/floor_area_ft2+aquisition_Smog_Air_impact*sum(
current_fuel_input_FC_kW)/floor_area_ft2;
system_Ecotox_impact =
sum(system_total_lca_impact(8:13))+maintanance_EIO_Ecotox_impact+product_EIO_Ecotox_impac
t+grid_Ecotox_impact*sum(current_grid_elec_kW)/floor_area_ft2+aquisition_Ecotox_impact*su
m(current_fuel_input_FC_kW)/floor_area_ft2;
system_HumanHCancer_impact =
sum(system_total_lca_impact(15:2:25))+maintanance_EIO_HumanHCancer_impact+product_EIO_Hum
anHCancer_impact+grid_HumanHCancer_impact*sum(current_grid_elec_kW)/floor_area_ft2+aquisi
tion_HumanHCancer_impact*sum(current_fuel_input_FC_kW)/floor_area_ft2;
system_HumanHNonCancer_impact =
sum(system_total_lca_impact(16:2:26))+maintanance_EIO_HumanHNonCancer_impact+product_EIO_
HumanHNonCancer_impact+grid_HumanHNonCancer_impact*sum(current_grid_elec_kW)/floor_area_f
t2+aquisition_HumanHNonCancer_impact*sum(current_fuel_input_FC_kW)/floor_area_ft2;
system_fuel_depletion_impact =
```

```
maintanance_EIO_fuel_depletion_impact+product_EIO_fuel_depletion_impact+(grid_fuel_depletion_impact*sum(current_grid_elec_kW)+aquisition_fuel_depletion_impact*sum(current_fuel_input_FC_kW))/floor_area_ft2;

%Parametric impact
 system_Global_Warming_Air_impact_p(op/10+1,os/210+1) = system_Global_Warming_Air_impact;
 system_Acidification_Air_impact_p(op/10+1,os/210+1) = system_Acidification_Air_impact;
 system_HH_Particulate_Air_impact_p(op/10+1,os/210+1) = system_HH_Particulate_Air_impact;
 system_Eutrophication_impact_p(op/10+1,os/210+1) =
system_Eutrophication_Air_impact+system_Eutrophication_Water_impact;
 system_Ozone_Depletion_Air_impact_p(op/10+1,os/210+1) =
system_Ozone_Depletion_Air_impact;
 system_Smog_Air_impact_p(op/10+1,os/210+1) = system_Smog_Air_impact;
 system_Ecotox_impact_p(op/10+1,os/210+1) = system_Ecotox_impact;
 system_HumanHCancer_impact_p(op/10+1,os/210+1) = system_HumanHCancer_impact;
 system_HumanHNonCancer_impact_p(op/10+1,os/210+1) = system_HumanHNonCancer_impact;
 system_water_consumption_p(op/10+1,os/210+1) = unit_wtrfengy_grid_elec_gal;
 system_fuel_depletion_p(op/10+1,os/210+1) = system_fuel_depletion_impact;

 %Parametric normalization
system_Global_Warming_Air_impact_N(op/10+1,os/210+1) =
system_Global_Warming_Air_impact_p(op/10+1,os/210+1)/24000;
system_Acidification_Air_impact_N(op/10+1,os/210+1) =
system_Acidification_Air_impact_p(op/10+1,os/210+1)/95;
system_HH_Particulate_Air_impact_N(op/10+1,os/210+1) =
system_HH_Particulate_Air_impact_p(op/10+1,os/210+1)/30;
system_Eutrophication_impact_N(op/10+1,os/210+1) =
system_Eutrophication_impact_p(op/10+1,os/210+1)/22;
system_Ozone_Depletion_Air_impact_N(op/10+1,os/210+1) =
system_Ozone_Depletion_Air_impact_p(op/10+1,os/210+1)/0.15;
system_Smog_Air_impact_N(op/10+1,os/210+1) =
system_Smog_Air_impact_p(op/10+1,os/210+1)/1400;
system_fuel_depletion_N(op/10+1,os/210+1)
=system_fuel_depletion_p(op/10+1,os/210+1)/17000;
system_Ecotox_impact_N(op/10+1,os/210+1)  =
system_Ecotox_impact_p(op/10+1,os/210+1)/11074;
system_HumanHCancer_impact_N(op/10+1,os/210+1)  =
system_HumanHCancer_impact_p(op/10+1,os/210+1)/1.0481E-3;
system_HumanHNonCancer_impact_N(op/10+1,os/210+1)  =
system_HumanHNonCancer_impact_p(op/10+1,os/210+1)/1.034E-3;

%LCA single Score
average_us_resident_impact(op/10+1,os/210+1) =
0.68*system_Global_Warming_Air_impact_N(op/10+1,os/210+1)+...
  0.01*system_Acidification_Air_impact_N(op/10+1,os/210+1)+...
  0.02*system_Eutrophication_impact_N(op/10+1,os/210+1) +...
  0.01*system_Ozone_Depletion_Air_impact_N(op/10+1,os/210+1) +...
0.05*system_fuel_depletion_N(op/10+1,os/210+1)+...
  0.05*system_Ecotox_impact_N(op/10+1,os/210+1);
```

Published with MATLAB® R2016b

D.6 The Prices of Electricity and Natural Gas

```
% cent per kwh
% https://www.npr.org/sections/money/2011/10/27/141766341/the-price-of-electricity-in-
your-state

miami_electricity_price = 11.7E-2;
atlanta_electricity_price = 11.1E-2;
chicago_electricity_price =  11.7E-2;
duluth_electricity_price = 10.9E-2;
phoenix_electricity_price = 11.1E-2;

% $ per 1000 cubic feet
% Commercial  and 2018 average
%https://www.eia.gov/dnav/ng/ng_pri_sum_dcu_SGA_m.htm
%natrual gas price for commercial

atlanta_naturegas_pirce = mean( [7.64 8.00    7.90    8.46    8.54    9.00    9.31    8.76
       9.03    8.56    8.04    7.36]);
phoenix_naturegas_pirce = mean( [ 9.20       9.13    9.16    9.23    9.44    9.38    9.14
       8.52    8.00    7.65]);
miami_naturegas_pirce = mean( [ 11.74 11.88   11.34   11.44   11.52   11.69   11.54 12.02
       11.25   11.49   11.19]);
chicago_naturegas_pirce = mean( [ 6.18       6.34    6.54    6.78    10.72   12.29   14.15
       13.52   12.72   8.18    6.42    6.61]);
duluth_naturegas_pirce = mean( [ 6.82 7.56    6.26    7.94    8.51    8.46    7.54    6.02
       6.65]);
```

Published with MATLAB® R2016b

D.7 Following Thermal Load: An Example of SOFC-Solar PVs-Li-ion Batteries

```
% Following Thermal Load

%Initiation
% use this for UNIQUE turbine output
num_of_demand = length(thermal_demand_kWh);
compare = zeros(num_of_demand,1);
current_turbine_elec_FC_kW= zeros(num_of_demand,1);
current_fuel_input_FC_kW = zeros(num_of_demand,1);
current_thermal_output_FC_kW = zeros(num_of_demand,1);
current_grid_elec_kW = zeros(num_of_demand,1);
current_backgrid_elec_kW= zeros(num_of_demand,1);
find_med = zeros(num_of_demand,1);


current_energystore_charge_kW = zeros(num_of_demand,1);
current_energystore_discharge_kW = zeros(num_of_demand,1);
current_wind_output_kW = zeros(num_of_demand,1);
current_solar_output_kW = zeros(num_of_demand,1);

buffer_a = 0;
buffer_b = 0;
buffer_c = 0;
amount_to_be_charge_kW = 0;
amount_to_be_discharge_kW = 0;

current_energystored_kWh = 0;
energy_storage_capacity_kWh = os;
solar_area_m2 = op;
round_trip_efficiency = 0.88;
heat_exchanger_efficincy = 0.8;


for iii = 1: num_of_demand


     compare = thermal_output_FC_kW > thermal_demand_FC_kWh(iii);
     find_med = find(compare);
     index_chosen = find_med(1);
     current_turbine_elec_FC_kW(iii)= elec_output_FC_kW(index_chosen);
     current_fuel_input_FC_kW(iii)= fuel_input_FC_kW(index_chosen);
     current_thermal_output_FC_kW(iii)= thermal_output_FC_kW(index_chosen);

      current_solar_output_kW(iii) = OneHour_Solar_Power_kW(iii)*solar_area_m2;




     buffer_a = elec_demand_FC_kWh(iii)-current_turbine_elec_FC_kW(iii)-
current_solar_output_kW(iii);
```

```
    if buffer_a <= 0   %charge

        current_grid_elec_kW(iii) = 0;
        amount_to_be_charge_kW = abs(buffer_a);
        buffer_b = current_energystored_kWh+amount_to_be_charge_kW;


        if current_turbine_elec_FC_kW(iii) >= elec_demand_FC_kWh(iii)
        useful_current_turbine_elec_FC_kW(iii) = elec_demand_FC_kWh(iii);
        useful_current_solar_output_kW(iii) = 0;

        else
        useful_current_turbine_elec_FC_kW(iii) = current_turbine_elec_FC_kW(iii);
        useful_current_solar_output_kW(iii) =
current_solar_output_kW(iii)+current_turbine_elec_FC_kW(iii)-elec_demand_FC_kWh(iii);

        end

        if buffer_b>=energy_storage_capacity_kWh
            current_energystored_kWh = energy_storage_capacity_kWh;
            current_energystore_charge_kW(iii) = amount_to_be_charge_kW-(buffer_b-
energy_storage_capacity_kWh);
            current_energystore_discharge_kW(iii) = 0;
            current_backgrid_elec_kW(iii) = abs(elec_demand_FC_kWh(iii)-
current_turbine_elec_FC_kW(iii)-current_solar_output_kW(iii)-
current_energystore_charge_kW(iii));

        else
            current_energystored_kWh = buffer_b;
            current_energystore_charge_kW(iii) = amount_to_be_charge_kW;
            current_energystore_discharge_kW(iii) = 0;
            current_backgrid_elec_kW(iii) = abs(elec_demand_FC_kWh(iii)-
current_turbine_elec_FC_kW(iii)-current_solar_output_kW(iii)-
current_energystore_charge_kW(iii));

        end

    else              %discharge

        amount_to_be_discharge_kW = abs(buffer_a);
        buffer_c = current_energystored_kWh-
round_trip_efficiency*amount_to_be_discharge_kW;

        useful_current_turbine_elec_FC_kW(iii) = current_turbine_elec_FC_kW(iii);
        useful_current_solar_output_kW(iii) = current_solar_output_kW(iii);

        if buffer_c <= 0
            current_energystore_charge_kW(iii) = 0;
            current_energystore_discharge_kW(iii) = abs(current_energystored_kWh);
            current_energystored_kWh = 0;
            current_backgrid_elec_kW(iii) = 0;
            current_grid_elec_kW(iii) = elec_demand_FC_kWh(iii)-
current_turbine_elec_FC_kW(iii)-current_solar_output_kW(iii)-
current_energystore_discharge_kW(iii);
```

```
        else
            current_energystore_charge_kW(iii) = 0;
            current_energystore_discharge_kW(iii) = amount_to_be_discharge_kW;
            current_energystored_kWh = buffer_c;
            current_backgrid_elec_kW(iii) = 0;
            current_grid_elec_kW(iii) = elec_demand_FC_kWh(iii)-
current_turbine_elec_FC_kW(iii)-current_solar_output_kW(iii)-
current_energystore_discharge_kW(iii);
        end

    end

end
```

Published with MATLAB® R2016b

D.8 Turbine Emission Calculation

```
%Initiation
wtrfengy_grid_elec_kg  = zeros(num_of_demand,1);
netmeter_wtrfengy_grid_elec_gal= zeros(num_of_demand,1);
emissions_grid_CO2_kg = zeros(num_of_demand,1);
netmeter_emissions_grid_CO2_kg= zeros(num_of_demand,1);
emissions_grid_NOx_kg = zeros(num_of_demand,1);
netmeter_emissions_grid_NOx_kg= zeros(num_of_demand,1);
emissions_turbine_CO2_kg = zeros(num_of_demand,1);
emissions_turbine_NOx_kg = zeros(num_of_demand,1);
emissions_turbine_VOC_kg =zeros(num_of_demand,1);
traditional_wtrfengy_grid_elec_gal=zeros(num_of_demand,1);
traditional_emissions_grid_CO2_kg=zeros(num_of_demand,1);
traditional_emissions_grid_NOx_kg=zeros(num_of_demand,1);

for jjj = 1 : num_of_demand

    % CCHP with solar and energy storage

    wtrfengy_grid_elec_gal(jjj) = water_for_energy_galperkWh.*current_grid_elec_kW(jjj);

    emissions_turbine_CO2_kg(jjj) =
turbCO2_emissions_kgperkWh.*current_turbine_elec_kW(jjj);

    emissions_turbine_NOx_kg(jjj) =
turbNOx_emissions_kgperkWh.*current_turbine_elec_kW(jjj);

    emissions_turbine_VOC_kg(jjj) =
turbVOC_emissions_kgperkWh.*current_turbine_elec_kW(jjj);
end


%CCHP system


    unit_emissions_turbine_CO2_kgperft2 = sum(emissions_turbine_CO2_kg)/floor_area_ft2;
    unit_emissions_turbine_NOx_kgperft2 = sum(emissions_turbine_NOx_kg)/floor_area_ft2;
    unit_emissions_turbine_VOC_kgperft2 = sum(emissions_turbine_VOC_kg)/floor_area_ft2;
    unit_wtrfengy_grid_elec_gal = sum(wtrfengy_grid_elec_gal)/floor_area_ft2;
```

Published with MATLAB® R2016b

D.9 LCIA of System Component: An Example of SOFC-Solar PVs-Li-ion Batteries

```
% oc = max(cooling_demand_kwh); %no chiller for fuel cell system
oe = max(thermal_demand_FC_kWh);

product_EIO_GW_impact =
(PV_Global_Warming_Air_impact*op+Battery_Global_Warming_Air_impact*os+...

Inverter_Global_Warming_Air_impact*0.2*op+SOFC_Global_Warming_Air_impact*FC_turbine_size+
...
    HE_Global_Warming_Air_impact*oe)/(20*floor_area_ft2);

product_EIO_AcidAir_impact =
(PV_Acidification_Air_impact*op+Battery_Acidification_Air_impact*os+...

Inverter_Acidification_Air_impact*0.2*op+SOFC_Acidification_Air_impact*FC_turbine_size+..
.
    HE_Acidification_Air_impact*oe)/(20*floor_area_ft2);

product_EIO_HHParticle_impcat =
(PV_HH_Particulate_Air_impact*op+Battery_HH_Particulate_Air_impact*os+...

Inverter_HH_Particulate_Air_impact*0.2*op+SOFC_HH_Particulate_Air_impact*FC_turbine_size+
...
    HE_HH_Particulate_Air_impact*oe)/(20*floor_area_ft2);

product_EIO_EutroAir_impact =
(PV_Eutrophication_Air_impact*op+Battery_Eutrophication_Air_impact*os+...

Inverter_Eutrophication_Air_impact*0.2*op+SOFC_Eutrophication_Air_impact*FC_turbine_size+
...
    HE_Eutrophication_Air_impact*oe)/(20*floor_area_ft2);

product_EIO_EutroWat_impact =
(PV_Eutrophication_Water_impact*op+Battery_Eutrophication_Water_impact*os+...

Inverter_Eutrophication_Water_impact*0.2*op+SOFC_Eutrophication_Water_impact*FC_turbine_s
ize+...
    HE_Eutrophication_Water_impact*oe)/(20*floor_area_ft2);

product_EIO_OzoneDep_impact =
(PV_Ozone_Depletion_Air_impact*op+Battery_Ozone_Depletion_Air_impact*os+...

Inverter_Ozone_Depletion_Air_impact*0.2*op+SOFC_Ozone_Depletion_Air_impact*FC_turbine_siz
e+...
    HE_Ozone_Depletion_Air_impact*oe)/(20*floor_area_ft2);

product_EIO_SmogAir_impact = (PV_Smog_Air_impact*op+Battery_Smog_Air_impact*os+...
    Inverter_Smog_Air_impact*0.2*op+SOFC_Smog_Air_impact*FC_turbine_size+...
    HE_Smog_Air_impact*oe)/(20*floor_area_ft2);
```

```
product_EIO_Ecotox_impact = (PV_Ecotox_impact*op+Battery_Ecotox_impact*os+...
    Inverter_Ecotox_impact*0.2*op+SOFC_Ecotox_impact*FC_turbine_size+...
    HE_Ecotox_impact*oe)/(20*floor_area_ft2);

product_EIO_HumanHCancer_impact =
(PV_HumanHCancer_impact*op+Battery_HumanHCancer_impact*os+...
    Inverter_HumanHCancer_impact*0.2*op+SOFC_HumanHCancer_impact*FC_turbine_size+...
    HE_HumanHCancer_impact*oe)/(20*floor_area_ft2);

product_EIO_HumanHNonCancer_impact =
(PV_HumanHNonCancer_impact*op+Battery_HumanHNonCancer_impact*os+...

Inverter_HumanHNonCancer_impact*0.2*op+SOFC_HumanHNonCancer_impact*FC_turbine_size+...
    HE_HumanHNonCancer_impact*oe)/(20*floor_area_ft2);

product_EIO_fuel_depletion_impact
=(PV_fuel_depletion_impact*op+Battery_fuel_depletion_impact*os+...
    Inverter_fuel_depletion_impact*0.2*op+SOFC_fuel_depletion_impact*FC_turbine_size+...
    HE_fuel_depletion_impact*oe)/(20*floor_area_ft2);

%EIO lCA and Traci Impact for maintanance
final_maintanance = zeros(428,1);

%Input Setup

%Maintanance and Operation
%Maintanance fee per year
% https://www.energy.gov/sites/prod/files/2016/09/f33/CHP-Microturbines_0.pdf
% 1.2cent/kWh zero doller

 maintanance_price_machine = sum(current_turbine_elec_FC_kW)*55*10E-3;
% maintanance_price_machine = 0;
% solar pand 5 dollar per m2 energy storage per year
 maintanance_price_solar_and_energy_storage = round(os/210)*50*10+op*3;
% maintanance_price_solar_and_energy_storage = 0;
final_maintanance(408) = maintanance_price_machine*10E-7 +
maintanance_price_solar_and_energy_storage*10E-7;


%run!
system_input_maintanance = final_maintanance;
run EIOLCA02_maintanance.m

% Emission and Traci Impact

maintanance_finalout_buffer = sum(finalout_maintanance);
maintanance_total_econ = maintanance_finalout_buffer(1); %  $M
maintanance_direct_econ = maintanance_finalout_buffer(2); %  $M

%per year
maintanance_EIO_GW_impact = maintanance_finalout_buffer(31)/floor_area_ft2;

maintanance_EIO_AcidAir_impact = maintanance_finalout_buffer(32)/floor_area_ft2;
```

```
maintanance_EIO_HHParticle_impcat =  maintanance_finalout_buffer(33)/floor_area_ft2;

maintanance_EIO_EutroAir_impact = maintanance_finalout_buffer(34)/floor_area_ft2;

maintanance_EIO_EutroWat_impact = maintanance_finalout_buffer(35)/floor_area_ft2;

maintanance_EIO_OzoneDep_impact = maintanance_finalout_buffer(36)/floor_area_ft2;

maintanance_EIO_SmogAir_impact = maintanance_finalout_buffer(37)/floor_area_ft2;

maintanance_EIO_Ecotox_impact =
(maintanance_finalout_buffer(38)+maintanance_finalout_buffer(41))/2/(20*floor_area_ft2);


maintanance_EIO_HumanHCancer_impact =
(maintanance_finalout_buffer(39)+maintanance_finalout_buffer(42))/2/(20*floor_area_ft2);


maintanance_EIO_HumanHNonCancer_impact =
(maintanance_finalout_buffer(40)+maintanance_finalout_buffer(43))/2/(20*floor_area_ft2);

maintanance_EIO_fuel_depletion_impact  = 0;
```

Published with MATLAB® R2016b

D.10 Main Code for Conventional Energy Generation

```
clear;
clc;

% 1 load building energy demand

 load('atlanta_new_medium_office_demand.mat')
% load('atlanta_new_small_office_demand.mat')
%  load('chicago_new_medium_office_demand.mat')
% load('miami_new_medium_office_demand.mat')
%  load('pheonix_new_small_office_demand.mat')

medium_office_area_ft2 = 17878.86;
medium_office_roof_area_m2 = 1660;
floor_area_ft2=medium_office_area_ft2;
roof_area_m2 = medium_office_roof_area_m2;

% large_office_area_ft2 = 498588;  %building type
% large_office_roof_area_m2 = 3860;
%
% floor_area_ft2=large_office_area_ft2;
% roof_area_m2 = large_office_roof_area_m2;

% small_office_area_ft2 = 5500.36;
% small_office_roof_area_m2 = 511;
%
% floor_area_ft2=small_office_area_ft2;
% roof_area_m2 = small_office_roof_area_m2;

% 2 Grid impact inventory

run grid_impact_inventory

load('Traci_inventory.mat');

run electricity_and_gas_price
run simapro_system_impact_inventory

%3.  gird impact calculation

atlanta_grid_Global_Warming_Air_impact =
sum(elec_demand2_kWh)*nosystem_Global_Warming_Air_impact_atlanta/floor_area_ft2;
atlanta_grid_Acidification_Air_impact=
sum(elec_demand2_kWh)*nosystem_Acidification_Air_impact_atlanta/floor_area_ft2;
atlanta_grid_HH_Particulate_Air_impact=
sum(elec_demand2_kWh)*nosystem_HH_Particulate_Air_impact_atlanta/floor_area_ft2;
atlanta_grid_Eutrophication_Air_impact=
sum(elec_demand2_kWh)*nosystem_Eutrophication_Air_impact_atlanta/floor_area_ft2;
atlanta_grid_Eutrophication_Water_impact=
sum(elec_demand2_kWh)*nosystem_Eutrophication_Water_impact_atlanta/floor_area_ft2;
atlanta_grid_Smog_Air_impact=
```

```
sum(elec_demand2_kWh)*nosystem_Smog_Air_impact_atlanta/floor_area_ft2;
atlanta_grid_Ozone_Depletion_Air_impact=
sum(elec_demand2_kWh)*nosystem_Ozone_Depletion_Air_impact_atlanta/floor_area_ft2;
atlanta_grid_Ecotox_impact=
sum(elec_demand2_kWh)*nosystem_Ecotox_impact_atlanta/floor_area_ft2;
atlanta_grid_fuel_depletion_impact=
sum(elec_demand2_kWh)*nosystem_fuel_depletion_impact_atlanta/floor_area_ft2;
atlanta_grid_HumanHCancer_impact=
sum(elec_demand2_kWh)*nosystem_HumanHCancer_impact_atlanta/floor_area_ft2;
atlanta_grid_HumanHNonCancer_impact=
sum(elec_demand2_kWh)*nosystem_HumanHNonCancer_impact_atlanta/floor_area_ft2;

atlanta_grid_Global_Warming_Air_impact_N  =
sum(elec_demand2_kWh)*nosystem_Global_Warming_Air_impact_atlanta_N/floor_area_ft2;
atlanta_grid_Acidification_Air_impact_N=
sum(elec_demand2_kWh)*nosystem_Acidification_Air_impact_atlanta_N/floor_area_ft2;
atlanta_grid_HH_Particulate_Air_impact_N=
sum(elec_demand2_kWh)*nosystem_HH_Particulate_Air_impact_atlanta_N/floor_area_ft2;
atlanta_grid_Eutrophication_Air_impact_N=
sum(elec_demand2_kWh)*nosystem_Eutrophication_Air_impact_atlanta_N/floor_area_ft2;
atlanta_grid_Eutrophication_Water_impact_N=
sum(elec_demand2_kWh)*nosystem_Eutrophication_Water_impact_atlanta_N/floor_area_ft2;
atlanta_grid_Smog_Air_impact_N=
sum(elec_demand2_kWh)*nosystem_Smog_Air_impact_atlanta_N/floor_area_ft2;
atlanta_grid_Ozone_Depletion_Air_impact_N=
sum(elec_demand2_kWh)*nosystem_Ozone_Depletion_Air_impact_atlanta_N/floor_area_ft2;
atlanta_grid_Ecotox_impact_N=
sum(elec_demand2_kWh)*nosystem_Ecotox_impact_atlanta_N/floor_area_ft2;
atlanta_grid_fuel_depletion_impact_N=
sum(elec_demand2_kWh)*nosystem_fuel_depletion_impact_atlanta_N/floor_area_ft2;
atlanta_grid_HumanHCancer_impact_N=
sum(elec_demand2_kWh)*nosystem_HumanHCancer_impact_atlanta_N/floor_area_ft2;
atlanta_grid_HumanHNonCancer_impact_N=
sum(elec_demand2_kWh)*nosystem_HumanHNonCancer_impact_atlanta_N/floor_area_ft2;

%4. furnace impact calcualtion
% Furnace emission
%furnace CO2 emissions(units: kg CO2/ kWh)

furnace_CO2emissions_kgperkWh =
(120000*0.453592/(1000000*0.000293071*1020))/0.8; %furnace efficiency 0.8

% furnace_NOxemissions_kgperkWh = 0.000424941;
furnace_NOxemissions_kgperkWh = (76*0.453592/(1000000*0.000293071*1020))/0.8;

furnace_VOCemissions_kgperkWh = (5.5*0.453592/(1000000*0.000293071*1020))/0.8;
furnace_SO2emissions_kgperkWh = (0.6*0.453592/(1000000*0.000293071*1020))/0.8;
furnace_CH4emissions_kgperkWh = (7.3*0.453592/(1000000*0.000293071*1020))/0.8;
furnace_N2Oemissions_kgperkWh = (0.64*0.453592/(1000000*0.000293071*1020))/0.8;

    trdl_emissions_furnace_CO2_kg =
furnace_CO2emissions_kgperkWh*sum(heat_demand2_kWh)/floor_area_ft2;

    trdl_emissions_furnace_NOx_kg =
```

```
furnace_NOxemissions_kgperkWh*sum(heat_demand2_kWh)/floor_area_ft2;

    trdl_emissions_furnace_VOC_kg =
furnace_VOCemissions_kgperkWh*sum(heat_demand2_kWh)/floor_area_ft2;

    trdl_emissions_furnace_SO2_kg =
furnace_SO2emissions_kgperkWh*sum(heat_demand2_kWh)/floor_area_ft2;

    trdl_emissions_furnace_CH4_kg =
furnace_CH4emissions_kgperkWh*sum(heat_demand2_kWh)/floor_area_ft2;

    trdl_emissions_furnace_N2O_kg =
furnace_N2Oemissions_kgperkWh*sum(heat_demand2_kWh)/floor_area_ft2;

furnace_emission = zeros(8,1);

furnace_emission(1) =  trdl_emissions_furnace_CO2_kg ;
furnace_emission(2) = trdl_emissions_furnace_NOx_kg;
furnace_emission(3) = trdl_emissions_furnace_SO2_kg;
furnace_emission(4) =  trdl_emissions_furnace_N2O_kg;
furnace_emission(5) =  trdl_emissions_furnace_CH4_kg ;
furnace_emission(6) = trdl_emissions_furnace_VOC_kg;

furnace_impact= lca_impact_matrix' *furnace_emission;

%4 natural gas aquisition for furnace

trdl_aquisition_Global_Warming_Air_impact =
aquisition_Global_Warming_Air_impact*sum(heat_demand2_kWh)*1.08/floor_area_ft2;
trdl_aquisition_Acidification_Air_impact =
aquisition_Acidification_Air_impact*sum(heat_demand2_kWh)*1.08/floor_area_ft2;
trdl_aquisition_HH_Particulate_Air_impact=aquisition_HH_Particulate_Air_impact*sum(heat_d
emand2_kWh)*1.08/floor_area_ft2;
trdl_aquisition_Eutrophication_Air_impact=aquisition_Eutrophication_Air_impact*sum(heat_d
emand2_kWh)*1.08/floor_area_ft2;
trdl_aquisition_Eutrophication_Water_impact=aquisition_Eutrophication_Water_impact*sum(he
at_demand2_kWh)*1.08/floor_area_ft2;
trdl_aquisition_Ozone_Depletion_Air_impact=aquisition_Ozone_Depletion_Air_impact*sum(heat
_demand2_kWh)*1.08/floor_area_ft2;
trdl_aquisition_Smog_Air_impact=aquisition_Smog_Air_impact*sum(heat_demand2_kWh)*1.08/flo
or_area_ft2;
trdl_aquisition_Ecotox_impact=aquisition_Ecotox_impact*sum(heat_demand2_kWh)*1.08/floor_a
rea_ft2;
trdl_aquisition_fuel_depletion_impact=aquisition_fuel_depletion_impact*sum(heat_demand2_k
Wh)*1.08/floor_area_ft2;
trdl_aquisition_HumanHCancer_impact=aquisition_HumanHCancer_impact*sum(heat_demand2_kWh)*
1.08/floor_area_ft2;
trdl_aquisition_HumanHNonCancer_impact=aquisition_HumanHNonCancer_impact*sum(heat_demand2
_kWh)*1.08/floor_area_ft2;
% 5. conventional overall impact

tradl_overall_Global_Warming_Air_impact_atlanta =
furnace_impact(1)+atlanta_grid_Global_Warming_Air_impact+trdl_aquisition_Global_Warming_A
ir_impact;
```

```
tradl_overall_Acidification_Air_impact_atlanta =
furnace_impact(2)+atlanta_grid_Acidification_Air_impact+trdl_aquisition_Acidification_Air
_impact;
tradl_overall_HH_Particulate_Air_impact_atlanta =
furnace_impact(3)+atlanta_grid_HH_Particulate_Air_impact+trdl_aquisition_HH_Particulate_A
ir_impact;
tradl_overall_Eutrophication_Air_impact_atlanta =
furnace_impact(4)+atlanta_grid_Eutrophication_Air_impact+trdl_aquisition_Eutrophication_A
ir_impact;
tradl_overall_Eutrophication_Water_impact_atlanta =
furnace_impact(5)+atlanta_grid_Eutrophication_Water_impact+trdl_aquisition_Eutrophication
_Water_impact;
tradl_overall_Ozone_Depletion_Air_impact_atlanta=
furnace_impact(6)+atlanta_grid_Ozone_Depletion_Air_impact+trdl_aquisition_Ozone_Depletion
_Air_impact;
tradl_overall_Smog_Air_impact_atlanta =
furnace_impact(7)+atlanta_grid_Smog_Air_impact+trdl_aquisition_Smog_Air_impact;
tradl_overall_Ecotox_impact_atlanta =
sum(furnace_impact(8:13))+atlanta_grid_Ecotox_impact+trdl_aquisition_Ecotox_impact;
tradl_overall_fuel_depletion_impact_atlanta =
atlanta_grid_fuel_depletion_impact+trdl_aquisition_fuel_depletion_impact+sum(heat_demand2
_kWh)*1.08*3.6/floor_area_ft2;
tradl_overall_HumanHCancer_impact_atlanta =
sum(furnace_impact(15:2:25))+atlanta_grid_HumanHCancer_impact+trdl_aquisition_HumanHCance
r_impact;
tradl_overall_HumanHNonCancer_impact_atlanta =
sum(furnace_impact(16:2:26))+atlanta_grid_HumanHNonCancer_impact+trdl_aquisition_HumanHNo
nCancer_impact;

tradl_overall_water_impact_atlanta =
sum(elec_demand2_kWh)*nosystem_water_consuption_gal_atlanta/floor_area_ft2;



tradl_overall_Global_Warming_Air_impact_atlanta_N =
furnace_impact(1)/24000+atlanta_grid_Global_Warming_Air_impact_N+trdl_aquisition_Global_W
arming_Air_impact/24000;
tradl_overall_Acidification_Air_impact_atlanta_N =
furnace_impact(2)/95+atlanta_grid_Acidification_Air_impact_N+trdl_aquisition_Acidificatio
n_Air_impact/95;
tradl_overall_HH_Particulate_Air_impact_atlanta_N =
furnace_impact(3)/30+atlanta_grid_HH_Particulate_Air_impact_N+trdl_aquisition_HH_Particul
ate_Air_impact/30;
tradl_overall_Eutrophication_Air_impact_atlanta_N =
furnace_impact(4)/22+atlanta_grid_Eutrophication_Air_impact_N+trdl_aquisition_Eutrophicat
ion_Air_impact/22;
tradl_overall_Eutrophication_Water_impact_atlanta_N =
furnace_impact(5)/22+atlanta_grid_Eutrophication_Water_impact_N+trdl_aquisition_Eutrophic
ation_Water_impact/22;
tradl_overall_Ozone_Depletion_Air_impact_atlanta_N=
furnace_impact(6)/0.15+atlanta_grid_Ozone_Depletion_Air_impact_N+trdl_aquisition_Ozone_De
pletion_Air_impact/0.15;
tradl_overall_Smog_Air_impact_atlanta_N =
furnace_impact(7)/1400+atlanta_grid_Smog_Air_impact_N+trdl_aquisition_Smog_Air_impact/140
```

```
0;
tradl_overall_Ecotox_impact_atlanta_N =
sum(furnace_impact(8:13))/11074+atlanta_grid_Ecotox_impact_N+trdl_aquisition_Ecotox_impac
t/11074;
tradl_overall_fuel_depletion_impact_atlanta_N =
atlanta_grid_fuel_depletion_impact_N+trdl_aquisition_fuel_depletion_impact/19000+sum(heat
_demand2_kWh)*1.08*3.6/floor_area_ft2/19000;
tradl_overall_HumanHCancer_impact_atlanta_N =
sum(furnace_impact(15:2:25))/0.0010481+atlanta_grid_HumanHCancer_impact_N+trdl_aquisition
_HumanHCancer_impact/0.0010481;
tradl_overall_HumanHNonCancer_impact_atlanta_N =
sum(furnace_impact(16:2:26)/0.000034)+atlanta_grid_HumanHNonCancer_impact_N+trdl_aquisiti
on_HumanHNonCancer_impact/0.000034;

%6.single score calculation

average_us_resident_impact_atlanta =
0.68*tradl_overall_Global_Warming_Air_impact_atlanta_N+...
  0.01*tradl_overall_Acidification_Air_impact_atlanta_N+...
  0.02*(tradl_overall_Eutrophication_Water_impact_atlanta_N
+tradl_overall_Ozone_Depletion_Air_impact_atlanta_N)+...
  0.01*tradl_overall_Ozone_Depletion_Air_impact_atlanta_N+...
   0.05*tradl_overall_fuel_depletion_impact_atlanta_N+...
  0.05*tradl_overall_Ecotox_impact_atlanta_N;


tradl_elec_price_atlanta =
sum(elec_demand2_kWh)*atlanta_electricity_price/floor_area_ft2;
tradl_gas_price_atlanta  =
sum(heat_demand2_kWh)*atlanta_naturegas_pirce/(293.0711*floor_area_ft2);
Tradl_overall_cost_atlanta = tradl_elec_price_atlanta+tradl_gas_price_atlanta;
Tradl_overall_cost_atlanta_NPV = pvvar([-Tradl_overall_cost_atlanta -
Tradl_overall_cost_atlanta -Tradl_overall_cost_atlanta -Tradl_overall_cost_atlanta -
Tradl_overall_cost_atlanta -Tradl_overall_cost_atlanta -Tradl_overall_cost_atlanta -
Tradl_overall_cost_atlanta -Tradl_overall_cost_atlanta -Tradl_overall_cost_atlanta -
Tradl_overall_cost_atlanta -Tradl_overall_cost_atlanta -Tradl_overall_cost_atlanta -
Tradl_overall_cost_atlanta -Tradl_overall_cost_atlanta -Tradl_overall_cost_atlanta -
Tradl_overall_cost_atlanta -Tradl_overall_cost_atlanta -Tradl_overall_cost_atlanta -
Tradl_overall_cost_atlanta],0.07)/-20;

run social_cost_apeep.m
Tradl_overall_Scost_atlanta =
Tradl_overall_cost_atlanta+sum(elec_demand2_kWh)*SLCC_grid_unit_atlanta_CO2/floor_area_ft
2+sum(elec_demand2_kWh)*SLCC_grid_unit_atlanta_NH3/floor_area_ft2+sum(elec_demand2_kWh)*S
LCC_grid_unit_atlanta_NOx/floor_area_ft2+sum(elec_demand2_kWh)*SLCC_grid_unit_atlanta_SO2
/floor_area_ft2+sum(elec_demand2_kWh)*SLCC_grid_unit_atlanta_VOC/floor_area_ft2+sum(elec_
demand2_kWh)*SLCC_grid_unit_atlanta_PM25/floor_area_ft2+...

trdl_emissions_furnace_CO2_kg*SLCC_unit_atlanta_CO2+trdl_emissions_furnace_NOx_kg*SLCC_un
it_atlanta_NOx+trdl_emissions_furnace_VOC_kg*SLCC_unit_atlanta_VOC+trdl_emissions_furnace
_SO2_kg*SLCC_unit_atlanta_SO2;
Tradl_overall_Scost_atlanta_NPV = pvvar([-Tradl_overall_Scost_atlanta -
Tradl_overall_Scost_atlanta -Tradl_overall_Scost_atlanta -Tradl_overall_Scost_atlanta -
Tradl_overall_Scost_atlanta -Tradl_overall_Scost_atlanta -Tradl_overall_Scost_atlanta -
```

```
Tradl_overall_Scost_atlanta -Tradl_overall_Scost_atlanta -Tradl_overall_Scost_atlanta -
Tradl_overall_Scost_atlanta -Tradl_overall_Scost_atlanta -Tradl_overall_Scost_atlanta -
Tradl_overall_Scost_atlanta -Tradl_overall_Scost_atlanta -Tradl_overall_Scost_atlanta -
Tradl_overall_Scost_atlanta -Tradl_overall_Scost_atlanta -Tradl_overall_Scost_atlanta -
Tradl_overall_Scost_atlanta],0.07)/-20;

%7 save


save('Results/tradl atlanta medium office')
```

Published with MATLAB® R2016b

D.11 Life Cycle Impact Inventory for All Technologies and System Components

```
clear;
clc;


%nature gas aquisition

aquisition_Global_Warming_Air_impact =0.219663386/10.28;
aquisition_Acidification_Air_impact =0.001903199/10.28;
aquisition_HH_Particulate_Air_impact=9.50076E-05/10.28;
aquisition_Eutrophication_Air_impact =2.67666E-05/10.28;
aquisition_Eutrophication_Water_impact=0/10.28;
aquisition_Ozone_Depletion_Air_impact=  3.75704E-12/10.28;
aquisition_Smog_Air_impact = 0.014570688/10.28;
aquisition_Ecotox_impact = 9.50076E-05/10.28;
aquisition_fuel_depletion_impact = 0.111113299/10.28;
aquisition_HumanHCancer_impact = 2.75807E-10/10.28;
aquisition_HumanHNonCancer_impact = 5.78E-09/10.28;


% wind turbine per kW


wind_Global_Warming_Air_impact =566902.9705/750;
wind_Acidification_Air_impact =   3941.738819/750;
wind_HH_Particulate_Air_impact= 875.672152/750;
wind_Eutrophication_Air_impact =4612.430698/750;
wind_Eutrophication_Water_impact=  0/750;
wind_Ozone_Depletion_Air_impact= 0.076600417/750;
wind_Smog_Air_impact = 45913.43194/750;
wind_Ecotox_impact = 187598680.3/750;
wind_fuel_depletion_impact =766402.9142/750;
wind_HumanHCancer_impact =  0.262043416/750;
wind_HumanHNonCancer_impact =  0.881552652/750;


% SOFC impact per kw

SOFC_Global_Warming_Air_impact =108064.4915/125;
SOFC_Acidification_Air_impact =   1027.165082/125;
SOFC_HH_Particulate_Air_impact= 161.2817375/125;
SOFC_Eutrophication_Air_impact =685.1187674/125;
SOFC_Eutrophication_Water_impact=  0/125;
SOFC_Ozone_Depletion_Air_impact= 0.011698509/125;
SOFC_Smog_Air_impact = 7079.587468/125;
SOFC_Ecotox_impact = 3613664.363/125;
SOFC_fuel_depletion_impact =105919.2541/125;
SOFC_HumanHCancer_impact =  0.041937121/125;
SOFC_HumanHNonCancer_impact = 0.105426072/125;


% PVs multi-Si per m2
```

```
PV_Global_Warming_Air_impact =173.953458;
PV_Acidification_Air_impact =   1.016335082;
PV_HH_Particulate_Air_impact= 0.159713238;
PV_Eutrophication_Air_impact =1.075954064;
PV_Eutrophication_Water_impact=  0;
PV_Ozone_Depletion_Air_impact= 4.76932E-05;
PV_Smog_Air_impact = 9.791487793;
PV_Ecotox_impact =1709.272645;
PV_fuel_depletion_impact =172.8263524;
PV_HumanHCancer_impact =  1.18265E-05;
PV_HumanHNonCancer_impact = 8.34474E-05;

% microgas turbine per kw

MT_Global_Warming_Air_impact =19030.87847/100;
MT_Acidification_Air_impact =  167.8366186/100;
MT_HH_Particulate_Air_impact= 31.7361973/100;
MT_Eutrophication_Air_impact =156.7197925/100;
MT_Eutrophication_Water_impact=  0/100;
MT_Ozone_Depletion_Air_impact= 0.001899668/100;
MT_Smog_Air_impact = 1159.496839/100;
MT_Ecotox_impact =848735.2687/100;
MT_fuel_depletion_impact =16539.10461/100;
MT_HumanHCancer_impact =  0.010174398/100;
MT_HumanHNonCancer_impact =0.029786109/100;

% lithium ion battery per kwh

Battery_Global_Warming_Air_impact =6.414654128*4.831;
Battery_Acidification_Air_impact =  0.103037132*4.831;
Battery_HH_Particulate_Air_impact= 0.012897203*4.831;
Battery_Eutrophication_Air_impact =0.149627861*4.831;
Battery_Eutrophication_Water_impact=  0*4.831;
Battery_Ozone_Depletion_Air_impact= 6.36361E-07*4.831;
Battery_Smog_Air_impact = 0.568870291*4.831;
Battery_Ecotox_impact =826.1280149*4.831;
Battery_fuel_depletion_impact =7.551891027*4.831;
Battery_HumanHCancer_impact =  1.90216E-06*4.831;
Battery_HumanHNonCancer_impact =3.51287E-05*4.831;


% inverter per kw

Inverter_Global_Warming_Air_impact =15589.36427/500;
Inverter_Acidification_Air_impact =  170.4758046/500;
Inverter_HH_Particulate_Air_impact= 23.91864035/500;
Inverter_Eutrophication_Air_impact =292.0989755/500;
Inverter_Eutrophication_Water_impact=  0/500;
Inverter_Ozone_Depletion_Air_impact= 0.003328049/500;
Inverter_Smog_Air_impact = 1000.755243/500;
Inverter_Ecotox_impact =1613414.534/500;
Inverter_fuel_depletion_impact =21530.7877/500;
Inverter_HumanHCancer_impact =  0.005837116/500;
```

```
Inverter_HumanHNonCancer_impact =0.062186314/500;



% ACAES per kw

ACAES_Global_Warming_Air_impact =59544.73794/100;
ACAES_Acidification_Air_impact =  428.8458065/100;
ACAES_HH_Particulate_Air_impact= 102.9161025/100;
ACAES_Eutrophication_Air_impact =  461.1485616/100;
ACAES_Eutrophication_Water_impact =0/100;
ACAES_Ozone_Depletion_Air_impact= 0.00547613/100;
ACAES_Smog_Air_impact = 3770.151085/100;
ACAES_Ecotox_impact = 2444210.708/100;
ACAES_fuel_depletion_impact = 49000.25011/100;
ACAES_HumanHCancer_impact =  0.043513648/100;
ACAES_HumanHNonCancer_impact = 0.091990722/100;



% chiller per kwh capacity

Chiller_Global_Warming_Air_impact = 27127.05182/100;
Chiller_Acidification_Air_impact =  316.4068861/100;
Chiller_HH_Particulate_Air_impact= 49.3889508/100;
Chiller_Eutrophication_Air_impact = 446.1569199/100;
Chiller_Eutrophication_Water_impact = 0/100;
Chiller_Ozone_Depletion_Air_impact= 0.003729167/100;
Chiller_Smog_Air_impact = 1982.413536/100;
Chiller_Ecotox_impact = 2274304.756/100;
Chiller_fuel_depletion_impact = 23808.38595/100;
Chiller_HumanHCancer_impact =  0.011864915/100;
Chiller_HumanHNonCancer_impact = 0.096804184/100;



%heat exchanger per kw base,

HE_Global_Warming_Air_impact = 2.387489058/12.6;
HE_Acidification_Air_impact =  0.010292603/12.6;
HE_HH_Particulate_Air_impact= 0.00328024/12.6;
HE_Eutrophication_Air_impact = 0.00976462/12.6;
HE_Eutrophication_Water_impact = 0/12.6;
HE_Ozone_Depletion_Air_impact= 1.54127E-07/12.6;
HE_Smog_Air_impact = 0.129903023/12.6;
HE_Ecotox_impact = 38.95894127/12.6;
HE_fuel_depletion_impact = 1.408372401/12.6;
HE_HumanHCancer_impact =  1.18903E-06/12.6;
HE_HumanHNonCancer_impact = 1.36475E-06/12.6;
```

Published with MATLAB® R2016b

D.12 Social Cost Inventory

```
%Atlanta County: Fulton, De kalb, 13121,13089
SLCC_unit_atlanta_CO2 = 42/1000;
SLCC_unit_atlanta_NH3 = (451563.761+516956.2344)/2/1000;
SLCC_unit_atlanta_NOx = (52101.63403+53418.88867)/2/1000;
SLCC_unit_atlanta_SO2 = (146905.186+147290.0447)/2/1000;
SLCC_unit_atlanta_VOC = (24971.51318+27912.85327)/2/1000;
SLCC_unit_atlanta_PM25 = (549333.5598+614031.6982)/2/1000;

%Chicago County: Cook, DuPage, 17031,17034

SLCC_unit_chicago_CO2 = 42/1000;
SLCC_unit_chicago_NH3 = (506581+884745.5239)/2/1000;
SLCC_unit_chicago_NOx = (57173.57788+68251.02661)/2/1000;
SLCC_unit_chicago_SO2 = (160760.0369+185277.4363)/2/1000;
SLCC_unit_chicago_VOC = (26771.10742+45734.7002)/2/1000;
SLCC_unit_chicago_PM25 = (588981.7346+1006180.412)/2/1000;

%Duluth County: St Louis, 27137

SLCC_unit_duluth_CO2 = 42/1000;
SLCC_unit_duluth_NH3 = 12208.30933/1000;
SLCC_unit_duluth_NOx = 10481.70752/1000;
SLCC_unit_duluth_SO2 = 39667.68896/1000;
SLCC_unit_duluth_VOC = 1454.856934/1000;
SLCC_unit_duluth_PM25 = 32036.7019/1000;

%Miami County:Dude,12025

SLCC_unit_miami_CO2 = 42/1000;
SLCC_unit_miami_NH3 = 135606.5652/1000;
SLCC_unit_miami_NOx = 20146.5073/1000;
SLCC_unit_miami_SO2 = 62577.13477/1000;
SLCC_unit_miami_VOC = 8822.646729/1000;
SLCC_unit_miami_PM25 = 194102.4834/1000;

%Phoenix County:Maricopa,04013
SLCC_unit_phoenix_CO2 = 42/1000;
SLCC_unit_phoenix_NH3 = 102370.3813/1000;
SLCC_unit_phoenix_NOx = 32681.3855/1000;
SLCC_unit_phoenix_SO2 = 43855.95288/1000;
SLCC_unit_phoenix_VOC = 6815.357666/1000;
SLCC_unit_phoenix_PM25 = 150460.7375/1000;


 %Grid

%Atlanta SERC

SLCC_grid_unit_atlanta_CO2 = 0.022011108*(145.82/100)*(40/35)*1.07;
SLCC_grid_unit_atlanta_NH3 = 0*(145.82/100)*1.07;
```

```
SLCC_grid_unit_atlanta_NOx = 0.001249554*(145.82/100)*1.07;
SLCC_grid_unit_atlanta_SO2 = 0.036988546*(145.82/100)*1.07;
SLCC_grid_unit_atlanta_VOC = 0*(145.82/100);
SLCC_grid_unit_atlanta_PM25 = 0.001600279*(145.82/100)*1.07;

%Chicago RFC

 SLCC_grid_unit_chicago_CO2 = 0.029814521*(145.82/100)*(40/35)*1.07;
SLCC_grid_unit_chicago_NH3 = 0*(145.82/100)*1.07;
SLCC_grid_unit_chicago_NOx = 0.001635588*(145.82/100)*1.07;
SLCC_grid_unit_chicago_SO2 = 0.044551388*(145.82/100)*1.07;
SLCC_grid_unit_chicago_VOC = 0*(145.82/100)*1.07;
SLCC_grid_unit_chicago_PM25 = 0.003914825*(145.82/100)*1.07;

%Duluth  MRO or MISO

 SLCC_grid_unit_duluth_CO2 = 0.022725117*(145.82/100)*(40/35)*1.07;
SLCC_grid_unit_duluth_NH3 = 0*(145.82/100)*1.07;
SLCC_grid_unit_duluth_NOx = 0.002447063*(145.82/100)*1.07;
SLCC_grid_unit_duluth_SO2 = 0.048309879*(145.82/100)*1.07;
SLCC_grid_unit_duluth_VOC = 0*(145.82/100)*1.07;
SLCC_grid_unit_duluth_PM25 = 0.002652246*(145.82/100)*1.07;

%Miami FRCC

 SLCC_grid_unit_miami_CO2 = 0.019683117*(145.82/100)*(40/35)*1.07;
SLCC_grid_unit_miami_NH3 = 0*(145.82/100)*1.07;
SLCC_grid_unit_miami_NOx = 0.000545913*(145.82/100)*1.07;
SLCC_grid_unit_miami_SO2 = 0.027232308*(145.82/100)*1.07;
SLCC_grid_unit_miami_VOC = 0*(145.82/100)*1.07;
SLCC_grid_unit_miami_PM25 = 0.002317758*(145.82/100)*1.07;

%Phoenix AMZN
 SLCC_grid_unit_phoenix_CO2 = 0.016186963*(145.82/100)*(40/35)*1.07;
SLCC_grid_unit_phoenix_NH3 = 0*(145.82/100)*1.07;
SLCC_grid_unit_phoenix_NOx = 0.001564671*(145.82/100)*1.07;
SLCC_grid_unit_phoenix_SO2 = 0.003609196*(145.82/100)*1.07;
SLCC_grid_unit_phoenix_VOC = 0*(145.82/100);
SLCC_grid_unit_phoenix_PM25 = 0.000487263*(145.82/100)*1.07;
```

Published with MATLAB® R2016b

D. 13 Choose Turbine Size: An Example of Microturbine

```
% Choose the right turbine size

if (maxthermal_output_30_kw > year_maxthermal_demand_kW)

    thermal_output_kW=thermal_output_30_kW;
    elec_output_kW = elec_output_30_kW;
    fuel_input_kW = fuel_input_30_kW;
    labels = labels30;
    turbNOx_emissions_kgperkWh = turbine30_NOxemissions_kgperkWh;
    turbVOC_emissions_kgperkWh = turbine30_VOCemissions_kgperkWh;
    turbCO2_emissions_kgperkWh = turbine30_CO2emissions_kgperkWh;
    fprintf('30 kW turbine\n');
    turbine_size = 30;
    microturbine_price_dollar = 4500*30;

elseif (maxthermal_output_65_kW > year_maxthermal_demand_kW)

    thermal_output_kW=thermal_output_65_kW;
    elec_output_kW = elec_output_65_kW;
    fuel_input_kW = fuel_input_65_kW;
    labels = labels65;
    turbNOx_emissions_kgperkWh = turbine65_NOxemissions_kgperkWh;
    turbVOC_emissions_kgperkWh = turbine65_VOCemissions_kgperkWh;
    turbCO2_emissions_kgperkWh = turbine65_CO2emissions_kgperkWh;
    fprintf('65 kW turbine\n');
    microturbine_price_dollar = 4500*65;
       turbine_size = 65;

elseif (maxthermal_output_95_kW >
year_maxthermal_demand_kW) %è¿™é‡Œemissionç›´æŽ¥ç”¨çš„æ˜¯65kwçš„ã€‚
    thermal_output_kW=thermal_output_95_kW;
    elec_output_kW = elec_output_95_kW;
    fuel_input_kW = fuel_input_95_kW;
    labels = labels95;
    turbNOx_emissions_kgperkWh = turbine65_NOxemissions_kgperkWh;
    turbVOC_emissions_kgperkWh = turbine65_VOCemissions_kgperkWh;
    turbCO2_emissions_kgperkWh = turbine65_CO2emissions_kgperkWh;
    fprintf('one 30 kW turbine and one 65kW turbine\n');
    microturbine_price_dollar = 4500*95;
       turbine_size = 95;

elseif (maxthermal_output_130_kW > year_maxthermal_demand_kW)
    thermal_output_kW=thermal_output_130_kW;
    elec_output_kW = elec_output_130_kW;
    fuel_input_kW = fuel_input_130_kW;
    labels = labels130;
    turbNOx_emissions_kgperkWh = turbine65_NOxemissions_kgperkWh;
    turbVOC_emissions_kgperkWh = turbine65_VOCemissions_kgperkWh;
    turbCO2_emissions_kgperkWh = turbine65_CO2emissions_kgperkWh;
    fprintf('two 65 kW turbine\n');
```

```
    microturbine_price_dollar = 4500*130;
       turbine_size = 130;

elseif (maxthermal_output_160_kW > year_maxthermal_demand_kW)
    thermal_output_kW=thermal_output_160_kW;
    elec_output_kW = elec_output_160_kW;
    fuel_input_kW = fuel_input_160_kW;
    labels = labels160;
    turbNOx_emissions_kgperkWh = turbine65_NOxemissions_kgperkWh;
    turbVOC_emissions_kgperkWh = turbine65_VOCemissions_kgperkWh;
    turbCO2_emissions_kgperkWh = turbine65_CO2emissions_kgperkWh;
    fprintf('one 30 kW turbine and two 65kW turbine\n');
    microturbine_price_dollar = 4500*160;
    turbine_size = 160;
elseif (maxthermal_output_200_kW > year_maxthermal_demand_kW)
    thermal_output_kW=thermal_output_200_kW;
    elec_output_kW = elec_output_200_kW;
    fuel_input_kW = fuel_input_200_kW;
    labels = labels200;
    turbNOx_emissions_kgperkWh = turbine200_NOxemissions_kgperkWh;
    turbVOC_emissions_kgperkWh = turbine200_VOCemissions_kgperkWh;
    turbCO2_emissions_kgperkWh = turbine200_CO2emissions_kgperkWh;
    fprintf('one 200 kW turbine\n');
    microturbine_price_dollar =4500*200;
       turbine_size = 200;


elseif (maxthermal_output_400_kW > year_maxthermal_demand_kW)
    thermal_output_kW=thermal_output_400_kW;
    elec_output_kW = elec_output_400_kW;
    fuel_input_kW = fuel_input_400_kW;
    labels = labels400;
    turbNOx_emissions_kgperkWh = turbine200_NOxemissions_kgperkWh;
    turbVOC_emissions_kgperkWh = turbine200_VOCemissions_kgperkWh;
    turbCO2_emissions_kgperkWh = turbine200_CO2emissions_kgperkWh;
    fprintf('two 200 kW turbine\n');
    microturbine_price_dollar = 4500*400;
       turbine_size = 400;

elseif (maxthermal_output_600_kW > year_maxthermal_demand_kW)
    thermal_output_kW=thermal_output_600_kW;
    elec_output_kW = elec_output_600_kW;
    fuel_input_kW = fuel_input_600_kW;
    labels = labels600;
    turbNOx_emissions_kgperkWh = turbine200_NOxemissions_kgperkWh;
    turbVOC_emissions_kgperkWh = turbine200_VOCemissions_kgperkWh;
    turbCO2_emissions_kgperkWh = turbine200_CO2emissions_kgperkWh;
    fprintf('one 600 kW turbine\n');
    microturbine_price_dollar = 4500*600;
       turbine_size = 600;
elseif (maxthermal_output_800_kW > year_maxthermal_demand_kW)
    thermal_output_kW=thermal_output_800_kW;
    elec_output_kW = elec_output_800_kW;
    fuel_input_kW = fuel_input_800_kW;
```

```
    labels = labels800;
    turbNOx_emissions_kgperkWh = turbine200_NOxemissions_kgperkWh;
    turbVOC_emissions_kgperkWh = turbine200_VOCemissions_kgperkWh;
    turbCO2_emissions_kgperkWh = turbine200_CO2emissions_kgperkWh;
    fprintf('one 800 kW turbine\n');
    microturbine_price_dollar = 4500*800;
       turbine_size = 800;

elseif (maxthermal_output_1000_kW > year_maxthermal_demand_kW)
    thermal_output_kW=thermal_output_1000_kW;
    elec_output_kW = elec_output_1000_kW;
    fuel_input_kW = fuel_input_1000_kW;
    labels = labels1000;
    turbNOx_emissions_kgperkWh = turbine200_NOxemissions_kgperkWh;
    turbVOC_emissions_kgperkWh = turbine200_VOCemissions_kgperkWh;
    turbCO2_emissions_kgperkWh = turbine200_CO2emissions_kgperkWh;
    fprintf('one 1000 kW turbine\n');
    microturbine_price_dollar =  4500*1000;
       turbine_size = 1000;
elseif  (maxthermal_output_2000_kW > year_maxthermal_demand_kW)
    thermal_output_kW = thermal_output_2000_kW;
    thermal_output_kW=thermal_output_2000_kW;
    elec_output_kW = elec_output_2000_kW;
    fuel_input_kW = fuel_input_2000_kW;
    labels = labels2000;
    turbNOx_emissions_kgperkWh = turbine200_NOxemissions_kgperkWh;
    turbVOC_emissions_kgperkWh = turbine200_VOCemissions_kgperkWh;
    turbCO2_emissions_kgperkWh = turbine200_CO2emissions_kgperkWh;
    fprintf('two 1000 kW turbine\n');
    microturbine_price_dollar = 4500*200;
       turbine_size = 2000;
 elseif  (maxthermal_output_2200_kW > year_maxthermal_demand_kW)
    thermal_output_kW = thermal_output_2200_kW;
    thermal_output_kW=thermal_output_2200_kW;
    elec_output_kW = elec_output_2200_kW;
    fuel_input_kW = fuel_input_2200_kW;
    labels = labels2200;
    turbNOx_emissions_kgperkWh = turbine200_NOxemissions_kgperkWh;
    turbVOC_emissions_kgperkWh = turbine200_VOCemissions_kgperkWh;
    turbCO2_emissions_kgperkWh = turbine200_CO2emissions_kgperkWh;
    fprintf('two 1000 kW and one 200kW turbine\n');
    microturbine_price_dollar = 4500*2200;
       turbine_size = 2200;
 elseif  (maxthermal_output_2400_kW > year_maxthermal_demand_kW)
    thermal_output_kW = thermal_output_2400_kW;
    thermal_output_kW=thermal_output_2400_kW;
    elec_output_kW = elec_output_2400_kW;
    fuel_input_kW = fuel_input_2400_kW;
    labels = labels2400;
    turbNOx_emissions_kgperkWh = turbine200_NOxemissions_kgperkWh;
    turbVOC_emissions_kgperkWh = turbine200_VOCemissions_kgperkWh;
    turbCO2_emissions_kgperkWh = turbine200_CO2emissions_kgperkWh;
    fprintf('two 1000 kW  and two 200kW turbine\n');
    microturbine_price_dollar = 4500*2400;
```

```
        turbine_size = 2400;

elseif  (maxthermal_output_2600_kW > year_maxthermal_demand_kW)
    thermal_output_kW = thermal_output_2600_kW;
    thermal_output_kW=thermal_output_2600_kW;
    elec_output_kW = elec_output_2600_kW;
    fuel_input_kW = fuel_input_2600_kW;
    labels = labels2600;
    turbNOx_emissions_kgperkWh = turbine200_NOxemissions_kgperkWh;
    turbVOC_emissions_kgperkWh = turbine200_VOCemissions_kgperkWh;
    turbCO2_emissions_kgperkWh = turbine200_CO2emissions_kgperkWh;
    fprintf('two 1000 kW and three 200kW turbine\n');
        turbine_size = 2600;
    microturbine_price_dollar = 4500*2600;
elseif  (maxthermal_output_2800_kW > year_maxthermal_demand_kW)
    thermal_output_kW = thermal_output_2800_kW;
    thermal_output_kW=thermal_output_2800_kW;
    elec_output_kW = elec_output_2800_kW;
    fuel_input_kW = fuel_input_2800_kW;
    labels = labels2800;
    turbNOx_emissions_kgperkWh = turbine200_NOxemissions_kgperkWh;
    turbVOC_emissions_kgperkWh = turbine200_VOCemissions_kgperkWh;
    turbCO2_emissions_kgperkWh = turbine200_CO2emissions_kgperkWh;
    fprintf('two 1000 kW and four 200kW turbine\n');
    microturbine_price_dollar = 4500*2800;
        turbine_size = 2800;
elseif  (maxthermal_output_3000_kW > year_maxthermal_demand_kW)
    thermal_output_kW = thermal_output_3000_kW;
    thermal_output_kW=thermal_output_3000_kW;
    elec_output_kW = elec_output_3000_kW;
    fuel_input_kW = fuel_input_3000_kW;
    labels = labels3000;
    turbNOx_emissions_kgperkWh = turbine200_NOxemissions_kgperkWh;
    turbVOC_emissions_kgperkWh = turbine200_VOCemissions_kgperkWh;
    turbCO2_emissions_kgperkWh = turbine200_CO2emissions_kgperkWh;
    fprintf('three 1000 kW  turbine\n');
    microturbine_price_dollar = 3000*160;
        turbine_size = 3000;
elseif  (maxthermal_output_3200_kW > year_maxthermal_demand_kW)
    thermal_output_kW = thermal_output_3200_kW;
    thermal_output_kW=thermal_output_3200_kW;
    elec_output_kW = elec_output_3200_kW;
    fuel_input_kW = fuel_input_3200_kW;
    labels = labels3200;
    turbNOx_emissions_kgperkWh = turbine200_NOxemissions_kgperkWh;
    turbVOC_emissions_kgperkWh = turbine200_VOCemissions_kgperkWh;
    turbCO2_emissions_kgperkWh = turbine200_CO2emissions_kgperkWh;
    fprintf('three 1000 kW and on 200kW turbine\n');
    microturbine_price_dollar = 4500*3200;
        turbine_size = 3200;
elseif  (maxthermal_output_3400_kW > year_maxthermal_demand_kW)
    thermal_output_kW = thermal_output_3400_kW;
    thermal_output_kW=thermal_output_3400_kW;
    elec_output_kW = elec_output_3400_kW;
```

```
    fuel_input_kW = fuel_input_3400_kW;
    labels = labels3400;
    turbNOx_emissions_kgperkWh = turbine200_NOxemissions_kgperkWh;
    turbVOC_emissions_kgperkWh = turbine200_VOCemissions_kgperkWh;
    turbCO2_emissions_kgperkWh = turbine200_CO2emissions_kgperkWh;
    fprintf('three 1000 kW turbine and two 200kW\n');
    microturbine_price_dollar = 4500*3400;
       turbine_size = 3400;
 elseif  (maxthermal_output_3600_kW > year_maxthermal_demand_kW)
    thermal_output_kW = thermal_output_3600_kW;
    thermal_output_kW=thermal_output_3600_kW;
    elec_output_kW = elec_output_3600_kW;
    fuel_input_kW = fuel_input_3600_kW;
    labels = labels3600;
    turbNOx_emissions_kgperkWh = turbine200_NOxemissions_kgperkWh;
    turbVOC_emissions_kgperkWh = turbine200_VOCemissions_kgperkWh;
    turbCO2_emissions_kgperkWh = turbine200_CO2emissions_kgperkWh;
    fprintf('three 1000 kW and three 200kW turbine\n');
    microturbine_price_dollar = 4500*3600;
       turbine_size = 3600;
 elseif  (maxthermal_output_3800_kW > year_maxthermal_demand_kW)
    thermal_output_kW = thermal_output_3800_kW;
    thermal_output_kW=thermal_output_3800_kW;
    elec_output_kW = elec_output_3800_kW;
    fuel_input_kW = fuel_input_3800_kW;
    labels = labels3800;
    turbNOx_emissions_kgperkWh = turbine200_NOxemissions_kgperkWh;
    turbVOC_emissions_kgperkWh = turbine200_VOCemissions_kgperkWh;
    turbCO2_emissions_kgperkWh = turbine200_CO2emissions_kgperkWh;
    fprintf('two 1000 kW four 200kW turbine\n');
    microturbine_price_dollar = 4500*3800;
       turbine_size = 3800;
 elseif  (maxthermal_output_4000_kW > year_maxthermal_demand_kW)
    thermal_output_kW = thermal_output_4000_kW;
    thermal_output_kW=thermal_output_4000_kW;
    elec_output_kW = elec_output_4000_kW;
    fuel_input_kW = fuel_input_4000_kW;
    labels = labels4000;
    turbNOx_emissions_kgperkWh = turbine200_NOxemissions_kgperkWh;
    turbVOC_emissions_kgperkWh = turbine200_VOCemissions_kgperkWh;
    turbCO2_emissions_kgperkWh = turbine200_CO2emissions_kgperkWh;
    fprintf('four 1000 kW turbine\n');
    microturbine_price_dollar = 4500*4000;
       turbine_size = 4000;

else
    fprintf('none');
end
```

Published with MATLAB® R2016b

REFERENCES

1. Arup. *Consumption-based GHG emissions of C40 cities*. (2018).
2. Affairs, D. of E. and S. *World Urbanization Prospects*. https://esa.un.org/unpd/wup/publications/files/wup2014-highlights.pdf (2014).
3. Darrow, K., Tidball, R., Wang, J. & Hampson, A. Catalog of CHP technologies. *US Environ. Prot. Agency, Washington, DC* 5–6 (2015).
4. Wu, D. & Wang, R. Combined cooling, heating and power: A review. *Prog. energy Combust. Sci.* **32**, 459–495 (2006).
5. Faisal, M. *et al.* Review of energy storage system technologies in microgrid applications: Issues and challenges. *Ieee Access* **6**, 35143–35164 (2018).
6. Zhang, J., Cho, H. & Knizley, A. Evaluation of financial incentives for combined heat and power (CHP) systems in U.S. regions. *Renew. Sustain. Energy Rev.* **59**, 738–762 (2016).
7. Mago, P. J., Fumo, N. & Chamra, L. M. Performance analysis of CCHP and CHP systems operating following the thermal and electric load. *Int. J. Energy Res.* **33**, 852–864 (2009).
8. James, J.-A. *et al.* Impacts of Combined Cooling, Heating and Power Systems, and Rainwater Harvesting on Water Demand, Carbon Dioxide, and NO x Emissions for Atlanta. *Environ. Sci. Technol.* **52**, 3–10 (2018).
9. Kroposki, B. *et al.* Benefits of power electronic interfaces for distributed energy systems. *IEEE Trans. energy Convers.* **25**, 901–908 (2010).
10. Chakraborty, S., Kramer, B. & Kroposki, B. A review of power electronics

interfaces for distributed energy systems towards achieving low-cost modular design. *Renew. Sustain. Energy Rev.* **13**, 2323–2335 (2009).

11. Yagoub, W., Doherty, P. & Riffat, S. B. Solar energy-gas driven micro-CHP system for an office building. *Appl. Therm. Eng.* **26**, 1604–1610 (2006).

12. Guan, X., Xu, Z. & Jia, Q.-S. Energy-efficient buildings facilitated by microgrid. *IEEE Trans. Smart Grid* **1**, 243–252 (2010).

13. Nuytten, T., Claessens, B., Paredis, K., Van Bael, J. & Six, D. Flexibility of a combined heat and power system with thermal energy storage for district heating. *Appl. Energy* **104**, 583–591 (2013).

14. Tveit, T.-M., Savola, T., Gebremedhin, A. & Fogelholm, C.-J. Multi-period MINLP model for optimising operation and structural changes to CHP plants in district heating networks with long-term thermal storage. *Energy Convers. Manag.* **50**, 639–647 (2009).

15. Rastegar, M. & Fotuhi-Firuzabad, M. Load management in a residential energy hub with renewable distributed energy resources. *Energy Build.* **107**, 234–242 (2015).

16. Mehleri, E. D., Sarimveis, H., Markatos, N. C. & Papageorgiou, L. G. Optimal design and operation of distributed energy systems: Application to Greek residential sector. *Renew. Energy* **51**, 331–342 (2013).

17. Shah, K. K., Mundada, A. S. & Pearce, J. M. Performance of US hybrid distributed energy systems: Solar photovoltaic, battery and combined heat and power. *Energy Convers. Manag.* **105**, 71–80 (2015).

18. Nosrat, A. H., Swan, L. G. & Pearce, J. M. Improved performance of hybrid

photovoltaic-trigeneration systems over photovoltaic-cogen systems including effects of battery storage. *Energy* **49**, 366–374 (2013).

19. Gu, W., Wu, Z. & Yuan, X. Microgrid economic optimal operation of the combined heat and power system with renewable energy. *IEEE PES Gen. Meet. PES 2010* 1–6 (2010) doi:10.1109/PES.2010.5590140.

20. Rodríguez, L. R., Lissén, J. M. S., Ramos, J. S., Jara, E. Á. R. & Domínguez, S. Á. Analysis of the economic feasibility and reduction of a building's energy consumption and emissions when integrating hybrid solar thermal/PV/micro-CHP systems. *Appl. Energy* **165**, 828–838 (2016).

21. Brandoni, C. & Renzi, M. Optimal sizing of hybrid solar micro-CHP systems for the household sector. *Appl. Therm. Eng.* **75**, 896–907 (2015).

22. Pedrazzi, S., Zini, G. & Tartarini, P. Modelling and simulation of a wind-hydrogen CHP system with metal hydride storage. *Renew. energy* **46**, 14–22 (2012).

23. Borello, D., Evangelisti, S. & Tortora, E. Modelling of a CHP SOFC system fed with biogas from anaerobic digestion of municipal waste integrated with solar collectors and storage unit. *Int. J. Thermodyn.* **16**, 28–35 (2013).

24. Brahman, F., Honarmand, M. & Jadid, S. Optimal electrical and thermal energy management of a residential energy hub, integrating demand response and energy storage system. *Energy Build.* **90**, 65–75 (2015).

25. Balcombe, P., Rigby, D. & Azapagic, A. Energy self-sufficiency, grid demand variability and consumer costs: Integrating solar PV, Stirling engine CHP and battery storage. *Appl. Energy* **155**, 393–408 (2015).

26. Bianchi, M., De Pascale, A. & Melino, F. Performance analysis of an integrated

CHP system with thermal and Electric Energy Storage for residential application. *Appl. Energy* **112**, 928–938 (2013).

27. Maleki, A., Hafeznia, H., Rosen, M. A. & Pourfayaz, F. Optimization of a grid-connected hybrid solar-wind-hydrogen CHP system for residential applications by efficient metaheuristic approaches. *Appl. Therm. Eng.* **123**, 1263–1277 (2017).
28. Celador, A. C., Odriozola, M. & Sala, J. M. Implications of the modelling of stratified hot water storage tanks in the simulation of CHP plants. *Energy Convers. Manag.* **52**, 3018–3026 (2011).
29. Shabani, B., Andrews, J. & Watkins, S. Energy and cost analysis of a solar-hydrogen combined heat and power system for remote power supply using a computer simulation. *Sol. Energy* **84**, 144–155 (2010).
30. Soheyli, S., Shafiei Mayam, M. H. & Mehrjoo, M. Modeling a novel CCHP system including solar and wind renewable energy resources and sizing by a CC-MOPSO algorithm. *Appl. Energy* **184**, 375–395 (2016).
31. Lee, D. & Thomas, V. M. Parametric modeling approach for economic and environmental life cycle assessment of medium-duty truck electri fi cation. *J. Clean. Prod.* **142**, 3300–3321 (2017).
32. Hosseini, M., Dincer, I. & Rosen, M. A. Hybrid solar–fuel cell combined heat and power systems for residential applications: Energy and exergy analyses. *J. Power Sources* **221**, 372–380 (2013).
33. Alipour, M., Mohammadi-Ivatloo, B. & Zare, K. Stochastic Scheduling of Renewable and CHP-Based Microgrids. *IEEE Trans. Ind. Informatics* **11**, 1049–1058 (2015).

34. US Department of Energy. *Combined Heat and Power Instalation Databasem Appciation Version 1.1.0*. (2018).

35. The Math Works. MATLAB. (2018).

36. Levihn, F. CHP and heat pumps to balance renewable power production: Lessons from the district heating network in Stockholm. *Energy* **137**, 670–678 (2017).

37. James, J.-A., Thomas, V. M., Pandit, A., Li, D. & Crittenden, J. C. Water, Air Emissions, and Cost Impacts of Air-Cooled Microturbines for Combined Cooling, Heating, and Power Systems: A Case Study in the Atlanta Region. *Engineering* **2**, 470–480 (2016).

38. Tempesti, D., Manfrida, G. & Fiaschi, D. Thermodynamic analysis of two micro CHP systems operating with geothermal and solar energy. *Appl. Energy* **97**, 609–617 (2012).

39. Ma, X., Wang, Y. & Qin, J. Generic model of a community-based microgrid integrating wind turbines, photovoltaics and CHP generations. *Appl. Energy* **112**, 1475–1482 (2013).

40. Yang, Y., Pei, W. & Qi, Z. Optimal sizing of renewable energy and CHP hybrid energy microgrid system. in *IEEE PES innovative smart grid technologies* 1–5 (IEEE, 2012).

41. Romero Rodríguez, L., Salmerón Lissén, J. M., Sánchez Ramos, J., Rodríguez Jara, E. Á. & Álvarez Domínguez, S. Analysis of the economic feasibility and reduction of a building's energy consumption and emissions when integrating hybrid solar thermal/PV/micro-CHP systems. *Appl. Energy* **165**, 828–838 (2016).

42. Bokrantz, R. & Fredriksson, A. Necessary and sufficient conditions for Pareto

efficiency in robust multiobjective optimization. *Eur. J. Oper. Res.* **262**, 682–692 (2017).

43. Lin, S.-H. & Gerber, D. J. Evolutionary energy performance feedback for design: Multidisciplinary design optimization and performance boundaries for design decision support. *Energy Build.* **84**, 426–441 (2014).

44. Martins, J. R. R. A. & Lambe, A. B. Multidisciplinary Design Optimization: A Survey of Architectures. *AIAA J.* **51**, 2049–2075 (2013).

45. Forest, F. & John, H. A Comparison of Multidisciplinary Design, Analysis and Optimization Processes in the Building Construction and Aerospace. (2007).

46. Best, R. E., Flager, F. & Lepech, M. D. Modeling and optimization of building mix and energy supply technology for urban districts. *Appl. Energy* **159**, 161–177 (2015).

47. Johnson, S. D. & Moyer, E. J. Feasibility of U.S. renewable portfolio standards under cost caps and case study for Illinois. *Energy Policy* **49**, 499–514 (2012).

48. US Department of Energy. *Renewable Energy Certificates (RECs)*. (2010).

49. Couture, T. D., Cory, K., Kreycik, C. & Williams, E. *Policymaker's Guide to Feed-in Tariff Policy Design*. (2010).

50. Wiser, R., Bolinger, M. & Barbose, G. Using the Federal Production Tax Credit to Build a Durable Market for Wind Power in the United States. *Electr. J.* **20**, 77–88 (2007).

51. Mahlia, T. M. I. & Chan, P. L. Life cycle cost analysis of fuel cell based cogeneration system for residential application in Malaysia. *Renew. Sustain. Energy Rev.* **15**, 416–426 (2011).

52. Roman, K. K. & Alvey, J. B. Selection of prime mover for combined cooling, heating, and power systems based on energy savings, life cycle analysis and environmental consideration. *Energy Build.* **110**, 170–181 (2016).

53. Marszal, A. J. & Heiselberg, P. Life cycle cost analysis of a multi-storey residential Net Zero Energy Building in Denmark. *Energy* **36**, 5600–5609 (2011).

54. Jacobsson, S. & Lauber, V. The politics and policy of energy system transformation—explaining the German diffusion of renewable energy technology. *Energy Policy* **34**, 256–276 (2006).

55. Mitchell, C. & Connor, P. Renewable energy policy in the UK 1990–2003. *Energy Policy* **32**, 1935–1947 (2004).

56. Kobos, P. H., Erickson, J. D. & Drennen, T. E. Technological learning and renewable energy costs: implications for US renewable energy policy. *Energy Policy* **34**, 1645–1658 (2006).

57. Tichi, S. G., Ardehali, M. M. & Nazari, M. E. Examination of energy price policies in Iran for optimal configuration of CHP and CCHP systems based on particle swarm optimization algorithm. *Energy Policy* **38**, 6240–6250 (2010).

58. Zheng, C. Y., Wu, J. Y., Zhai, X. Q. & Wang, R. Z. Impacts of feed-in tariff policies on design and performance of CCHP system in different climate zones. *Appl. Energy* **175**, 168–179 (2016).

59. Jiang, X. Z., Zeng, G., Li, M. & Shi, L. Evaluation of combined cooling, heating and power (CCHP) systems with energy storage units at different locations. *Appl. Therm. Eng.* **95**, 204–210 (2016).

60. Li, M., Mu, H., Li, N. & Ma, B. Optimal design and operation strategy for

integrated evaluation of CCHP (combined cooling heating and power) system. *Energy* **99**, 202–220 (2016).

61. Yan, J., Broesicke, O., Wang, D., Li, D. & Crittenden, J. Parametric Life Cycle Assessment for Distributed Combined Cooling, Heating and Power integrated with Solar Energy and Energy Storage. *J. Clean. Prod.* **Manuscript**, (2019).

62. Deng, J., Wang, R. Z. & Han, G. Y. A review of thermally activated cooling technologies for combined cooling, heating and power systems. *Prog. Energy Combust. Sci.* **37**, 172–203 (2011).

63. Betz, F. Combined cooling, heating, power, and ventilation (CCHP/V) systems integration. in *University* (Citeseer, 2009).

64. Yang, L. *et al.* Design of high-performance cathode materials with single-phase pathway for sodium ion batteries: A study on P2-Nax(LiyMn1-y)O2compounds. *J. Power Sources* **381**, 171–180 (2018).

65. LCI, U. S. Life-Cycle Inventory, v. 1.6. 0. *Golden, CO Natl. Renew. Energy Lab.* (2008).

66. Pre. Simapro. (2019).

67. Yang, Y., Ingwersen, W. W., Hawkins, T. R., Srocka, M. & Meyer, D. E. USEEIO: A new and transparent United States environmentally-extended input-output model. *J. Clean. Prod.* **158**, 308–318 (2017).

68. US Environmental Protection Agency. Emissions & Generation Resource Integrated Database (eGRID). (2016).

69. Bare, J. TRACI 2.0: the tool for the reduction and assessment of chemical and other environmental impacts 2.0. *Clean Technol. Environ. Policy* **13**, 687–696

(2011).

70. Ryberg, M., Vieira, M. D. M., Zgola, M., Bare, J. & Rosenbaum, R. K. Updated US and Canadian normalization factors for TRACI 2.1. *Clean Technol. Environ. Policy* **16**, 329–339 (2014).

71. Gloria, T. P., Lippiatt, B. C. & Cooper, J. Life Cycle Impact Assessment Weights to Support Environmentally Preferable Purchasing in the United States. *Environ. Sci. Technol.* **41**, 7551–7557 (2007).

72. Baer, P., Brown, M. A. & Kim, G. The job generation impacts of expanding industrial cogeneration. *Ecol. Econ.* **110**, 141–153 (2015).

73. Mago, P. J. & Chamra, L. M. Analysis and optimization of CCHP systems based on energy, economical, and environmental considerations. *Energy Build.* **41**, 1099–1106 (2009).

74. US Department of Energy. EnergyPlus 9.1.0. (2019).

75. Crawley, D. B., Lawrie, L. K., Pedersen, C. O. & Winkelmann, F. C. Energy plus: energy simulation program. *ASHRAE J.* **42**, 49–56 (2000).

76. US Department of Energy. Commercial Reference Buildings. https://www.energy.gov/eere/buildings/commercial-reference-buildings (2011).

77. Deru, M. *et al.* US Department of Energy commercial reference building models of the national building stock. (2011).

78. Torcelini, P. *et al. DOE commercial building benchmark models*. (2008).

79. Makita, K. Waste heat energy application for absorption chillers. in *3rd International District Cooling Conference & Trade Show, Dubai* (2008).

80. Corporation, C. T. *Product Specification Model C200-Capstone MicroTurbineTM*.

(2009).

81. Sandia National Laboratories. PVPerformance Modeling Collaborative. (2016).

82. Brooks, W. & Dunlop, J. Photovoltaic (PV) installer resource guide. *North Am. Board Certif. Energy Pract. (NABCEP), Tech. Rep* (2012).

83. nternational Fire Code. *International Fire Code [IFC605.11]*. (2012).

84. Tesla, I. *Tesla Powerwall Limited warranty （USA）*. (2017).

85. Energy Information Administration. State Profile and Energy Estimates. (2019).

86. Leung, D. Y. C. & Yang, Y. Wind energy development and its environmental impact: A review. *Renew. Sustain. Energy Rev.* **16**, 1031–1039 (2012).

87. Wu, Y. & Hong, J. A literature review of wind forecasting technology in the world. in *2007 IEEE Lausanne Power Tech* 504–509 (2007). doi:10.1109/PCT.2007.4538368.

88. Maydew, R. C. & Klimas, P. C. Aerodynamic performance of vertical and horizontal axis wind turbines. *J. Energy* **5**, 189–190 (1981).

89. Wilcox, S. & Marion, W. *Users manual for TMY3 data sets*. (National Renewable Energy Laboratory Golden, CO, 2008).

90. Justus, C. G. & Mikhail, A. Height variation of wind speed and wind distributions statistics. *Geophys. Res. Lett.* **3**, 261–264 (1976).

91. Ray, M. L., Rogers, A. L. & McGowan, J. G. Analysis of wind shear models and trends in different terrains. *Univ. Massachusetts, Dep. Mech. Ind. Eng. Renew. Energy Res. Lab.* (2006).

92. Choi, N. J., Nam, S. H., Jeong, J. H. & Kim, K. C. Numerical study on the horizontal axis turbines arrangement in a wind farm: Effect of separation distance

on the turbine aerodynamic power output. *J. Wind Eng. Ind. Aerodyn.* **117**, 11–17 (2013).

93. SD WIND ENERGY. SD WIND ENERGY. (2019).

94. US Environmental Protection Agency. Catalog of CHP Technologies. (2015).

95. Conti, J. J. *et al.* Annual energy outlook 2014. *US Energy Inf. Adm.* 2 (2014).

96. Wang, S. & Jiang, S. P. Prospects of fuel cell technologies. *Natl. Sci. Rev.* **4**, 163–166 (2017).

97. Chiappini, D., Facci, A. L., Tribioli, L. & Ubertini, S. SOFC management in distributed energy systems. *J. Fuel Cell Sci. Technol.* **8**, 31015 (2011).

98. Geisbrecht, R. A. & Williams, M. C. Fuel cell-fuel cell hybrid system. (2003).

99. Barnhart, C. J. & Benson, S. M. On the importance of reducing the energetic and material demands of electrical energy storage. *Energy Environ. Sci.* **6**, 1083 (2013).

100. Budt, M., Wolf, D., Span, R. & Yan, J. A review on compressed air energy storage: Basic principles, past milestones and recent developments. *Appl. Energy* **170**, 250–268 (2016).

101. Mahlia, T. M. I., Saktisahdan, T. J., Jannifar, A., Hasan, M. H. & Matseelar, H. S. C. A review of available methods and development on energy storage; technology update. (2014) doi:10.1016/j.rser.2014.01.068.

102. Department of Energy. Global Energy Storage Database. *2019*.

103. Luo, X. *et al.* Modelling study, efficiency analysis and optimisation of large-scale Adiabatic Compressed Air Energy Storage systems with low-temperature thermal storage. *Appl. Energy* **162**, 589–600 (2016).

104. Bennett, C. O. & Myers, J. E. *Momentum, heat, and mass transfer*. vol. 370 (McGraw-Hill New York, 1982).

105. Bouman, E. A., Øberg, M. M. & Hertwich, E. G. Environmental impacts of balancing offshore wind power with compressed air energy storage (CAES). *Energy* **95**, 91–98 (2016).

106. Mongird, K. *et al.* Energy Storage Technology and Cost Characterization Report. *Pacific Northwest Natl. Lab. PNNL-28866 (July 2019)* (2019).

107. Mohendroo, M. Some common mistakes to avoid in estimating and applying discount rates. *Deloitte, Spring* (2014).

108. Koomey, J. & Krause, F. Introduction to environmental externality costs. *CRC Handb. Energy Effic. ed. Frank Kreith Ronald E. West (Boca Raton, Fla. CRC)* (1997).

109. Matthews, H. S., Hendrickson, C. & Horvath, A. External costs of air emissions from transportation. *J. Infrastruct. Syst.* **7**, 13–17 (2001).

110. Ayres, R. U. & Kneese, A. V. Production, consumption, and externalities. *Am. Econ. Rev.* **59**, 282–297 (1969).

111. Muller, N. Z. & Mendelsohn, R. The Air Pollution Emission Experiments and Policy Analysis Model (APEEP) Technical Appendix. *Yale Univ. New Haven, CT, USA* **1**, (2006).

112. National Academies of Sciences and Medicine, E. *Valuing climate damages: updating estimation of the social cost of carbon dioxide*. (National Academies Press, 2017).

113. Bureau of Lavor Statistics. Consumer Price Index. https://www.bls.gov/cpi/

(2019).

114. Environmental Systems Research Institute. ArcGIS Desktop: Release 10.7.1. (2018).

115. Agency, U. S. E. P. Emissions & Generation Resource Integrated Database (eGRID). (2002).

116. Michel, A. N. Analysis of the 2017 Tax Cuts and Jobs Act. *Herit. Found. December* **19**, 2017 (2017).

117. Weinzierl, M. & Scherf, R. Donald Trump and the Tax Cuts and Jobs Act. (2018).

118. Mendelsohn, M. & Feldman, D. *Financing US Renewable Energy Projects Through Public Capital Vehicles: Qualitative and Quantitative Benefits. National Renewable Energy Laboratory*. (2013).

119. University of Michigan. *Commercial Building Factsheet*. (2019).

VITA

Junchen Yan

Junchen was born in Dalian and grew up in Beijing, China. He received a B.S. in Electrical and Electronic Engineering from Imperial College London in 2014 and an M.S. in Chemical Engineering from Georgia Institute of Technology in 2016 before his doctorate in Sustainable Engineering.

During the challenging research life, this motto inspired and continuously supported him:

Prosperity comes to the common people and to those of mean abilities; but it is the part of a great man to overcome the disasters and terrors of mortals. Valor is eager for danger and thinks only of its aim not what it will suffer, since even what it will suffer is a part of its glory. Soldiers glory in their wounds and joyfully speak of the blood which they were so fortunate to shed.

---Seneca, On Providence.